hGBP1 coordinates Chlamydia restriction and inflammasome activation through sequential GTP hydrolysis

Inaugural Dissertation to obtain the academic degree
Doctor rerum naturalium (Dr. rer. nat.)

submitted to the Department of Biology, Chemistry, Pharmacy
of Freie Universität Berlin

Audrey Helena Xavier

Berlin, 2020

The present work was carried out between August 2016 and August 2020 at the Max-Delbrück-Center for Molecular Medicine (MDC-Berlin) and the Max-Planck-Institute for Infection Biology (MPIIB Berlin) under the supervision of Prof. Dr. Oliver Daumke (MDC) and Prof. Dr. Thomas F. Meyer (MPIIB).

Selbstständigkeitserklärung

Hiermit bestätige ich, dass ich die vorliegende Arbeit selbstständig und unter Zuhilfenahme der angegebenen Literatur erstellt habe.

Berlin den

_____

Unterschrift

1. Reviewer: Prof. Dr. Oliver Daumke, Department of Protein Crystallography, Max Delbrück Center for Molecular Medicine

2. Reviewer: Prof. Dr. Christian Freund, Department of Biochemistry, Freie Universität Berlin

Date of defense: 15.02.2021

Publication

Part of this PhD thesis has been published in the following manuscript:

hGBP1 Coordinates Chlamydia Restriction and Inflammasome Activation through Sequential GTP Hydrolysis. Xavier A, Al-Zeer MA, Meyer TF, Daumke O. *Cell Rep*. 2020;31(7):107667. doi:10.1016/j.celrep.2020.107667

Content

1. Introduction

1.1 Pathogen detection by the innate immune system

An effective microbial immune response is based on the detection of pathogens by the host immune system. In the course of an evolutionary “arms-race”, vertebrates have developed two major branches of immunological defense, the innate and adaptive immune system (Dawkins et al., 1979). These branches include a subset of humoral and cellular immune mechanisms, which can efficiently recognize and clear pathogen infection. An integer part of the innate branch is the recognition of distinct pathogenic or danger signatures, the pathogen-associated molecular patterns (PAMPs) or danger-associated molecular patterns (DAMPs), by pattern recognition receptors (PRRs). Recognition of PAMPs or DAMPs is essential to the host organism to distinguish self from an invading pathogen or detect a cellular imbalance and to consequently activate a downstream signaling cascade (Janeway, 1989). Accordingly, pathogens have developed strategies to avoid detection by the host system. Invading the host cell and replicating intracellularly enables pathogens to escape detection by extracellular immune responses, such as the complement system, phagocytes and antibodies (Kumar and Valdivia, 2009). In most cases, an invading pathogen will enter the host cell within a vacuolar compartment, as the result of phagocytosis or by facilitating their own endocytosis. To prevent lysis by the host cell, pathogens must avoid fusion of their compartment with lysosomes. Only a few microbial pathogens can replicate directly in the cytosol (Kumar and Valdivia, 2009), as the broad spectrum of host cytosolic defense mechanisms enforce the necessity to reside in sheltered compartments, generally referred to as pathogen containing vacuoles (PCV) (Case et al., 2014; Paciello et al., 2013). The host cytosolic defense system initiates the secretion of pro-inflammatory cytokines, chemokines, and the recruitment of effector immune cells. In addition, inflammatory host cell death (pyroptosis) can be induced by the activation of inflammasome complexes. In general, these mechanisms lead to the elimination of the pathogens or infected cells. However, chronic, or erroneous activation can lead to immunodeficiency, septic shock, or autoimmune disease.

1.2 The effector immune response

Detection of PAMPs and DAMPs by PRRs of antigen presenting cells (APCs) leads to transcriptional upregulation of genes involved in inflammatory responses (Akira and Takeda, 2004; Akira et al., 2006). These genes encode type I interferons, chemokines, pro-inflammatory cytokines and proteins that in turn regulate PRR signaling and expression. Inflammation is coordinated by the proinflammatory cytokines tumor necrosis factor (TNF), interleukin (IL)-1, and IL-6 (Akira et al., 2006). Proinflammatory cytokines are regulated on the transcriptional and translational level. However, IL-1β has an additional control mechanism. Transcription of IL-1β is initiated by toll-like receptor (TLR) signaling, but expression occurs as the 31 kDa precursor protein, Pro-IL-1β, which is matured by proteolytic cleavage by caspase-1. Caspase-1 activation is mediated by the inflammasome complex composed of adaptor molecules, a cytosolic PRR and Pro-Caspase-1 (Mariathasan et al., 2006; Martinon et al., 2002). The most well characterized inflammasome complex thus far consists of the cytosolic NOD-like receptor (NLR) called NLRP3. NLRP3 has a tripartite structure with a pattern sensory domain, the C-terminal leucine rich repeat (LRR), a central nucleotide binding (or NACHT) domain and an N-terminal pyrin domain (PYD). The PYD recruits the adaptor molecule apoptosis-associate speck-like protein containing a caspase recruitment domain (ASC). ASC is composed of a PYD and a caspase activation and recruitment domain (CARD) domain. The latter engages in homotypical interaction with the CARD of caspase 1, facilitating its autoproteolysis and activation. Following the proteolytic processing of Pro-IL-1β, the mature 17 kDa cytokine is secreted from the cell, either passively by pyroptosis or by active vesicle transport (Agostini et al., 2004; Kanneganti et al., 2007; Nickel and Rabouille, 2009). IL-1β can induce the expression of hundreds of genes that lead to the recruitment of immune cells (such as T cells and B cells) to the site of infection (Weber et al., 2010).

1.3 Inflammasomes

Inflammasomes are cytosolic signaling complexes initiated by pattern recognition receptors and serve as activation platforms for inflammatory caspases, like mouse caspase-1 and caspase-11 or human caspase-1, caspase-4 and caspase-5 (Man et

al., 2015). Inflammatory caspase activation leads to IL-1β processing and pyroptosis. IL-1β is a key regulator of inflammatory responses, thus over-production is associated with autoinflammatory syndromes, such as gout and periodic fever syndromes. A canonical and the non-canonical pathway can be distinguished. Canonical inflammasome complexes consist of a sensor molecule and an adaptor molecule that activates caspase 1-mediated downstream signaling. There are two classes of sensor molecules: NLRs and AIM2-like receptors (ALRs). Sensor proteins have an effector domain such as the CARD, PYD or baculoviral inhibitor of apoptosis (IAP) repeat domain for interaction with an adaptor molecule or for direct caspase 1 activation, a NACHT domain and a LRR domain. The most common adaptor molecule is ASC. ASC is composed of a PYD and a CARD domain. The latter engages in homotypical interaction with the CARD of caspase 1. The canonical pathway refers to the downstream activation of caspase 1, whereas the non-canonical pathway results in processive cleavage of mouse caspase 11 or human caspase 4/5 (Lu and Wu, 2015) (see Fig. 1). The canonical pathway is initiated by the sensing of pathogenic ligands via receptor molecules of the NLR or pyrin and HIN200 domain-containing (PYHIN) family, whereas in case of the non-canonical pathway caspase 11 (human caspase-4) is supposed to directly sense bacterial lipopolysaccharides (LPS) (Shi et al., 2014).Upon entry of gram-negative bacteria, IFN-induced factors are suggested to liberate LPS, which can be sensed by components of the non-canonical inflammasome that subsequently activate Gasdermin D-mediated pyroptosis or cytokine release via the NLRP3- caspase-1-pathway (Kayagaki et al., 2015; Man et al., 2016; Meunier et al., 2014).

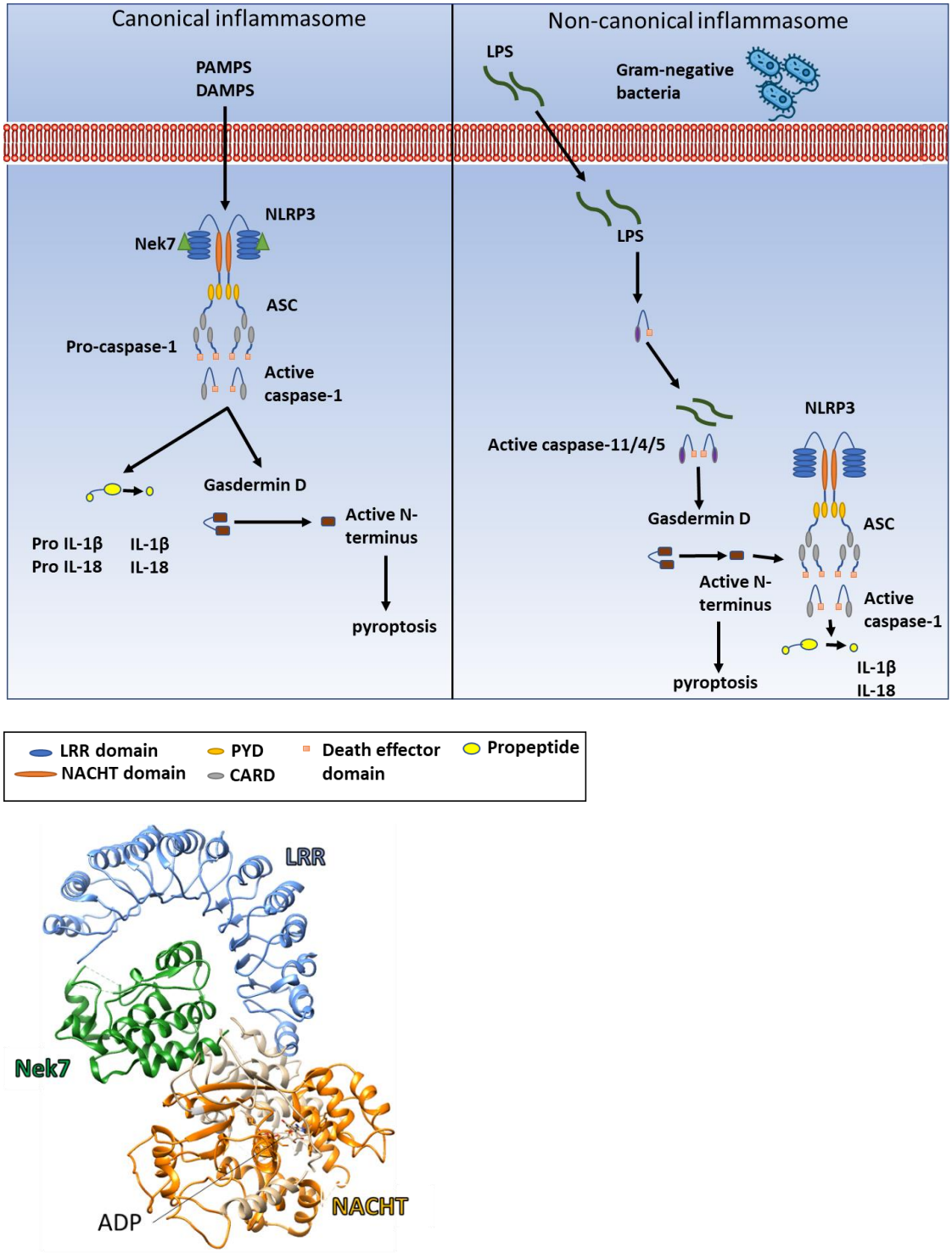

Figure 1 Canonical and non-canonical inflammasome pathways. The canonical inflammasome pathway is activated by a plethora of pathogen or danger signatures. Nek7 (green) is recruited to the LRR domain (blue) of NLRP3 and stabilizes inflammasome formation as depicted in the crystal structure of NLRP3 NACHT-LRR bound to Nek7 (6NPY). NLRP3 recruits pro-caspase-1 through the adaptor protein ASC leading to autoproteolytic activation of pro-caspase-1 (grey + yellow) to caspase-1. Caspase-1 processes the pro-inflammatory cytokine pro- IL-1β (bright yellow) to mature IL-1β, which is secreted from the cell. Caspase-1 induces pyroptosis by cleaving Gasdermin D (brown). The non-canonical inflammasome murine caspase-11 or human caspase-4/-5 is activated by LPS of gram-negative bacteria and cleaves Gasdermin D to induce pyroptosis. Caspase-11 also leads to NLRP3 activation and NLRP3-mediated cytokine processing. This figure was adapted from (Rathinam and Fitzgerald, 2016).

1.3.1 NOD-like receptors

Based on the effector function of their N-termini, NLRs can be divided into four subfamilies (see Fig. 2): The acidic transactivation domain (NLRA), the baculoviral inhibitory repeat-like domain (NLRB), the CARD (NLRC) and the PYD (NLRP) and four functional groups: inflammasome assembly, autophagy, signal transduction and transcription activation (Motta et al., 2015; Ting et al., 2008). The NLRs perceive a plethora of ligands derived from either pathogen (viral RNA, flagellin, peptidoglycan, toxins) environmental substances (asbestos, alum, skin irritants, UV radiation) or the host cell itself (ATP, uric acid, cholesterol crystals) (Davis et al., 2011). The latter is a form of recognition of cellular stress or a homeostatic imbalance of the cell. There are eight members of NLRs that can form inflammasomes (NLRP1, NLRP2, NLRP3, NLRP6, NLRP7, NLRP12, NLRC4 and NAIP). NLRP1 recognizes anthrax lethal toxin and MDP, a peptidoglycan motif common to gram-negative and gram-positive bacteria (Kang et al., 2008; Levinsohn et al., 2012). Since it contains a CARD, NLRP1 can directly interact with procaspase-1 and form an active inflammasome. NLRC4 lacks the pyrin domain and can form two different types of inflammasome complexes. NAIP and NLRC4 form an inflammasome complex that recognizes flagellin and components of the type III secretion system, making it an indicator of bacterial infection (Amer et al., 2006; Franchi et al., 2006; Kofoed and Vance, 2011). NLRC4 can also recruit ASC, which leads to the activation of procaspase-1 and processive cleavage of Pro-IL-1β and Pro-IL-18 and consecutive pyroptosis (Miao et al., 2010). NLRP6 and NLRP12 are involved in negative regulation of nuclear factor kappa-light-chain-enhancer of activated B cells (NF-κB) and NLRP6 is associated with increased susceptibility to colitis and colon cancer (Anand et al., 2012; Chen et al., 2011), whereas NLRP12 is associated with atopic dermatitis (Macaluso et al., 2007). NLRP7 can recognize bacterial lipopeptide (Khare et al., 2012) and mutations in NLRP7 are associated with endometrial cancer and testicular seminoma (Ohno et al., 2008; Okada et al., 2004).

However, the most well characterized NLR inflammasome consists of NLRP3. NLRP3 has been attributed to recognize a vast variety of PAMPs and DAMPS such as alum, ATP and uric acid (Davis et al., 2011). This rather promiscuous form of activation has challenged scientists trying to discover a common mechanism. Currently, NLRP3 is thought to be activated by multiple, mutually non-exclusive upstream danger signals,

such as K^+, or Cl^- efflux or Ca^{2+} flux, lysosomal damage, mitochondrial dysfunction, metabolic changes or Golgi fragmentation (Chen and Chen, 2018; Groß et al., 2016; Hornung et al., 2008; Martinon et al., 2006a; Muñoz-Planillo et al., 2013; Wolf et al., 2016; Zhou et al., 2011). Despite the abundance of data characterizing NLRP3 activation signals, many pathways are overlapping, interconnected or even conflicting. Recently, NIMA-related kinase 7 (Nek7) was demonstrated to specifically interact with NLRP3 and stabilize the oligomeric state of the inflammasome, which proved to be essential for ASC speck formation and caspase-1 recruitment (He et al., 2016; Sharif et al., 2019; Shi et al., 2016).

NLRs are required to sense PAMPS and DAMPS in the cytosol and are thus essential to the host immune response. However, NLRs are also involved in other essential biological processes. So far, the activation mechanism of many NLRs is poorly characterized and demands further investigation.

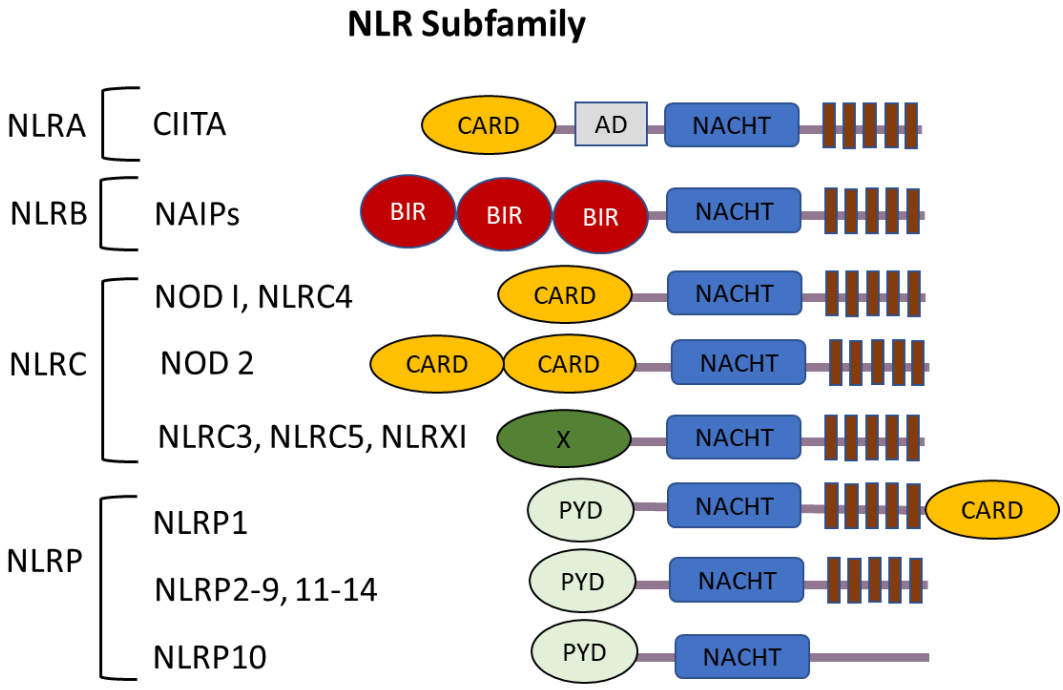

Figure 2 The NLR subfamily. The cytosolic NOD-like receptors (NLRs) comprise 22 identified intracellular pattern-recognition receptors in humans. Mammalian NLRs are divided into subfamilies according to their N-terminal effector domains. The N-terminal domains are caspase activation and recruitment domain (CARD, yellow), transactivator domain (AD, grey), baculoviral inhibitor of apoptosis repeat domain (BIR, red) or pyrin domain (PYD, mint green). The c-terminal leucine rich repeat domain (LRR) is indicated in crimson. The NLR subfamilies are categorized into subfamilies by the initial of the domain name: NLRA (based on AD), NLRB (based on BIR), NLRC (based on CARD) and NLRP (based on PYD). This figure was adapted from InvivoGen (www.invivogen.com).

1.4 IL-1β signaling

IL-1β is an important key regulator of the inflammatory response. Upon binding of IL-1β to the type 1 receptor (IL-1R1), signal transduction depends on three generations of mitogen-activated protein kinases (MKKK/MAP3K/MEKKs) and their downstream proteins (see Fig. 3). This leads to the activation of transcription factors to orchestrate the expression of host defense proteins. Upon binding of IL-1α or IL-1β ligands to IL-1R1, the co-receptor IL-1 receptor accessory protein (IL-1RAP) associates with IL-1R1 and activates signal transduction. (Greenfeder et al., 1995). The Toll- and IL-1R–like (TIR) domains on the cytoplasmic side of IL-1R1 lead to proximity induced recruitment of myeloid differentiation primary response gene 88 (MYD88), Toll-interacting protein (TOLLIP) (Dinarello, 2009) and IL-1 receptor-associated kinase 4 (IRAK4). They form a stable complex and IL-1 receptor-associated kinases IRAK4, IRAK2 and IRAK1 are phosphorylated. This results in the recruitment and oligomerization of tumor necrosis factor-associated factor 6 (TRAF6) (Brikos et al., 2007; Cao et al., 1996a; Cao et al., 1996b). Afterwards, TRAF6 and phosphorylated IRAK1 and IRAK2 separate from the complex and localize to the membrane, where they form a new complex with TGF-β-activated kinase 1 (TAK1) and TAK1-binding proteins TAB1 and TAB2 (Dinarello, 2009). This newly formed TAK1-TAB1-TAB2-TRAF6 complex moves back to the cytosol, where TRAF6 is ubiquitinated and TAK1 is phosphorylated (Dinarello, 2009).

Moving downstream, the signal can follow two different main paths: IKK – IκB – NF-κB and/or MKK – MAPK/JNK/ERK (Figure 3). In the first path, phosphorylated TAK1 initiates the degradation of the nuclear factor kappa-B inhibitor (IκB) via inhibitor of nuclear factor kappa-B kinase subunit beta (IKKβ) and subsequent activation of nuclear factor 'kappa-light-chain-enhancer' of activated B-cells (NF-κB) that can translocate into the nucleus (Oeckinghaus and Ghosh, 2009). NF-κB regulates the expression of pro-inflammatory cytokines IL-1,8 and 6, tumor necrosis factor α (TNF-α) and Interferon-γ (IFN-γ) (Kojima et al., 1999; Wang et al., 2014). In the second path, TAK1 can activate MAPK p38, c-Jun N-terminal kinases (JNK) and extracellular signal-regulated kinases (ERK) by binding to MKK proteins (Sato et al., 2005). This leads to the activation of transcription factors such as c-Jun, c-Fos, c-Myc and ATF2 that regulate cell cycle progression, translation and expression of innate effector proteins, such as β-defensins (Chang and Karin, 2001; Chiu et al., 1988; Meade and

O'Farrelly, 2019). Taken together, IL-1 cytokines secreted by inflammasomes are required to regulate an intricate network of inflammatory processes that mediate inflammation, pathogen clearance and immune cell recruitment, activation, differentiation and proliferation in response to PAMPs and DAMPs.

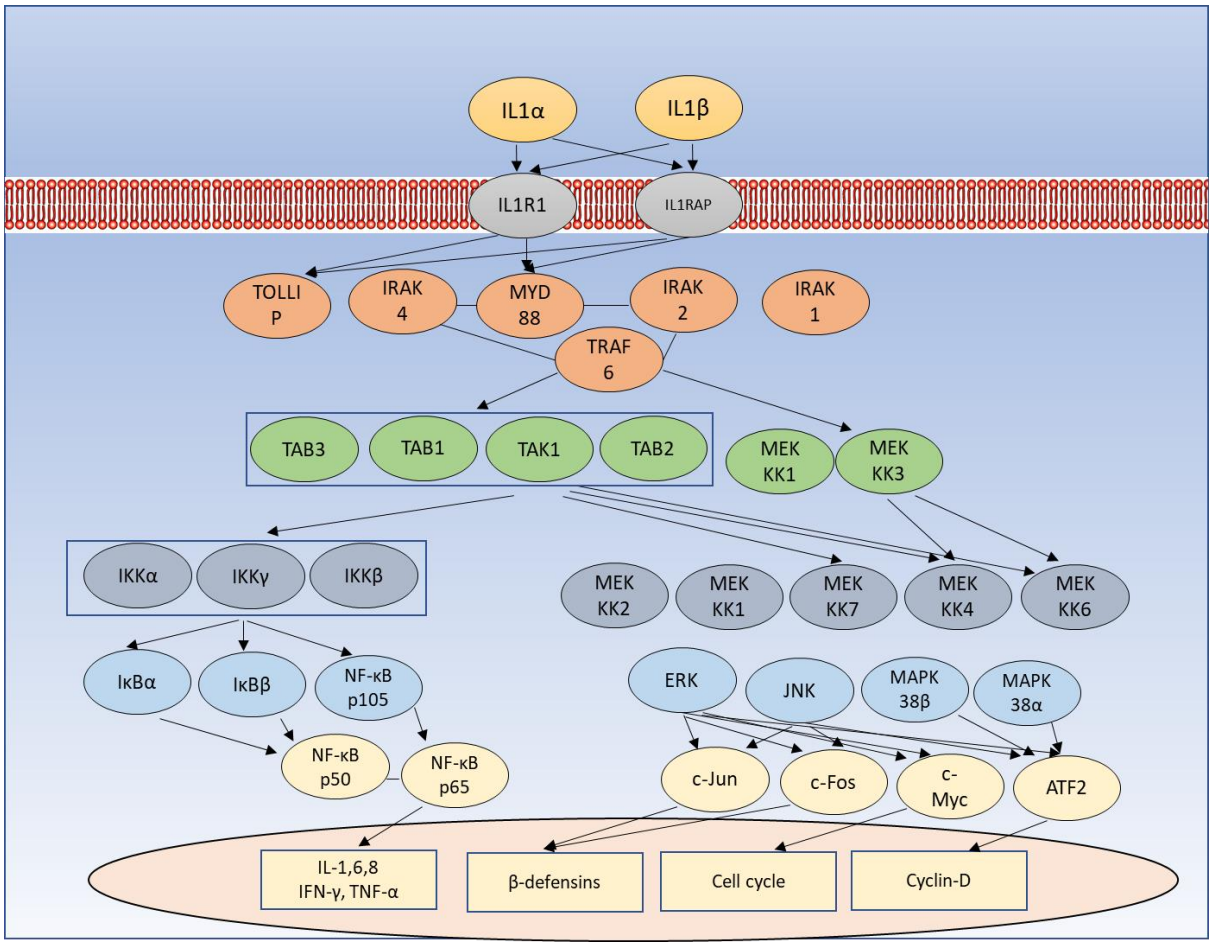

Figure 3 Detailed architecture of IL-1β signaling pathway. Protein-protein interactions of the IL-1β pathway are indicated by black lines (protein complex) or black arrows (transient interaction). IL-β binding to IL-1 receptors can lead to the activation of two major pathways via the myeloid differentiation primary response gene 88 (MYD88)-tumor necrosis factor-associated factor 6 (TRAF6) complex. The two major axis lead to the activation of master regulators of transcription such as nuclear factor kappa-B kinase NF-κB or c-myc. The transcription factors then translocate into the nucleus and lead to the activation of major immune or cell proliferation pathways. This figure was adapted from (Acuner Ozbabacan et al., 2014).

1.5 Macrophages in pathogen clearance

The most versatile antigen presenting cell type and guardian of innate immunity are macrophages. An invading pathogen is likely to be detected by macrophages, which are highly specialized phagocytes responsible for engulfing cellular debris, foreign substances, microbes and dead cells. Blood circulating monocytes that are recruited to the site of inflammation, infection or injury can differentiate into two types of macrophages, the pro-inflammatory M1 or anti-inflammatory M2 (see Fig. 4) (Mills et al., 2000; Nathan et al., 1983). The pro-inflammatory subtype can be evoked by stimuli such as the gram-negative bacterial ligand LPS or interferon gamma, whereas the pro-resolving subtype M2 is regulated by the inhibitors IL-4 and IL-13 (Martinez and Gordon, 2014). M2 macrophages have a high phagocytosis capacity and clear apoptotic cells and promote wound healing (Ferrante and Leibovich, 2012; Sica and Mantovani, 2012). However, in an ongoing injury or inflammation, monocytes exhibit a certain plasticity that allows them to switch between pro-inflammatory at the early stage of inflammation and pro-resolving during wound healing (Krzyszczyk et al., 2018). LPS binds to the TLR4 and forms a complex together with myeloid differentiation factor 2 (mD2) receptor. Downstream signaling events following this receptor complex formation depend on different sets of adaptor proteins. The adaptor MyD88 and MyD88 like adapter leads to the activation of NF-κB in early signaling events, whereas a later response requires TIR-domain-containing adapter-inducing interferon-β (TRIF) and TRIF-related adapter molecule (TRAM), and is followed by the late activation of NF-κB and IRF3, and induction of cytokines like IL-1β, chemokines, and other transcription factors as well as components of inflammasome (Danis et al., 1990; Hazuda et al., 1988; Liu et al., 2017). IFN-γ stimulated macrophages show increased anti-microbial activity, antigen processing and presentation, upregulation of cellular reactive oxygen species (ROS) and nitric oxide synthase (NOS) production and induction of autophagy (Gunjan et al., 2018). IFN-γ binds to the IFN-γ receptor (IFNGR), which leads to the recruitment of Janus kinases JAK1 and JAK2 to the receptor complex. Upon recruitment, autophosphorylated JAK1 phosphorylates JAK2, which enables recruitment of signal transducer and activator of transcription 1 (STAT1). Activated STAT1 translocates to the nucleus and induces the expression of interferon stimulated genes (ISGs) and other interferon response factors (Schneider et al., 2014). This alerted state of macrophages allows effective clearance of

pathogens by phagocytosis, effector cell recruitment and induction of pro-inflammatory cytokines.

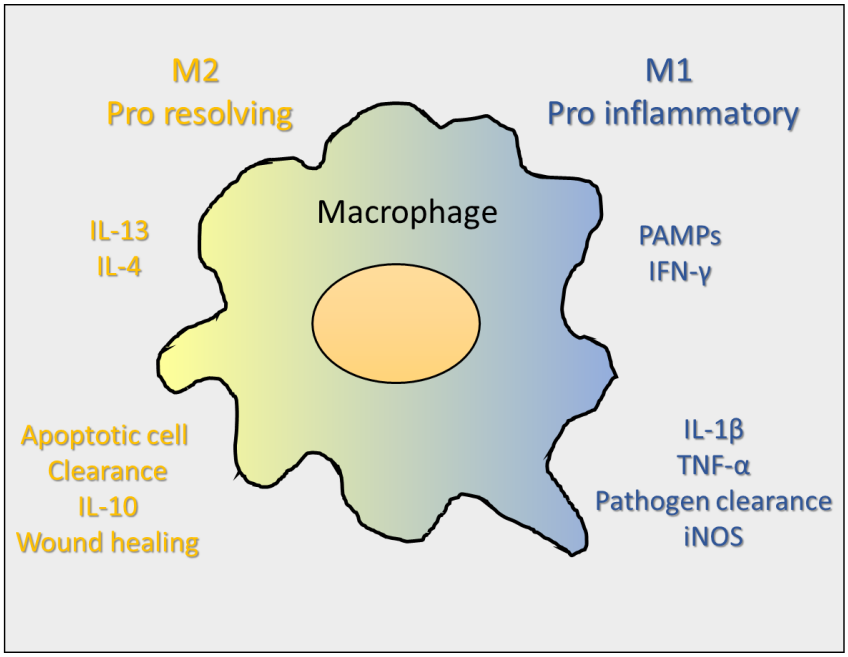

Figure 4 Two phenotypes of macrophage polarization. Macrophages can be differentiated into two phenotypes: M1 macrophages (pro-inflammatory, pathogen clearing) are differentiated by IFN-γ or PAMPs and are characterized by production of iNOS and pro-inflammatory cytokines such as TNFα and IL-1β. M2 macrophages (anti-inflammatory, pro-resolving, apoptotic cell and damaged molecule clearing, wound healing) are induced by IL-4 and IL-13 and characterized by anti-inflammatory cytokine IL-10 production. This figure was adapted from (Bohlson et al., 2014).

1.6 IFN-γ - a versatile factor in antimicrobial immunity

IFN-γ is an extremely versatile cytokine in navigating host resistance against pathogens leading to the upregulation of numerous antimicrobial processes. One such mechanism is that IFN-γ stimulation rapidly facilitates phagolysosomal acidification and production of reactive nitrogen/oxygen species in infected macrophages and thus enables pathogen clearance (Schroder et al., 2004). At the same time, IFN-γ promotes autophagy of intracellular microbes as an effector immune response and induces the expression of various lysosomal components, granules and secreting factors that regulate inflammation and robust anti-microbial activity (Gunjan et al., 2018).

Another group of Interferon stimulated genes, the IFN-induced dynamin-related GTPase families play a key role in these mechanisms. The proteins consists of the 47 kDa immunity-related GTPases (IRGs), the 65 kDa guanylate-binding proteins (GBPs) and the 200–285 kDa very large inducible GTPases (VLIGs or GVINs) and the human transmembrane protein IRGM (see Fig. 5) (Kim et al., 2016). IRGs are not only pivotal in recruiting the various components of the autophagic machinery to bacterial phagosomes, but also have been implied in engaging in lysis of PCVs, releasing microbial components into the cytosol (Man et al., 2016). Although IRGs are expressed in mammals, this subset of GTPases is not present in primates. Thus, similarly to rodent IRGs, human IRGM facilitates trafficking of autophagic constituents to PCVs (Petkova et al., 2013). GBPs, as the single largest IFN-induced GTPase family remaining functional in primates, have emerged as a key factor in human cell autonomous immunity. Upon endocytosis of pathogens, GBPs are recruited to the PCV or to the membrane of cytosolic bacteria, where they engage in a so-far mechanistically uncharacterized membrane remodeling event, leading to the restriction of bacterial and protozoic growth within the cell (Tretina et al., 2019). Furthermore, GBPs are suggested to reduce virion infectivity and target replication complexes of ribonucleic acid viruses (Braun et al., 2019). Interestingly, GBPs are not only involved in pathogen killing, but also flexibly mediating inflammasome activation over various pathways, leading to the release of cytokines or inflammatory cell death (Kim et al., 2016). However, the exact mechanisms underlying GBP-mediated cell autonomous immunity have remained elusive.

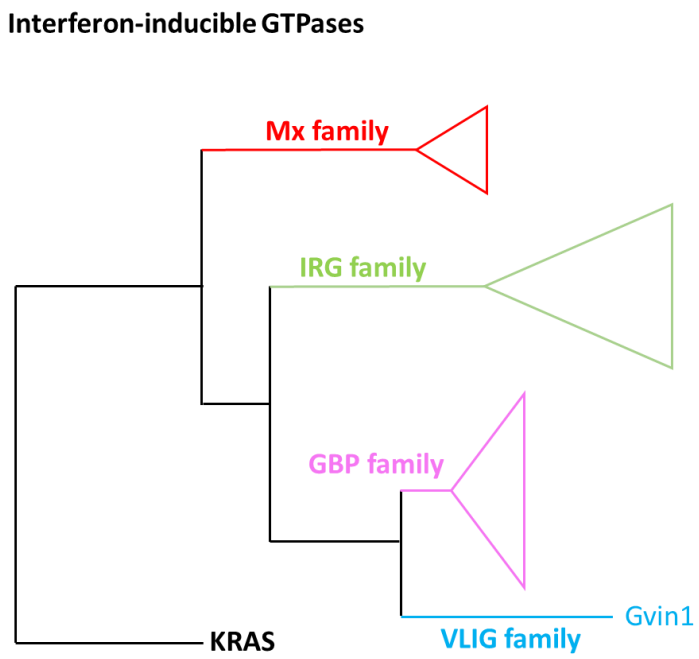

Figure 5 Phylogenetic tree of Interferon-inducible GTPases. Interferon(IFN)-inducible GTPases are clustered according to their genetic distance and the size of the triangle is proportional to the number of family members as well as the relative homology between them. KRAS (black) is the most distant relative of the IFN-inducible family. KRAS and the MX family (red) are induced by IFN-α/β, whereas all other families are induced by IFN-γ. Mx proteins are involved in viral and IRG and GBPs are involved in pathogen restriction. The IRG (green) and VLIG (blue) family exist in mammals but not in primates. This figure was adapted from (Pilla-Moffett et al., 2016).

1.6.1 GBPs confer pathogen resistance and induce inflammasome activation

GBPs are important members of the of host defense *in vivo* against bacterial and viral pathogens and parasites including *T. gondii, L. monocytogenes, M. bovis, F. novicida*, *C. trachomatis,* influenza virus and HIV (Degrandi et al., 2013; Haldar et al., 2013; Kim et al., 2011; Krapp et al., 2016; Meunier et al., 2015; Nordmann et al., 2012; Shenoy et al., 2012; Yamamoto et al., 2012). Several studies have shown a crucial role of GBP membrane recruitment and oligomerization for the antimicrobial function (Britzen-Laurent et al., 2010; Shenoy et al., 2012). Consistently, GBPs have been demonstrated to homo- or hetero-oligomerize (Britzen-Laurent et al., 2010; Shenoy et al., 2012). During infection, GBPs target PCVs, such as the *T. gondii* PV (Degrandi et al., 2007; Degrandi et al., 2013; Kravets et al., 2012; Yamamoto et al., 2012), *C. trachomatis* inclusions (Haldar et al., 2013) and bacterial vacuoles of *M. bovis (Kim et al., 2011)* and *S. typhimurium* (Meunier et al., 2014). GBPs require isoprenylation for successfully targeting membranes (Modiano et al., 2005; Tietzel et al., 2009). They do not only restrict vacuolar pathogens, but they also target cytosolic pathogens, such as *L. monocytogenes*, *F. novicida,* HIV (Kim et al., 2011; Krapp et al., 2016; Meunier et al., 2015). Subsequent studies revealed that GBPs on mouse chromosome 3 (Gbp^{ch3}) play a role in the activation of the non-canonical inflammasome and caspase 11-induced pyroptosis (Pilla et al., 2014). Another model describing the role of GBP in host defense implies that GBP targeting to PCVs and bacteria leads to rupture of PCVs and subsequent release of bacterial components into the cytosol. In addition, the exposure of pathogenic components results in indirect activation of inflammasomes since they act as ligands of pattern recognition receptors (see Fig. 6) (Man et al., 2015; Meunier et al., 2014). The duration of LPS stimulation may play a crucial role for GBP action. Thus, Pilla et. al. demonstrated that prolonged incubation with LPS shows reduced inflammasome activation (Pilla et al., 2014). Another study revealed that during *C. muridarum* infection, GBPs are required for inflammasome activation though GBPs fail to target the *C. muridarum* inclusions (Finethy et al., 2015). This implies that vacuolar or bacterial lysis is not the sole mechanism by which GBPs operate.

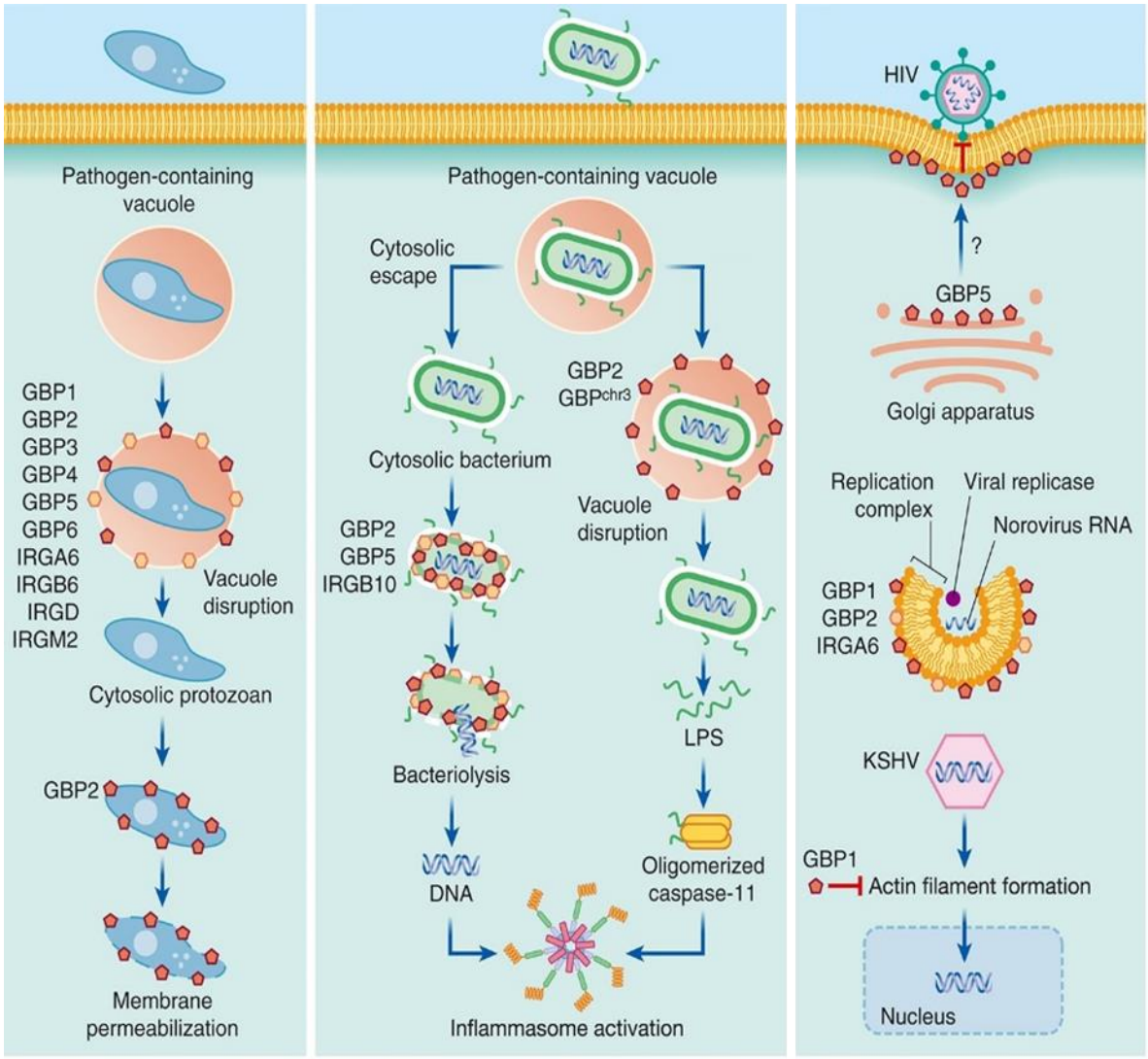

Figure 6 Schematic model of the function of GBPs and IRGs in response to infection in mice. The first panel shows the recruitment of GBPs and IRGs to the membrane of the pathogen-containing vacuole (PCV) in immune and non-immune cells infected with *Toxoplasma gondii*. GBPs and IRGs form higher order oligomer complexes on the PCV that leads to vacuolar disintegration and the escape of the toxoplasma into the cytoplasm. GBP2 further attacks and destroys the Toxoplasma membrane leading to pathogen killing. The second panels (middle) reveals how GBPs and IRGs attack the membrane of cytosolic bacteria such as *Francisella novicida*. Rupture of the pathogen membrane leads to release of bacterial DNA into the cytosol that is detected by the DNA-sensing AIM2 inflammasome. GBPs are also recruited to the PCV surrounding vacuolar bacteria including *Salmonella enterica* serovar Typhimurium. Rupture of the vacuole leads to the release of lipopolysaccharides (LPS) that activates murine caspase-11 and the non-canonical NLRP3 inflammasome. The last panel (right) shows that Golgi-membrane bound GBP5 interferes with the infectivity of the RNA human immunodeficiency virus and simian immunodeficiency virus. GBPs and IRGs can be recruited to the replication complex induced by the RNA virus norovirus to compromise viral replication. GBP1 binds to actin monomers and disrupts actin filament formation which interferes with the delivery of the DNA virus Kaposi's sarcoma-associated herpesvirus to the host nucleus. This figure was adapted from (Ngo and Man, 2017).

1.6.2 GBPs are members of the dynamin superfamily

GBPs belong to the family of dynamin related large GTP-binding proteins. GTPases of the dynamin superfamily share the property to hydrolyze nucleotides and form higher order helical oligomer assemblies on membrane tubules *in vitro*. The energy generated by GTP hydrolysis is translated into mechanical work often associated with membrane remodeling and thus, dynamin superfamily proteins are known as mechano-chemical enzymes (see Fig. 7) (Daumke and Praefcke, 2016; Faelber et al., 2013). Dynamin superfamily GTPases have a low intrinsic affinity for nucleotides, which makes them catalytically independent from guanine nucleotide exchange factors. The relatively high GTPase activity of dynamin superfamily members increases with oligmerization (cooperativity) and stabilization of the oligomers on membrane platforms (Gao et al., 2010; Ghosh et al., 2006a; Praefcke et al., 2004a; Tuma and Collins, 1994; Warnock et al., 1996). Like other dynamin-related GTPases, GBPs show nucleotide-dependent oligomerization and fast cooperative GTPase activity (Ghosh et al., 2006b). However, unlike its peers membrane binding does not influence the GTP hydrolysis rate (Fres et al., 2010). Most recombinantly expressed dynamin superfamily members, such as Dynamin, Opa-1 and EHDs can form higher order oligomer assemblies on a membrane or protein filament template (Faelber et al., 2019; Faelber et al., 2011; Stoeber et al., 2012). However, GBPs can only form distinct ring-shaped oligomers in the presence of nucleotide and when isoprenylated *in vitro*. These ring-shaped oligomers can further stack into rod shaped super structures and form completely independent of a stabilizing membrane tubule (Shydlovskyi et al., 2017). Intensive phenotypical studies *in vivo* as well as the helical assembly and conformational changes upon GTP hydrolysis of dynamin on membrane tubules *in vitro* suggests a mechanism of membrane fission, while opposing movements in atlastin suggests that oligomerization tethers ER-tubules (Praefcke and McMahon, 2004a). Recent evidence shows that recombinantly expressed GBP1 can tether giant unilamellar vesicles *in vitro* and induces hemi-fusion (Shydlovskyi et al., 2017). While GBPs share close homology to atlastin-1, the functional relevance of GBP-mediated ring formation remains largely unknown.

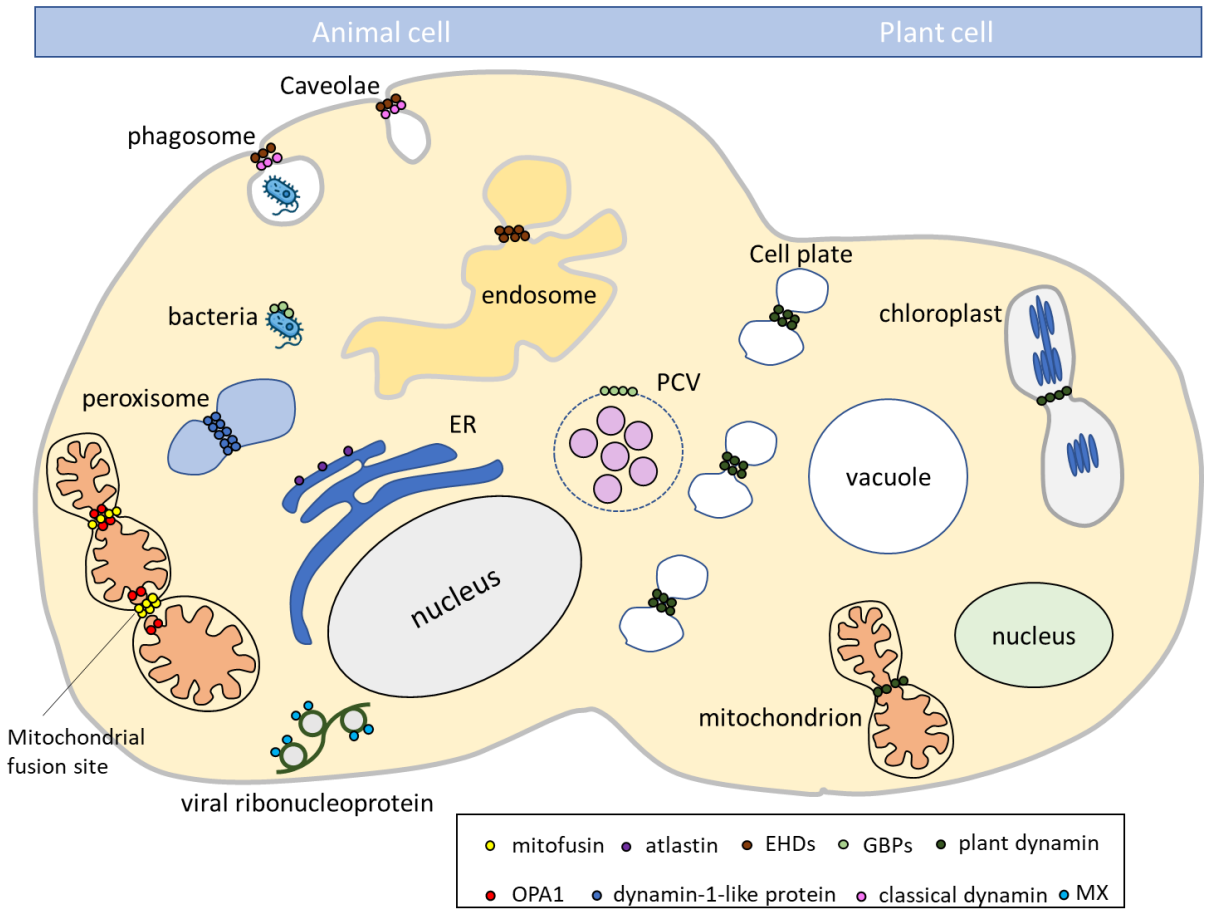

Figure 7 Dynamin superfamily proteins: Cellular localization and function. Figure modified from (Praefcke and McMahon, 2004b)

1.7 Mechanisms of GTP hydrolysis of dynamin superfamily

Proteins of the dynamin superfamily share a common architecture consisting of an N-terminal large GTPase (LG-domain) domain responsible for nucleotide hydrolysis followed by one or more helical bundles that carry out the mechanical movement induced by it. Upon nucleotide binding, proteins of the dynamin superfamily dimerize, which stimulates GTP hydrolysis. The catalytic LG-domain contain 5 motifs that are required for nucleotide binding and hydrolysis (see Fig. 8) (Saraste et al., 1990). The G1 motif describes the P-loop with consensus sequence GxxxxGKS/T, where the serine/threonine residue coordinates the Mg^{2+}-ion essential for GTP hydrolysis. Another important role of the P-loop is the stabilization of the transition state of GTP hydrolysis. In the case of dynamin, S41 coordinates a catalytic cation, whereas in GBP1 and atlastin-1, the side chain of R48 rotates into the nucleotide binding pocket

to stabilize the negative charge induced by the transition state (Bian et al., 2011; Byrnes and Sondermann, 2011a; Praefcke et al., 1999a). The G2 and G3 (also known as switch I and switch II) motif also stabilize the Mg^{2+}-ion and interact with the γ-phosphate of the nucleotide directly and undergo nucleotide dependent conformational changes. In dynamin, the G4 motif mediates specific binding to the guanine base *in trans* via D211 of the opposing monomer (Chappie et al., 2010). In EHDs, the G4 motif is followed by a methionine residue that sterically inhibits the binding of the guanine base, thus EHDs bind ATP instead (Daumke et al., 2007). Lastly, the G5 motif is not well conserved among the dynamin superfamily but may interact with the guanine base or ribose backbone of the nucleotide.

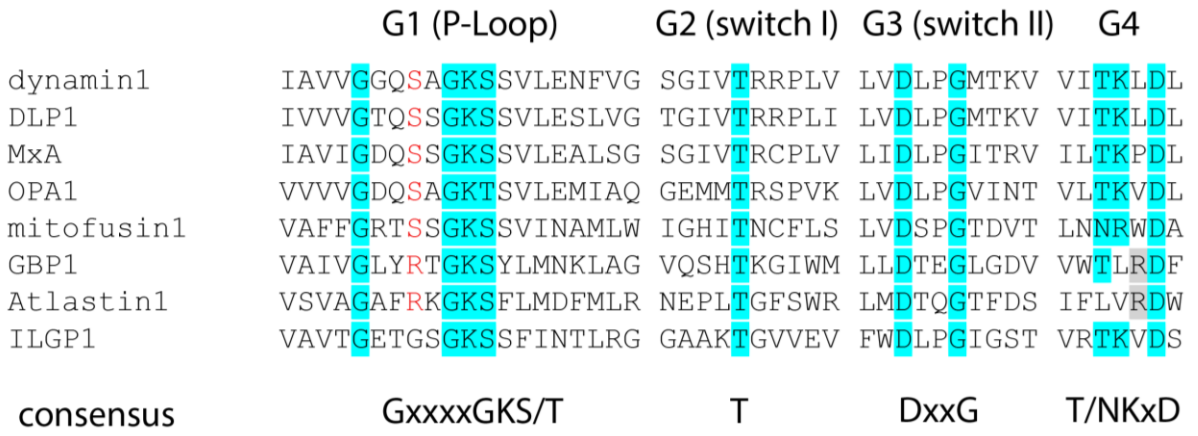

Figure 8 Nucleotide binding and hydrolysis of dynamin superfamily proteins. Sequence alignment of dynamin superfamily proteins in the G1-G4 motifs. Conserved canonical residues are highlighted in blue, other conserved residues in light grey. The catalytic arginine and serine in the P-loop are shown in red.

1.7.1 GTP hydrolysis in GBPs

The LG domain of GBPs also contains the 4 main GTP binding motifs (G1-G4) but shows specific deviations from the consensus motifs that are largely shared with atlastin-1. In addition, GBPs have a distinct biochemical property amongst dynamin GTPases, i.e. they hydrolyze GTP to GMP in two consecutive cleavage reactions (Schwemmle and Staeheli, 1994). The crystal structure of full-length hGBP1 has been solved in the nucleotide-free state and in complex with the non-hydrolysable GTP

analogue GMPPNP (Prakash et al., 2000). The structures show that GBP1 has a 36-kDa N-terminal large G (LG) domain and a 32-kDa carboxy-terminal α-helical elongated domain (Fig. 9a). Crystal structures of the N-terminal G domain of human GBP1 trapped at intermediate steps of GTP and GDP hydrolysis uncovered the molecular basis for nucleotide-dependent dimerization and cleavage of GTP (Ghosh et al., 2006b). These structures reveal that homo-dimerization occurs in a parallel head-to-head fashion and is regulated by structural changes in the switch regions leading to activation of GTPase activity (Fig. 9b). Structural information also shed light on the unique two-step cleavage mechanism of GTP by GBP1. Upon GTP cleavage, conformational changes in the LG-domain push the ribose backbone of the nucleotide forward inside the binding pocket to position the β-phosphate in the same position previously occupied by the γ-phosphate and thus enabling the consecutive cleavage with the exact same mechanism. R48 in the phosphate binding loop has been shown to have a crucial catalytic role in the GTPase reaction; a dimerization-dependent flip of its side chain into the nucleotide-binding pocket has been observed stabilizing the transition state of GTP hydrolysis (Fig. 9c). In addition, a catalytic serine stabilizes a water molecule for GTP hydrolysis.

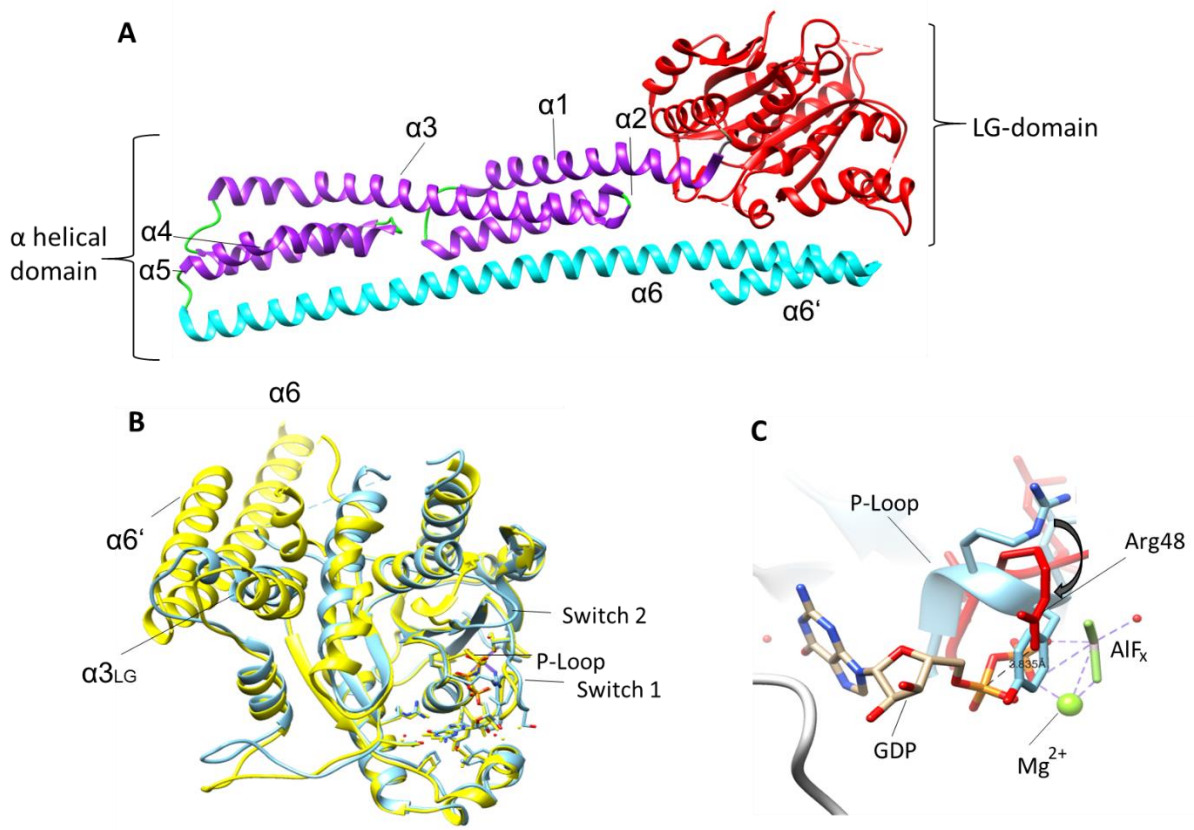

Figure 9 Dimerization induced conformational changes of hGBP1 (a) hGBP1 full length crystal structure. hGBP1 consists of an N-terminal LG domain (red) and a C-terminal α-helical elongated domain (purple, cyan). The C-terminal helix α6 (cyan) interacts with the LG domain (red). Flexible loops are displayed in green. (b) Superimposition of hGBP1 LG domain (cyan) and hGBP1 full length in yellow. Upon dimerization. helix $\alpha3_{LG}$ moves towards the C-terminal helices α6 and α6'. (c) Phosphate binding-loop of the structure of hGBP1 LG domain bound to GDP•AlF_3 (red) superimposed on the P-Loop of the GMPPNP-bound full length hGBP1 crystal structure (cyan). The major flip of Arg48 towards α-phosphate group of GBP • AlF_3 is indicated by an arrow.

In GBP1, K51, S52 as well as R48 are essential for GTP hydrolysis. However, GBP1 mutants K51A and S52N cannot bind and hydrolyze GTP and do not dimerize, whereas mutant R48A can bind GTP, dimerizes but cannot hydrolyze the nucleotide. The switch I region of GBP1 does not only contribute in stabilizing the Mg^{2+}-ion and transition state of hydrolysis, but also interacts with another large loop that binds the opposing molecule in *trans*. Residues H74 and K76 of the Switch I region have been proposed to specifically inhibit the second cleavage step of GTP hydrolysis (Praefcke et al., 2004b). GBP1 mutants H74A and K76A retain cooperativity but exhibit a 4-5 fold reduced GTPase activity and no GMP production. The neighboring residues T75 and S73 undergo major rearrangements during GTP hydrolysis and stabilize a catalytic water molecule (Praefcke et al., 2004a). Of note, GBP5 cannot hydrolyze

GTP to GMP but only to GDP (Neun et al., 1996b). Residues of the P-loop, switch I and switch II region are highly conserved amongst GBPs as well as residues H74 and K76 (Praefcke et al., 2004a). This difference in hydrolysis mechanisms implies that residues outside the conserved motifs play an important role in preference of one-step versus two-step GTP cleavage. GBPs bind GMP, GDP and GTP with similar affinity and hydrolyze GTP to GMP by two successive cleavages of two phospho-anhydride bonds (Ghosh et al., 2006a; Praefcke et al., 1999b). Subsequent studies indicated that the helical domain undergoes large-scale conformational rearrangements upon GTPase domain dimerization and membrane binding (Vöpel et al., 2014), as expected for a dynamin superfamily protein. While biophysical and biochemical studies suggest that the energy generated by the second cleavage step could be utilized in formation of polymers (Shydlovskyi et al., 2017), the physiological role of this process has thus far not been addressed.

1.8 Chlamydia trachomatis

The Chlamydiaceae family of the chlamydiae phylum comprises 11 species that are pathogenic to humans or animals. Some species that are pathogenic to animals, such as the avian pathogen *Chlamydia psittaci*, or the fetal species *Chlamydia abortus*, can be transmitted to humans (Bachmann et al., 2014; Pospischil et al., 2002). *Chlamydia trachomatis* and *Chlamydia pneumoniae* are the major species that infect humans and contribute to a variety of diseases (see Fig. 10) (Malhotra et al., 2013). *Chlamydia trachomatis* (C. *trachomatis*) is the world's leading cause of bacterial sexually transmitted infection. According to the world health organization, about 131 million new cases occur annually, where infection is most prevalent among sexually active young women and men (14-25 years) (WHO, 2018). C. *trachomatis* infects squamocolumnar cells which are located between the single layered cervical canal and multiple layered ectocervix in women or penile epithelial cells in men (Anttila et al., 2001; Cates and Wasserheit, 1991). Different chlamydia strains or serotypes are also known to infect genital, ocular or respiratory tissues. Chronic infection may lead to ectopic pregnancies, infertility and pelvic pain as well as pelvic inflammatory disease (PID) in women (Pavletic et al., 1999). C. *trachomatis* infections can be easily treated with antibiotics, however infection often remains undetected due to its asymptomatic progress, which earned C. *trachomatis* the term "stealth pathogen" (Hafner, 2015; Redgrove and McLaughlin, 2014).

C. *trachomatis* is an obligate intracellular gram-negative bacterium; thus it depends on host metabolites and protein machineries in order to survive (Bachmann et al., 2014). C. *trachomatis* can currently be classified in 19 different serovars that were historically established based on antigenic variation in the major outer membrane protein (MOMP) encoded by *OmpA* (Wang et al., 1985). Serovars A-C are common cause of trachoma, while serovars D-K cause urogenital infections. Serovars L1-L3 are associated with invasive lymphoma granuloma venereum (LGV) (Elwell et al., 2016).

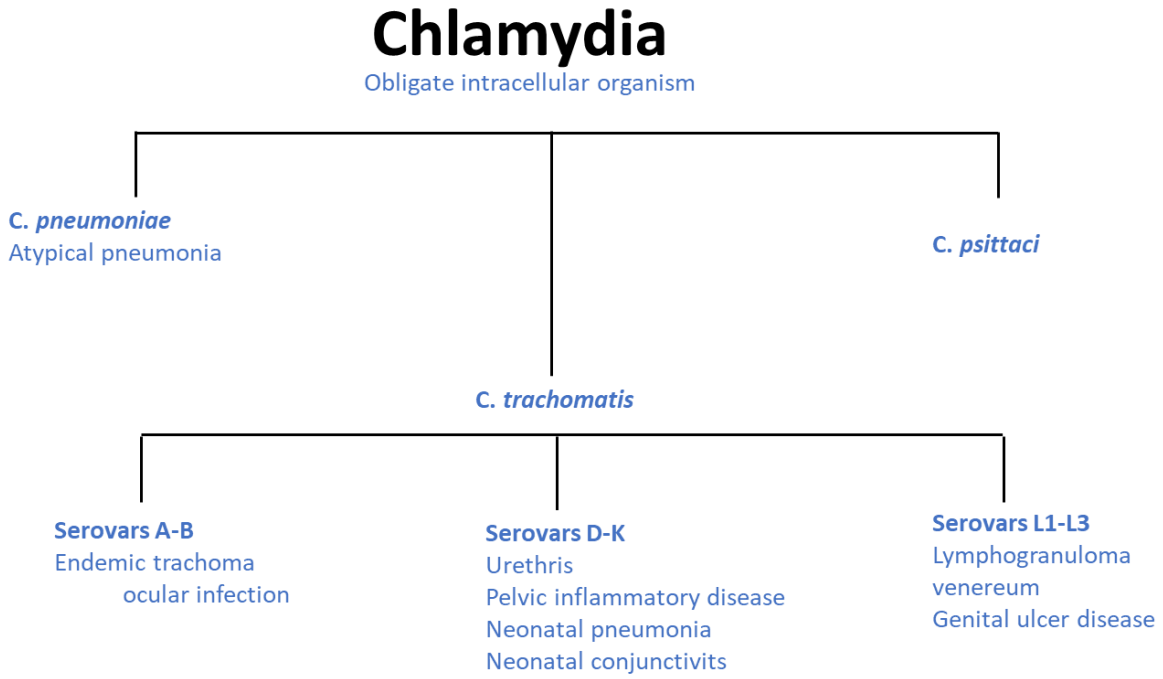

Figure 10 Phylogenetic tree of Chlamydia species and serovars. The Chlamydia genus is divided into the species C. *pneumoniae, C. psittaci* and *C. trachomatis. C. trachomatis* is divided in various serovars. Diseases caused by different species and serovars are displayed underneath.

1.8.1 Chlamydia life cycle

C. *trachomatis* is an intracellular pathogen with a unique biphasic life cycle (see Fig. 11) (Hackstadt et al., 1997). Upon docking to the host cell via the formation of a trimolecular bridge of bacterial adhesin, host receptors and host heperan sulfate proteoglycans, infectious elementary bodies (EB) activate a host cell signaling cascade that allows entry of the pathogen into the host cytoplasm (Elwell et al., 2016; Rosmarin et al., 2012). Pre-synthesized type III secretion system effectors are injected into the host cell, where a subset of these effectors activate cytoskeletal rearrangements and facilitate host endocytosis. Internalized EBs rapidly differentiate into a second growth and replication phase called reticulate bodies (RB), initiated by the synthesis of bacterial proteins. RBs reside within a host membrane-derived pathogen containing vacuole termed inclusion that is actively uncoupled from the host endolysosomal pathway. During this growth phase, C. *trachomatis* expresses inclusion membrane proteins (Inc) that vastly exploit the retromer complex for nutrient

acquisition (Hackstadt et al., 1999). Furthermore, *C. trachomatis* acquires sphingomyelin and cholesterol from the Golgi apparatus, which is fragmented into Golgi mini-stacks that surround the inclusion in order to facilitate lipid delivery (Heuer et al., 2009). The Chlamydia inclusion is transported via microtubules to the microtubule organizing center (MTOC) (Clausen et al., 1997; Mital and Hackstadt, 2011). RBs start to divide exponentially and the inclusion secrets other effectors that modulate many host cell pathways involved in cell cycle progression, metabolism and cell death (Omsland et al., 2014; Sun et al., 2016). The last stage of the life cycle embodies the secretion of EB effector proteins followed by differentiation into EBs. Infectious EBs can now be released from the host cell via lysis or extrusion and start attaching to neighboring cells (Hybiske and Stephens, 2007).

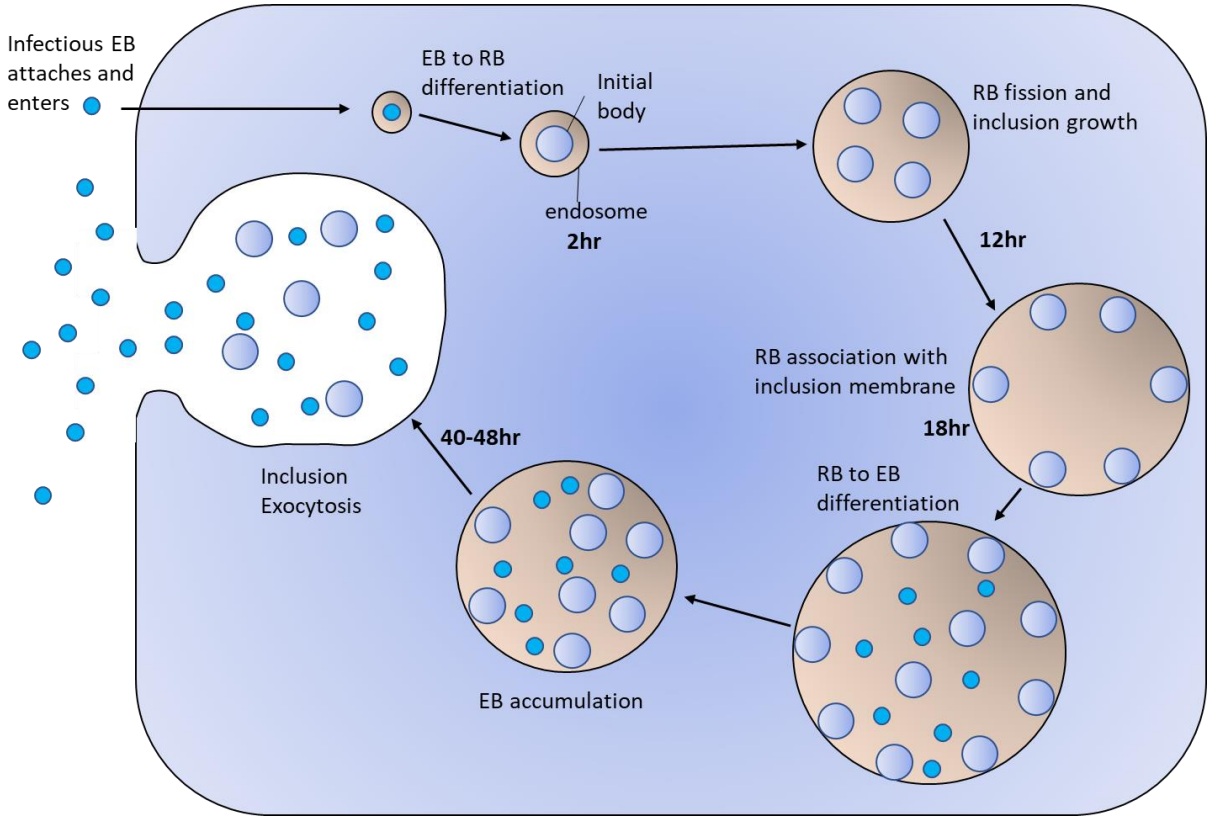

Figure 11 Chlamydia trachomatis (C. *trachomatis*) life cycle. (C. *trachomatis*) is an obligate intracellular pathogen that resides within a specialized PCV and has a biphasic developmental cycle. Epithelial cells of the cervix are invaded by an infectious, but metabolically inactive, elementary body (EB). Upon endocytosis, the EB is engulfed by a membrane of the endosomal trafficking pathway, which allows it to replicate undetected within the cell. Within the inclusion, the EB grows into a larger metabolically active reticulate body (RB), which divides by binary fission. The RBs transform back into infective EBs within 2 days, which are released from the infected cell to infect neighboring cells. Figure modified from (Brunham and Rey-Ladino, 2005).

1.8.2 Modulation of the innate immune response by Chlamydia

Like other intracellular pathogens, chlamydia infection is detected by PRRs, which leads to cell-autonomous immunity and pro-inflammatory cytokine release (Bastidas et al., 2013). Multiple bacterial patterns such as LPS or peptidoglycans are recognized by TLR4 and TLR2 and subsequently activate the MYD88 dependent TRAF6-NFkB signaling axis that lead to the activation of the innate immune response (Shimada et al., 2012a). The bacterial second messenger cGAMP or cycling di-AMP can activate the cytosolic sensor synthase stimulator of interferon genes (STING) leading to the expression of ISG (Zhang et al., 2014). ISGs such as GBPs and IRG recognize and localize to chlamydia inclusions and promote bacterial clearance (Al-Zeer et al., 2013). Chlamydia infection leads to NLRP3 inflammasome activation that requires the generation of ROS and K^+ efflux (Abdul-Sater et al., 2010). Chlamydial virulence factors can prevent or impair the innate immune response. A C. *pneumoniae* protease can cleave TRAF3 preventing phosphorylation and activation of interferon regulatory factor 3 (IRF3) augmenting ISG expression (Wolf and Fields, 2013). The C. *trachomatis* deubiquitinase dub1 can remove ubiquitination of IκBα, which leads to the stabilization of the inhibitory p65-p50-IkB complex and prevents nuclear translocation of NF-κB (Wolf et al., 2009). C. *pneumoniae* also prevents nitric oxide induction by downregulating the expression of inducible nitric oxide synthase (iNOS) (Abu-Lubad et al., 2014), while C. *trachomatis* downregulates the expression of interferon- induced protein with tetratricopeptide repeats 1 (IFIT1) and IFIT2 through the T3SS effector TepP (Chen et al., 2014). Other proteins such as CP0236 retain activating factors at the inclusion membrane (Wolf et al., 2009) and thus preventing detection by the innate immune system.

2. Objective of this study

Human guanylate binding protein 1 (hGBP1) belongs to the dynamin superfamily of GTPases and is involved in cell-autonomous defense against intracellular bacteria and parasites. During infection, hGBP1 is recruited to cytosolic pathogens, such as *Shigella flexneri* and pathogen-containing vacuoles, such as *Chlamydia trachomatis* inclusions, restricts pathogenic growth, and induces the activation of the inflammasome pathway and inflammatory cell death (pyroptosis). Amongst dynamin GTPases, hGBP1 has the unique catalytic activity to hydrolyze GTP to GMP in two consecutive cleavage steps. However, the functional significance of this activity in pathogenic restriction and inflammasome activation has remained elusive. In order to address this question, a structure-guided mutant that specifically abrogates GMP production, while maintaining fast cooperative GTP hydrolysis, was generated. The physiological function of this mutant was tested via complementation experiments in the monocyte precursor cell line THP-1 infected with the obligate intracellular pathogen C. *trachomatis*.

3. Materials and Methods

3.1 Materials

3.1.1 Structures

Structures displayed in this thesis are listed in the Appendix A.

3.1.2 Instruments

Instruments used in this thesis are listed in the Appendix B.

3.1.3 Chemicals

Chemicals used in this thesis are listed in the Appendix C.

3.1.4 Enzymes

Enzymes used in this thesis are listed in Appendix D.

3.1.5 Kits

Kits used in this thesis are listed in the Appendix E.

3.1.6 Media

Media used in this thesis are listed in Appendix F

3.1.7 Buffers

Buffers used in this thesis are listed in Appendix G

3.1.8 Constructs

Constructs used in this thesis are listed in Appendix H.

3.1.9 S1 bacterial strains

Table 1 S1 bacterial strains

Bacterial strain	Application
E.coli Dh5α	Molecular cloning
E.coli BL21 DE3	Protein expression
E.coli Top10	Lentivirus vectors molecular cloning
E.coli Stbl3	Lentivirus vectors amplification

3.1.10 Plasmids

pGEX-6P-1 (AmpR, GE Healthcare); pSKB2-LNB (KanR, based on pET28, Merck, Darmstadt, DE; Multiple cloning site exchanged against that of pGEX-6P-1, PreScission Protease cleavage site, O. Daumke, MDC-Berlin); pET-Duet-1 (KanR, Novagen); pLenti-CRISPR-V2 (AmpR, PuroR, CMV promotor, based on 3rd generation lentivirus vector); pLenti CMV GFP hygro (AmpR, HygroR, CMV promotor, based on 3rd generation lentivirus vector that expresses eGFP, genes are cloned into BamHI, SalI to replace eGFP gene expression), psPAX2 (AmpR, 2nd generation lentiviral packaging vector), pVSVG (AmpR, 2nd generation lentiviral envelope vector).

3.1.11 Media and Buffers

Buffers used in this thesis and their compositions are listed in the Appendix F. Media are listed in Appendix G.

3.1.12 Experimental model and subject details

3.1.12.1 Cell Lines

THP-1 cell lines (American Type Culture Collection TIB-202) were cultured in RPMI 1640 with 10% fetal bovine serum (FBS). hGBP1 knock-out cell lines were generated by transfection of lentiCRISPRv2 containing hGBP1 single guide RNA sequences and single cell dilution. hGBP1 WT and mutant cell lines were generated by infection with

lentiviruses generated in HEK293T cell line (ATCC CRL-11268) expressing hGBP1 proteins.

3.1.12.2 Human Primary Macrophages

Human primary macrophages were isolated from peripheral blood mononuclear cells (PBMCs) from healthy female donors, aged 20-40 years according to protocol number EA1/203/16 as approved by the ethics commission of Charité, Berlin. Human primary macrophages were cultured by adherence from PBMCs in RPMI 1640 with 10% FBS and 50 ng/ml human macrophage colony-stimulating factor (M-CSF) for 6 d.

3.1.12.3 Microbe strain and culture

C. trachomatis serovar L2 (ATCC VR-902B) was routinely, cultured, prepared, and propagated in HeLa cells (American Type Culture Collection CCL-2.1) as previously described (Al-Zeer et al., 2013).

3.2 Methods

3.2.1 Molecular Biology

3.2.1.1 Polymerase Chain reaction (PCR)

DNA fragments were amplified with KOD Hot Start polymerase (Merck Millipore, DE) according to manufacturer’s instructions.

3.2.1.2 Restriction digest

DNA was digested with restriction endonucleases (Type II) from New England Biolabs (NEB) according to the manufacturer’s procedures.

3.2.1.3 Agarose gel electrophoresis

1% agarose gels were prepared and run according to standard procedures.

3.2.1.4 DNA purification

Excised DNA bands were purified using the QIAquick Gel Extraction Kit (Qiagen) according to the manufacturer's protocol.

3.2.1.5 Ligation

Concentration of plasmids and inserts was determined using the absorption at 259 nm. 10 ng and a six-fold molar excess of insert were ligated using T4 DNA Ligase from NEB according to the manufacturer's protocol.

3.2.1.6 Preparation of chemically competent E. coli cells

Chemically competent *E. coli* bacteria were prepared according to (Chung et al., 1989).

3.2.1.7 Transformation of chemically competent E. coli cells

Plasmids were transformed using the heat shock method according to standard protocols. *E. coli* DH5α was used for plasmid propagation and E. *coli* BL21 (DE3) strain for protein expression. (Chung et al., 1989)

3.2.1.8 Storage of E. coli cells

For long-term storage of bacteria, 1 mL of a 5 mL LB overnight bacterial culture was mixed with 0.5 mL sterile glycerol and stored at -80 °C.

3.2.1.9 Site-directed mutagenesis

Site-directed mutagenesis was carried out by QuickChange mutagenesis (Stratagene) according to the manufacturer's protocol.

3.2.1.10 Expression constructs

The hGBP1 mutants, R48A, K76A and G68A, were generated using the plasmid pQE80L-hGBP1 (a kind gift from Gerrit Praefcke) and the QuikChange site-directed mutagenesis kit (Stratagene, USA). The PCR product was cloned into a modified pET28 vector (pSKB-LNB2) and the mutation was verified by DNA sequencing. An overview of the constructs used in this thesis can be found in Appendix H.

3.2.2 Biochemistry

3.2.2.1 Protein preparation

WT and mutant hGBP1 variants with an N-terminal His6 tag were expressed using pSKB-LNB2 in *E. coli* strain BL21(DE3). The cells were grown at 37 °C in TB medium, and protein expression was induced at an optical density of 0.6-0.8 by the addition of 50 µM isopropyl-β-d-thiogalactopyranoside (IPTG), followed by overnight incubation at 18 °C. Upon centrifugation, the cells were suspended in 50 mM Tris–HCl (pH 8.0), 5 mM $MgCl_2$, 300 mM NaCl, 5 mM β-mercaptoethanol, 10% (v/v) glycerol, 20 mM imidazole, 100 µM phenylmethylsulfonyl fluoride (PMSF) (Roth, Germany) and 1 µM DNase I (Roche) and mechanically lysed in a microfluidizer (Microfluidics). Following centrifugation (30,000 × g, 1 h, 4 °C), the protein in the cleared lysate was applied to a NiNTA column (GE Healthcare) and eluted with 20 mM Tris–HCl (pH 8.0), 5 mM $MgCl_2$, 100 mM NaCl, 5 mM β-mercaptoethanol, 10% glycerol and 20 mM imidazole using a 20 mM to 500 mM imidazole gradient. It was followed by gel filtration via Superdex 200 (GE healthcare) in 50 mM HEPES pH 7.5,150 mM NaCl, 5 mM $MgCl_2$ and 2 mM dithiothreitol. Fractions containing monomeric hGBP1 were pooled and concentrated using Amicon filters with a 10 kDa cut-off to 10 mg/ml, shock-frozen in liquid nitrogen and stored at -80 °C. The concentration of hGBP1 was determined by ultraviolet spectrophotometry at 276 nm with the calculated molar absorption coefficient of 45,450 M^{-1} cm^{-1}.

3.2.2.2 Protein purification of farnesylated hGBP1

Farnesylated hGBP1 was purified according to (Fres et al., 2010). The plasmid pGEX-6P-I-hGBP1 was transformed into competent BL21 (DE3) E. coli cells (Novagen) containing the pRSF-FTase α/β construct for coexpression. Cultures were

supplemented with carbenicillin (50 µg/ml) and kanamycin (50 µg/ml) induced with 100 µM isopropyl β-D-thiogalactopyranoside at an OD600 of 0.6–0.8. Cells were cultured for 16 h at 20°C, collected by centrifugation at 6,000 g for 20 min, and resuspended in 50 mM Tris/HCl, pH 8.0, 300 mM NaCl, 5 mM $MgCl_2$, 20 mM imidazole, 10 mM β-mercaptoethanol. The cells were disrupted by multiple passage in a microfluidizer (Microfluidics). Unbroken cells and large debris were removed by centrifugation at 60,000 g for 60 min at 4°C. The His-tagged hGBP1 was further purified using Nickel-Sepharose 6 Fast Flow (GE Healthcare) and eluted with an imidazole gradient to 1,000 mM in 130 mM KCl. Farnesylated and unmodified proteins were separated by Butyl Sepharose High Performance or Butyl Sepharose 4B Fast Flow (GE Healthcare) using a decreasing salt gradient from 1.5 M $(NH4)_2SO_4$ to 0 mM in 50 mM Tris/HCl, pH 8.0, 2 mM MgCl2, 2 mM DTT. The removal of salt was carried out by gel filtration on Superdex 200 (GE Healthcare).

3.2.2.3 GTP hydrolysis assay

Non-farnesylated hGBP1 WT and mutants at the indicated concentrations were incubated with 1 mM GTP at 37 °C in buffer A (20 mM HEPES pH 7.5, 150 mM NaCl, 2 mM $MgCl_2$). Aliquots of the reaction were taken at the given time points, diluted in excess buffer A and flash-frozen in liquid nitrogen. Nucleotides were separated via reversed-phase chromatography (C-18, Hypersil) and their ratios quantified by integration of the 260 nm absorbance.

3.2.2.4 Liposome preparation

Liposomes were prepared by mixing 50 µl of Folch liposomes (total bovine brain lipids fraction I from Sigma (25 mg/ml) to 200 µl of a Chloroform/Methanol (1:0.3 v/v) mixture and dried under Argon stream. The liposomes were resuspended in Liposome Buffer and sonicated in water bath for 30 sec.

3.2.2.5 Liposome co-sedimentation assays

Liposomes (1 mg/ml) were incubated at room temperature with 10 µM of the indicated fhGBP1 construct in the presence of 1 mM GTP or 200 µM GDP, 300 µM AlF_3 and 10

mM NaF or no nucleotide for 10 min in 50 µl reaction volume, followed by 213,000 g spin for 10 min at 20 C. The final reaction buffer contained 25 mM HEPES/NaOH (pH 7.5), 150 mM NaCl and 1 mM $MgCl_2$. The supernatant and pellet were analyzed via SDS-PAGE.

3.2.2.6 Electron microscopy

10 µM fhGBP1 WT was incubated in the presence of 1 mM GTP and the reaction subsequently diluted at 1:10 and spotted for 5 min at room temperature on carbon-coated copper grids and negatively stained with 2% uranyl acetate. 10 µM fhGBP1 G68A was incubated in the presence of 200 µM GDP, 300 µM AlF3 and 10 mM NaF for 15 min at room temperature, diluted at 1:10 and spotted on carbon-coated copper grids and negatively stained with 2% uranyl acetate. Electron grids were imaged with a transmission electron microscope at 80 kV and acquisition was done with a CCD camera.

3.2.2.7 Structural analysis and sequence alignment

Crystal structures were analyzed with PyMOL (Molecular Graphics System Version 1.8. Schroedinger, LLC) and Chimera (Pettersen et al., 2004) The molecular superposition was created in Chimera. Sequence alignments were performed with MUSCLE (Madeira et al., 2019) and figures prepared with Chimera.

3.2.3 Cell and infection biology

3.2.3.1 Cell culture treatments and C. trachomatis infection

Human primary monocyte–derived macrophages (hMDMs) were prepared by adherence from whole-blood fractions of healthy donors. Primary monocytes were cultured in RPMI 1640 with 10% FBS and treated with 50 ng/ml M-CSF for 6 d. THP-1 cells were cultured in RPMI with 10% FCS.

When indicated, THP-1 cells were differentiated with 100 nM phorbol 12-myristate 13-acetate (PMA) for 24 h. *C. trachomatis* bacteria were cultured as previously described

(Al-Zeer et al., 2013) and infected at MOI 5 for inclusion count and infectivity assay, or at MOI 30 for inflammasome activation. For allopurinol specificity and inflammasome control experiments, THP-1 cells or hMDM were transfected either with 1 µg Flagellin (i.e., NLRC4 inflammasome stimulation) or 1 µg poly(dA:dT) (i.e., AIM2 inflammasome stimulation) for 6 h using Profect P1 reagent (Targeting Systems) or Lipofectamine RNAimax (Invitrogen), respectively. THP-1 cells or hMDMs were primed for 16 h with 100 nM LPS or 100 nM LPS + 100 nM IFN-γ, respectively, and treated with 5 mM ATP (NLRP3) for 4 h or transfected with 1 µg LPS (CAS4) for 6 h using FuGENE HD transfection reagent (Promega). For NLRP3 inhibition experiments, THP-1 cells or hMDMs were treated with 300 nM MCC950 for 1 h prior to 24 h infection with *C. trachomatis*. For cell death pathway determination, THP-1 hGBP1 R48A mutant cells were treated with 12 µM IM-54, 1 µM Bafilomycin-A1, 40 µM necrostatin-1, 5 µM ferrostatin-1 or 15 µg/ml Ac-YVAD-CMK 1 h prior to 24 h infection with *C. trachomatis*. For the metabolite feedback experiments, THP-1 hGBP1 KO cells and THP-1 hGBP1 G68A mutant cells were treated with 0.5 mM or 1 mM guanine or guanosine for 1 h post infection (p.i.) with *C. trachomatis*.

3.2.3.2 siRNA transfection

THP-1 cells were seeded in a 12 well plate in 1 ml Opti-MEM at a density of $5x10^5$/ml. Per well transfection, 246.5 µl of Opti-MEM + 3.75 µl of 20 µM siRNA were mixed with 246.5 µl of Opti-MEM with 3.75 µl siRNAmax transfection reagent from Invitrogen and incubated for 10 min at RT. 500 µl of transfection mix were transfected per well of THP-1 by drop by drop release. 6 hrs post transfection, the Opti-MEM was replaced by 2 ml RPMI + IFN-γ at 50 ng/ml and LPS at 100 ng/ml. Cells were further infected with C. *trachomatis* or harvested 48 hrs post transfection.

3.2.3.3 CRISPR/Cas9-mediated knockout of hGBP1 and complementation in THP-1

hGBP1 single guide RNA sequences from Feng Zhang´s Gecko database were cloned into lentiCRISPR v2 and transfected into THP-1 cells with Fugene HD transfection reagent (Promega). Two days after transfection, the cells were diluted into single clones and seeded into 96 well plates. Successful knockout of hGBP1 was confirmed via immunoblotting (rat anti hGBP1 1:1000, Santa Cruz biotechnology).

hGBP1 knockout cells were complemented with lentiviral constructs that express GBP1 WT, R48A, K76A or G68A. The genes exhibit two silent mutations on the sgRNA sequence to disable targeting by Cas9. Lentiviruses were generated in HEK293T cells by transfection with a lentivirus vector containing GFP (as empty vector control), FLAG-hGBP1 WT, FLAG-hGBP1 G68A, FLAG-hGBP1 R48A and its packaging vectors PsPax2 and VSVG. The vector contains a hygromycin resistance gene. 6 hours after transfection the media was replaced with fresh DMEM and 48-56 h post transfection the media was filtered with a 0.4 µm filter and applied to 1.0.x 10^7 THP-1 cells. 24 h post infection with virus, the media was changed to fresh RPMI + 10% FCS media. After 3 days, THP-1 cells positive for GBP1 expression were selected via hygromycin at increasing concentrations from 100-400 µg/ml over 2 weeks. GBP1 expression was tested via immunoblotting against FLAG and endogenous GBP1.

3.2.3.4 Immunostaining and ASC speck count

THP-1 cells were differentiated for 24 h with 100 nM PMA and infected with *C. trachomatis* at MOI 5 or 30 for 24 h. Cells were fixed in 4% Paraformaldehyde (PFA) or 2% PFA for a specific UA staining. After fixation, the cells were permeabilized with 0.3% Triton-X100 for 10 min and blocked in 3% bovine serum albumin (BSA) in phosphate-buffered saline or 10% horse serum, 100 mM glycine for 1 h at room temperature. The cells were stained for *C. trachomatis* inclusions (goat anti-MOMP 1:150), ASC (rabbit anti-ASC 1:300, Proteintech), Xanthine Oxidase (mouse anti XO, 1:50 Santa Cruz biotechnology), hGBP1 (rat anti hGBP1 1:50, Santa Cruz biotechnology), rabbit anti uric acid (UA, 1:1500), at 4 °C, overnight. ASC specks were counted by evaluating 500 cells per experiment.

3.2.3.5 Inclusion count

THP-1 cells were differentiated with 100 nM PMA for 24 h and stimulated with 100 nM IFN-γ, 100 nM LPS for 24 h. The cells were infected with *C. trachomatis* at MOI 5. After 1 h of infection, the media was changed to fresh RPMI, and the cells incubated for another 23 h. The cells were fixed 24 h post infection (p.i.) with 4% PFA and stained for *C. trachomatis* and 4′,6-diamidino-2-phenylindole (DAPI). The number of inclusions

per nuclei was determined following three independent experiments. In each experiment, 500 cells were evaluated. Significance was determined by one-way ANOVA.

3.2.3.6 Infectivity assay

Host cells were seeded in 6-well plates, treated as above, infected with *C. trachomatis* diluted in infectious medium at MOI 5 and incubated at 35 °C and 5% CO_2. Two hours p.i., the cells were washed and loaded with fresh medium containing 100 U/ml IFN-γ. Control infected cells were not treated with the cytokine. The cell cultures were then incubated as above for 48 h. The formation of infectious *C. trachomatis* progeny in a secondary infection was assessed by infectivity titration assay (Al-Zeer et al., 2009). Briefly, the infected cells were mechanically destroyed using glass beads. Resulting lysates were serially diluted in infectious medium and then used to inoculate HeLa cells for 2 h. The cells were then washed and further incubated for 24 h in RPMI medium with 5% FBS and 1 µg/ml cycloheximide. One day later, the cells were fixed with 4% PFA and stained for *C. trachomatis*, as described above. Forty confocal images were taken per sample and experiment at 400x magnification, and the area of each image calculated and divided by the area of one well. The infectivity titer is expressed as the number of inclusions (IFU/ml) IFU/ml = no. inclusions in 10 fields/10 × no. fields in a well × dilution factor. Significance was determined by a Student´s t-test.

3.2.3.7 LDH cytotoxicity assay

THP-1 cells (1.7 x 10^5 per well) or hMDMs (2.0 x 10^5 per well) were stimulated with 100 nM IFN-γ and 100 nM LPS for 16 h and infected with *C. trachomatis* at MOI 30 for 24h in a 96-well plate or 24-well plate (hMDMs). LDH release upon infection was measured using CytoTox-ONE™ Homogeneous Membrane Integrity Assay kit (Promega, according to manufacturer´s instructions). LDH release was calculated by subtraction of cell culture background and normalization to average maximum according to the Promega manual. Significance was determined by two-way ANOVA.

3.2.3.8 ELISA

THP-1 cells (1.7 x 10^5 per well) or hMDMs (2.0 x 10^5 per well) were stimulated with 100 nM IFN-γ and 100 nM LPS for 16 h and infected with *C. trachomatis* at MOI 30 for 24 h in a 96-well plate or 24-well plate (hMDMs). IL-1β measurements were conducted using the Human IL-1 beta/IL-1F2 DuoSet ELISA kit according to the manufacturer´s instructions. Significance was determined by two-way ANOVA.

3.2.3.9 mtROS measurement

THP-1 cells (2 x 10^5 per well) were stimulated with 100 nM IFN-γ and 100 nM LPS for 16 h and infected with *C. trachomatis* at MOI 30 for 24 h in a 96-well plate. Mitochondrial ROS were measured by reaction with MitoSOX™ Red dye in a microplate reader according to manufacturer´s instructions (fluorescence Ex.: 400 nm/ Em.: 595 nm). Significance was determined by two-way ANOVA.

3.2.3.10 Uric acid measurement

THP-1 cells (2 x 10^5 per well) were stimulated with 100 nM IFN-γ and 100 nM LPS for 16 h and infected with *C. trachomatis* at MOI 30 for 24 h in a 96-well plate. Uric acid concentration in cell culture supernatants was measured using Uric acid/Uricase Assay Kit from Cell Biolabs, inc. according to the manufacturer´s instructions. Briefly, uric acid reacts with water and oxygen in the presence of the enzyme uricase to produce allantoin and H_2O_2. In the presence of HRP, a fluorescence probe reacts with H_2O_2 in a 1:1 stoichiometry to produce a highly fluorescent product (Ex.: 535 nm/ Em.: 595 nm), which can be measured using a microplate reader.

3.2.4 Quantification and statistical analysis

3.2.4.1 Image Analysis

For inclusion and ASC speck counting, approximately 30-40 images were taken per experiments representing approximately 500 cells. Nuclei, *C. trachomatis* inclusions and ASC specks were manually counted from immunostaining and analyzed

statistically using one-way ANOVA in Graphpad Prism software. Infectivity titer was determined by counting *C. trachomatis* inclusions and nuclei from 40 images per sample and the area of each image calculated and divided by the area of one well. The infectivity titer is expressed as the number of inclusions (IFU/ml) IFU/ml = no. inclusions in 10 fields/10 × no. fields in a well × dilution factor. Significance was determined by Student´s t-test using Graphpad Prism software.

3.2.4.2 Cell Biological Assays

ELISA, LDH and mtROS assays were analyzed using two-way ANOVA and Uric acid measurements using one-way ANOVA in Graphpad Prism software for three independent experiments.

4. Results

4.1 The hGBP1 G68A mutant retains fast, cooperative GTP hydrolysis while displaying reduced GMP production.

Since the two-step cleavage mechanism of GTP to GMP by hGBP1 requires the movement of the ribose backbone of the cleaved GDP moiety, a point mutation in the G-domain of hGBP1 was designed to sterically lock GDP in the nucleotide binding site and thus prevent the second hydrolysis step (Fig. 12). Several glycine residues surround GTP in the catalytic site and provide the necessary peptide backbone flexibility that enables nucleotide relocation. Amongst these glycines, Gly68 was chosen for two reasons. First, consistent with the reported crystal structure (Ghosh et al., 2006b), Gly68 is in close proximity to the ribose moiety of GDP during GTP hydrolysis, and its mutation into a bulkier amino acid might consequently interfere with nucleotide displacement. Second, when the sequence of hGBP1 is compared to that of hGBP5 that can cleave GTP only to GDP (Neun et al., 1996a; Wehner and Herrmann, 2010), Gly68 is substituted with alanine in hGBP5 (Fig. 12).

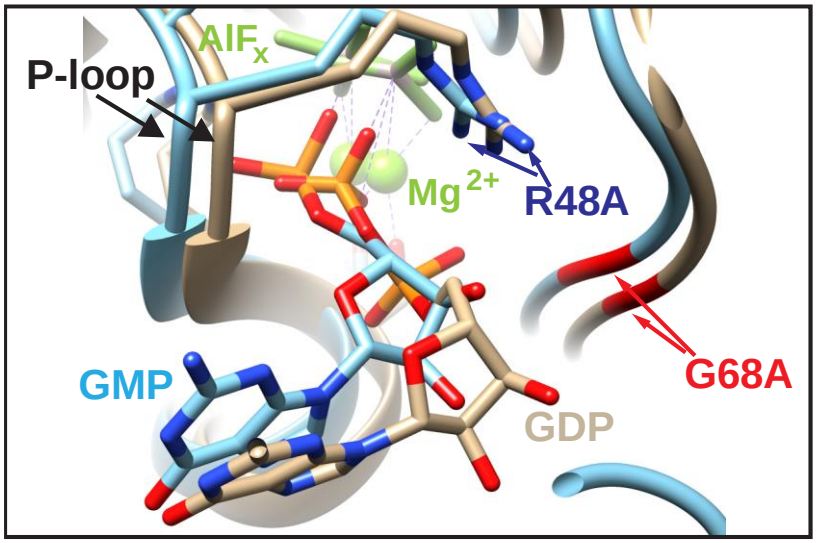


```
hGBP1 55 MNKLAGKKKGFSLGSTVQSHTKGIWM 80
hGBP2 55 MNKLAGKKNGFSLGSTVKSHTKGIWM 80
hGBP5 55 MNKLAGKNKGFSVASTVQSHTKGIWI 80
```

Figure 12 Design of a structure- based GMP production mutant in the LG domain.
(Top) Superimposition of hGBP1 G-domain structures bound to GDP·AlF_x (brown, pdb 2b92) and GMP·AlF_x (blue, pdb 2b8w). (Bottom) Sequence alignment of human GBP1, GBP2 and GBP5. Position 68 is marked in red.

Thus, recombinant hGBP1 WT and G68A mutants were generated and purified (see section 3.2.2.1) The G68A mutant of hGBP1 retained a similar GTP hydrolysis rate to that of the wild-type (WT) protein (Fig. 13A). However, the G68A mutation completely abolished GMP production (Fig. 13B-13D). Mutations in K76 or H74 in the conserved switch I region of the G-domain have been previously shown to abrogate GMP production (Praefcke et al., 2004b). However, unlike G68A, the K76A mutation led to a general reduction in GTP hydrolysis (Fig. 13A). Mutating R48, which stabilizes the transition state of GTP hydrolysis, to alanine completely abolished GTP hydrolysis (Fig. 13A-C), which is also consistent with previous data (Praefcke et al., 2004b).

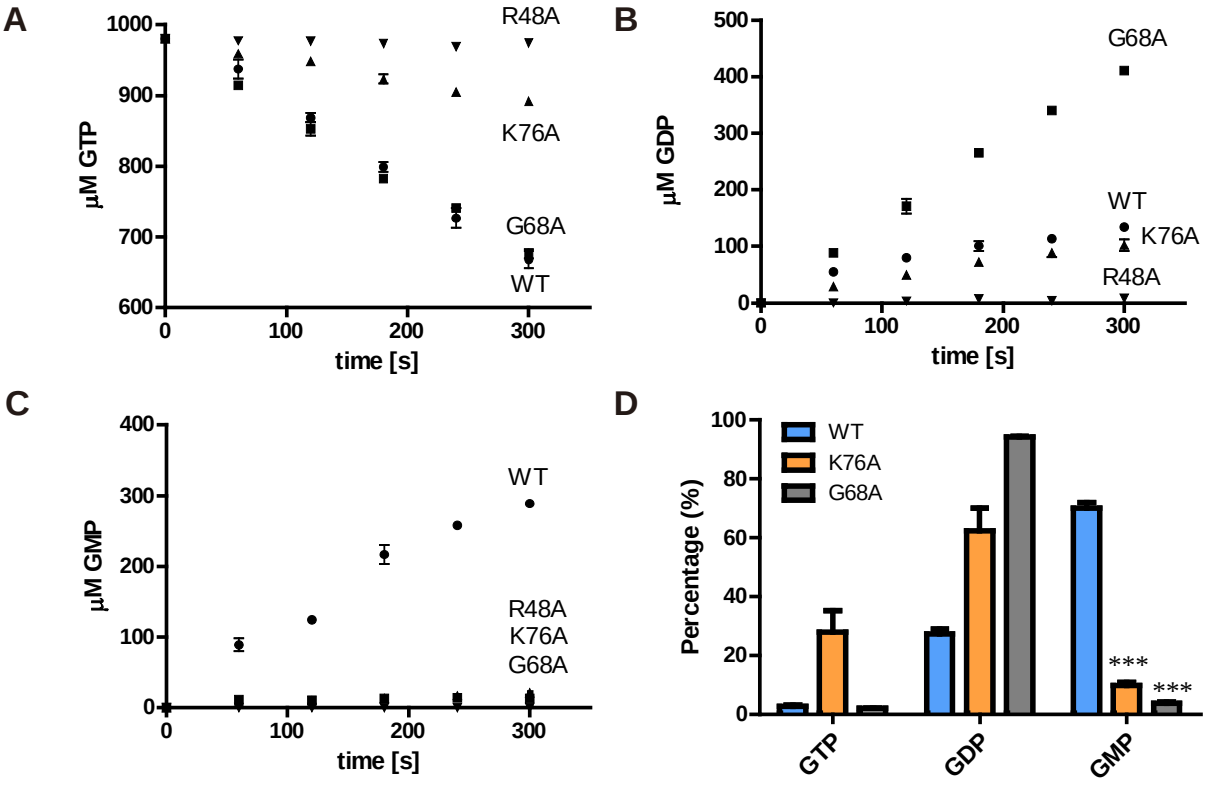

Figure 13 Linear rates of GTP hydrolysis, GDP and GMP production by hGBP1 WT and point mutants. GTP hydrolysis (A), GDP production (B) and GMP production (C) of 2 µM hGBP1 WT (•), G68A (▪), K76A (▲) or R48A (▼) were followed by an HPLC-based approach. Data represent the average of two independent measurements ± range. Error bars smaller than the data points are not indicated. (D) End product formation of GTP hydrolysis after reacting with 2 µM of indicated hGBP1 proteins for 30 minutes, n=3. Error bars indicate the standard error of the mean (SEM). *P<0.05, **P<0.01, ***P<0.001, two-way ANOVA.

To further compare the specific catalytic activities of the mutants, a detailed time- and concentration-dependent enzymatic characterization was performed. These results indicate that in comparison to the WT protein, I show that the dimerization- dependent GTP hydrolysis activity of the G68A mutant was not impaired. While the K76A mutation retained cooperativity, this mutation led to a 4-fold decrease in the maximal GTP hydrolysis activity (Fig. 14).

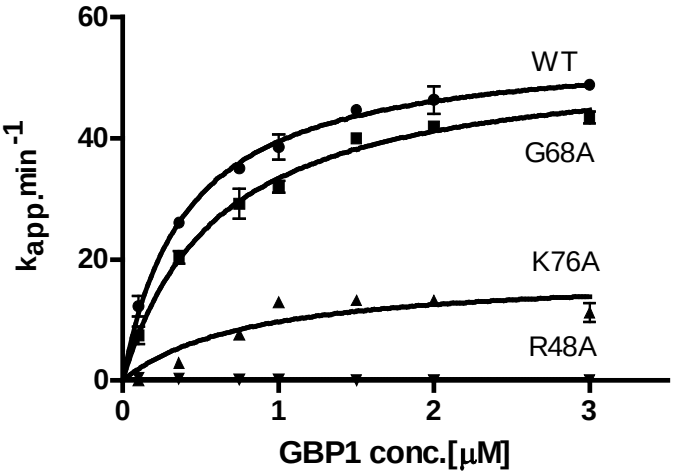

Figure 14 Dimerization-dependent GTP hydrolysis rate of hGBP1 WT and point mutants. Cooperative GTP hydrolysis rate of indicated hGBP1 proteins obtained by plotting specific activity against protein concentration. Data represent the average of two independent measurements ± range. Error bars smaller than the data points are not indicated.

Previous studies indicated that *in vitro* farnesylated hGBP1 can bind liposomes composed of bovine brain lipids (Folch liposomes) and form ring-like structures in the presence of transition state analog GDP AlF_x, indicating that GTP hydrolysis is important for the mechano-chemical function of hGBP1 on membranes. Critically, in line with its generally reduced GTP hydrolysis activity, it has been shown that K76A mutant fails to bind liposomes and to form such high order oligomeric state (Shydlovskyi et al., 2017). In contrast, recombinantly expressed and farnesylated hGBP1 G68A bound to Folch liposomes (Fig. 15) and formed ring-like structures (Fig. 16), comparable to hGBP1 WT (see section 3.2.2.6 for experimental details).

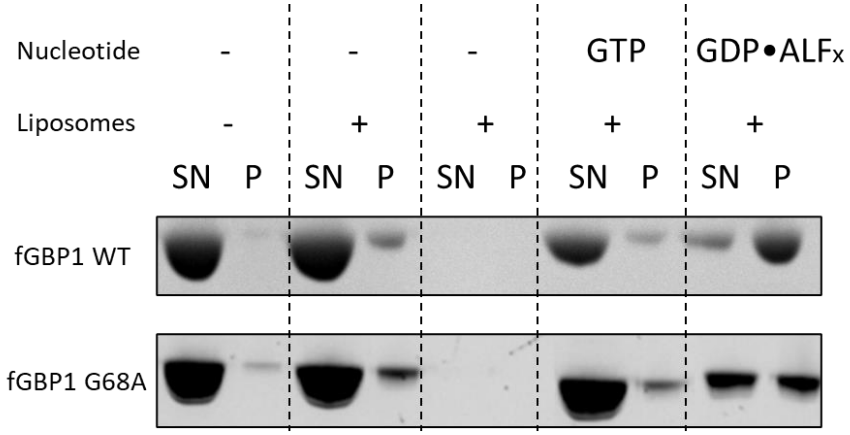

Figure 15 Liposome co-sedimentation assay. Folch liposome co-sedimentation assay of fGBP1 WT and fGBP1 G68A in the absence or presence of nucleotide. P, Pellet fraction; SN, supernatant.

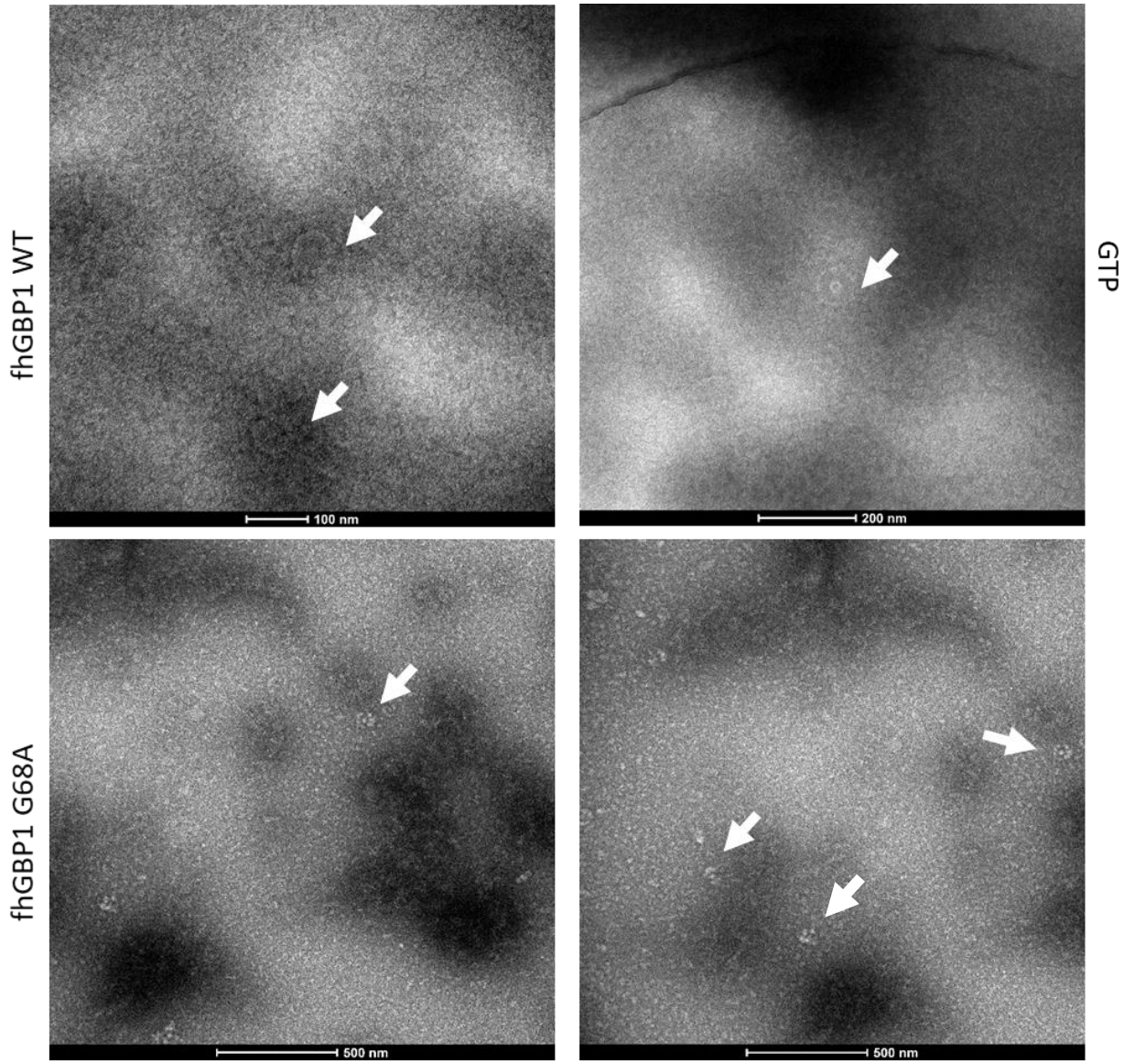

Figure 16 Negative stain electron microscopy images of fhGBP1 WT and G68A. (Top) negative stain EM images of a reaction of 10 µM fhGBP1 WT in the presence of 1 mM GTP at 1:10 dilution. (Bottom) negative stain EM images of a reaction of 10 µM fhGBP1 G68A in the presence of 200 µM GDP, 300 µM AlF_3 and 10 mM NaF at 1:10 dilution.

Collectively, among the tested hGBP1 mutants that abolished GMP production, the G68A mutant hydrolyzed GTP most similar to WT. Therefore, this mutant was utilized for the subsequent functional studies.

4.2 Consecutive GTP hydrolysis is dispensable for the restriction of *C. trachomatis.*

In order to characterize the role of the second-step GDP hydrolysis for pathogen restriction, hGBP1 was knocked out in THP-1 cells, a human monocyte cell line, using CRISPR-Cas9 technology (see section 3.2.3.3). Subsequently, the KO cells were reconstituted with lentivirus-expressed WT hGBP1, the hGBP1 mutants, R48A, K76A, G68A, or GFP as a negative control. The depletion of endogenous hGBP1 and expression of exogenous constructs were confirmed by Western blot (Fig. 17).

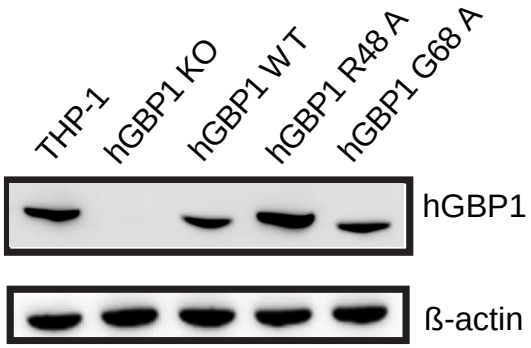

Figure 17 Western blot of hGBP1 WT and point mutants in THP-1. CRISPR-Cas9-mediated knock-out of hGBP1 and stable overexpression of hydrolysis mutants as shown by immunoblotting against endogenous hGBP1 and β-actin. Cell lines were stimulated with IFN-γ for 16 h.

Parental THP-1 cells and the newly generated cell lines were infected with *C. trachomatis*, followed by immunostaining against major outer membrane protein (MOMP), an antigen of *C. trachomatis* (see Fig. 18A) In agreement with a previous study, hGBP1 KO cells presented an increased number and size of *C. trachomatis* inclusions (Fig. 18A-18C) (Al-Zeer et al., 2013). Re-expression of WT hGBP1, but not the R48A mutant, reduced *C. trachomatis* inclusions, indicating that hGBP1-mediated GTP hydrolysis is vital for *C. trachomatis* restriction. The switch I mutant K76A showed impaired restriction of *C. trachomatis* although not to the same extent as the GTP hydrolysis-deficient hGBP1 mutants re-expressed in the KO cells (Fig. 19). This is consistent with the impaired GTP hydrolysis activity of K76A mutant, and K76A mutant was thus not further investigate in this study. Surprisingly, the G68A mutant restricted *C. trachomatis* comparably to WT hGBP1-expressing cells (Fig. 18A-18C).

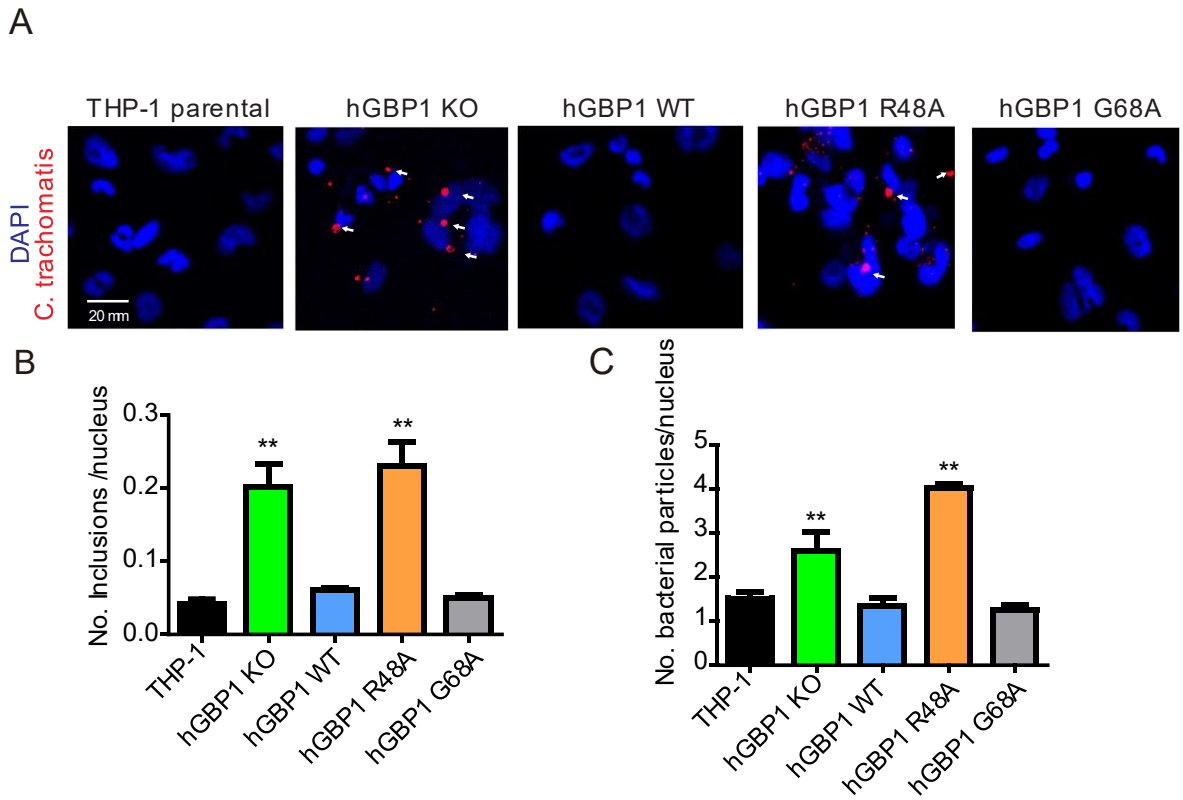

Figure 18 hGBP1 G68A mutant is able to restrict C. *trachomatis*. (A) Representative images of indicated THP-1 cell lines stimulated with IFN-γ and infected with *C. trachomatis* at MOI 5 for 24 h. White arrows indicate inclusions. Red, *C. trachomatis*. Blue, DAPI. The scale bars are 20 µm. (B, C) *C. trachomatis* inclusions larger (B) or smaller (C) than the size of 2 µm diameter were quantified by scanning the nuclei (30-40 per image) of all cells as indicated in (A) (n=3).

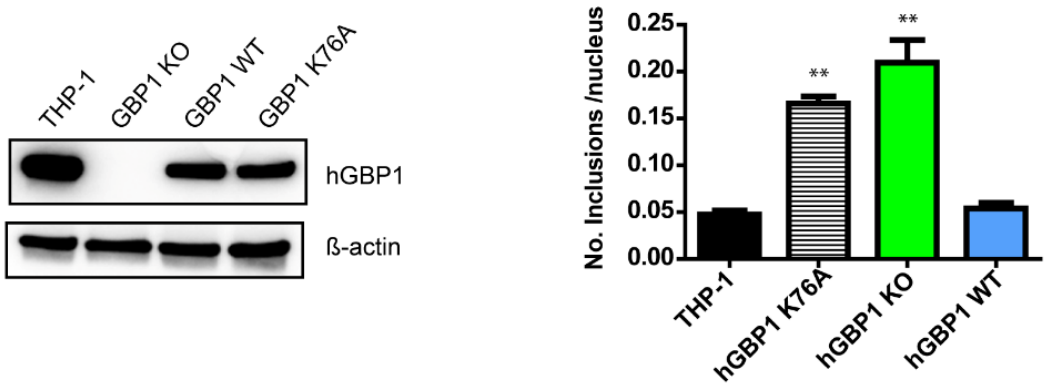

Figure 19 Cell line THP-1 hGBP1 K76A does not restrict *C. trachomatis* growth. Western blot confirming re-expression of the hGBP1 K76A in THP-1 hGBP1 KO cells (left) and inclusion count (right) of THP-1 stimulated with IFN-γ and infected with *C. trachomatis* at MOI 5 for 24 h. *C. trachomatis* inclusions larger than the size of 2 µm diameter were quantified by normalization to the number of nuclei (30-40 per image).

To further substantiate these findings, the requirement of consecutive GTP hydrolysis for restricting infectious *C. trachomatis* progeny was tested by conducting a re-infection assay in HeLa cells. In this assay, *C. trachomatis* are isolated from infected THP-1 cells and re-infected to HeLa cells. This quantifies actual viability of the bacteria as opposed to simple inclusion counts, which could potentially include inactive or non-infectious bacteria. While hGBP1 KO cells and R48A mutants increased the production of *C. trachomatis* elementary bodies, WT hGBP1-expressing cells and G68A mutants significantly reduced their production (Fig. 20A and 20B). Thus, consecutive GTP hydrolysis is dispensable for hGBP1-mediated Chlamydia restriction.

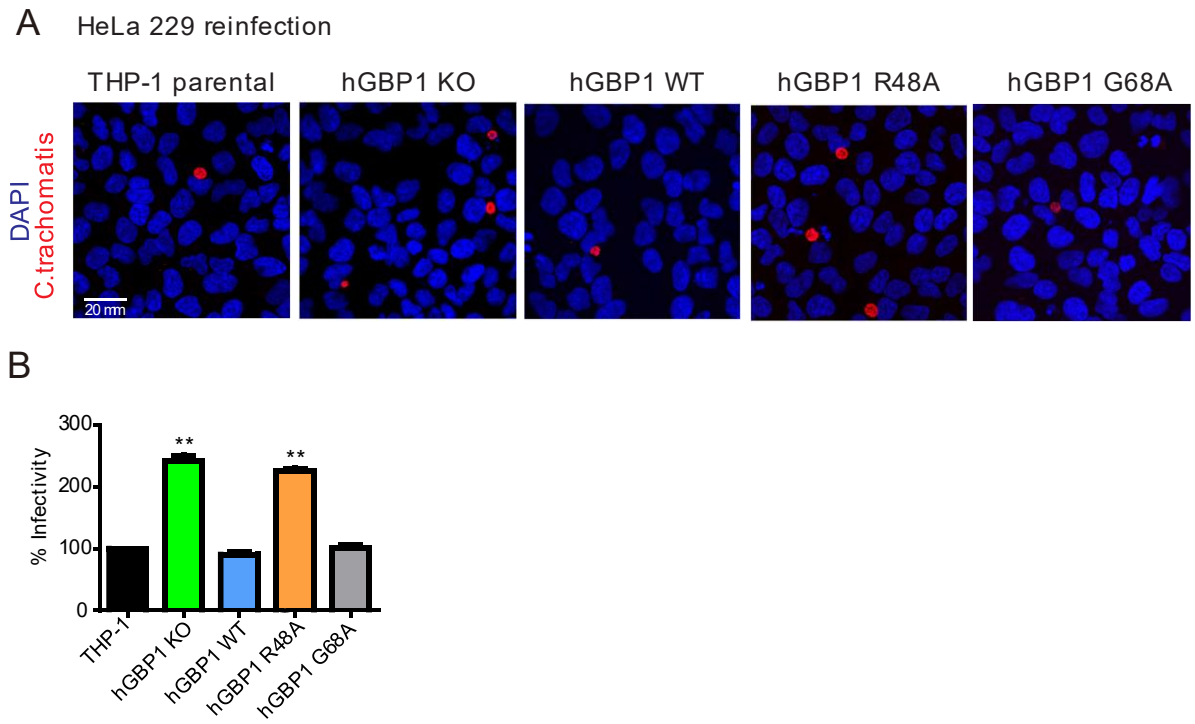

Figure 20 hGBP1 G68A can restrict C. *trachomatis* infectious progeny (A) Influence of hGBP1 mutants on *C. trachomatis* infectious progeny. *C. trachomatis* inclusions were isolated from the infected various THP-1 cells; the infectivity was determined by the re-infection of HeLa 229 cells, normalized to the parental THP-1 cells. Representative images of reinfection (B) Bar diagram of re-infection of HeLa 229 from C. *trachomatis* infected THP-1 GBP1 cell lines. Red, *C. trachomatis*. Blue, DAPI. All error bars indicate SEM. *P<0.05, **P<0.01, one-way ANOVA.

4.3 Consecutive GTP hydrolysis is required for inflammasome activation

It has previously been demonstrated that GBPs are required for inflammasome activation (Fisch et al., 2019; Man et al., 2015; Meunier et al., 2014; Meunier et al., 2015; Pilla et al., 2014). Inflammasome activation leads to Gasdermin D-mediated cell death (pyroptosis), caspase-1-dependent processing, and the secretion of interleukin-1β (IL-1β). Therefore, the inflammasome activation of *C. trachomatis*-infected THP-1 cells was evaluated by measuring lactate dehydrogenase (LDH) release (a readout of cell death) and IL-1β secretion. As expected, KO cells showed a significant reduction in cell death rate as compared with the parental cells (Fig. 21A and 21B). These defects were rescued by re-expression of hGBP1 WT. In contrast, expression of the R48A mutant failed to rescue IL-1β secretion (Fig. 10A).

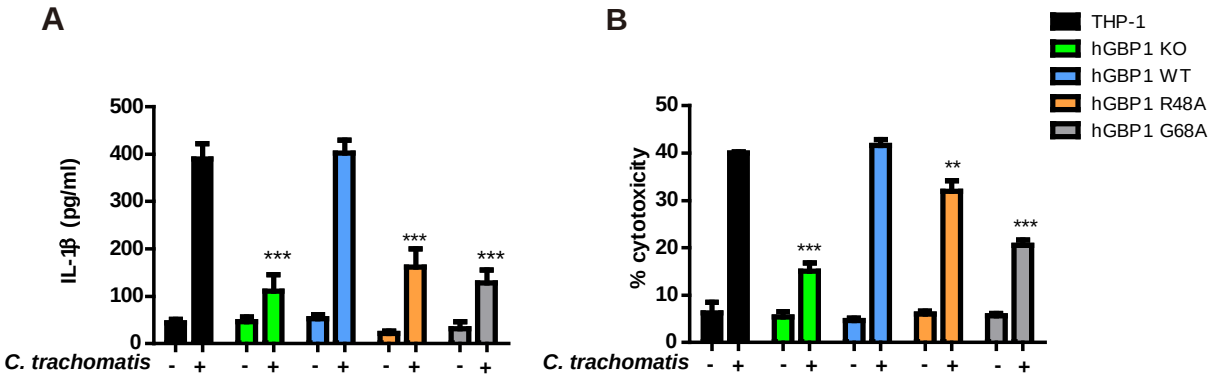

Figure 21 The consecutive hydrolysis of hGBP1 is required for cytokine release and pyroptosis. (A) Inflammasome activation was examined by IL-1β ELISA. Cell lines were infected with *C. trachomatis* at MOI 30 for 24 h, n=3; two-way ANOVA.(B) Cell death was measured by measuring release of lactate dehydrogenase in LPS + IFN-γ stimulated THP-1 cells infected with *C. trachomatis* at MOI 30 for 24 h, n=3; two-way ANOVA.

Unexpectedly, R48A cells showed somewhat increased cell death despite the clear blockade of inflammasome activation (Fig. 21B). Screening of inhibitors that target various cell death mechanisms showed that R48A mutants died due to necroptosis (Fig. 22). Therefore, infected cells can engage in necroptotic cell death when hydrolysis activity of hGBP1 is compromised, but not when hGBP1 is completely absent. The surprising link between the hGBP1 R48A mutation and the induction of necroptosis needs further investigation.

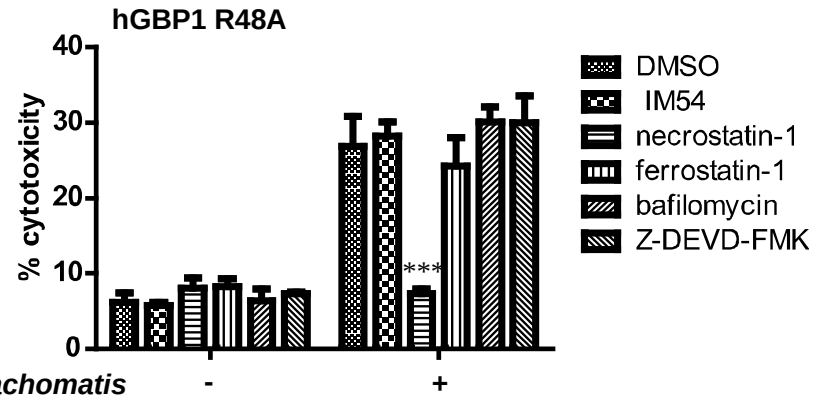

Figure 22 THP-1 hGBP1 R48A dies by necroptosis. LDH release of THP-1 hGBP1 R48A cell line stimulated with IFN-γ + LPS for 16 h, followed by infection with *C. trachomatis* at MOI 30 for 24 h. Cells were co-treated with indicated cell death inhibitors for 24 h, n=3; two-way ANOVA. Cell death inhibitors - IM54, necrostatin-1, ferrostatin-1, bafilomycin and Z-DEVD-FMK that inhibit necrosis, necroptosis, ferroptosis, autophagy and apoptosis, respectively.

Interestingly, the G68A mutant failed to induce cell death and secrete IL-1β in an infection-dependent manner, which was comparable with KO cells (Fig. 21A and 21B). Also, the status of caspase-1 activation by Western blotting of cell culture supernatants was examined. In comparison to KO cells, G68A mutants reduced the secretion of mature caspase-1 subunit p20 (Fig. 23). These findings lead to the conclusion that the reduced secretion of caspase-1 and inflammatory cytokines are the results of impaired inflammasome activation.

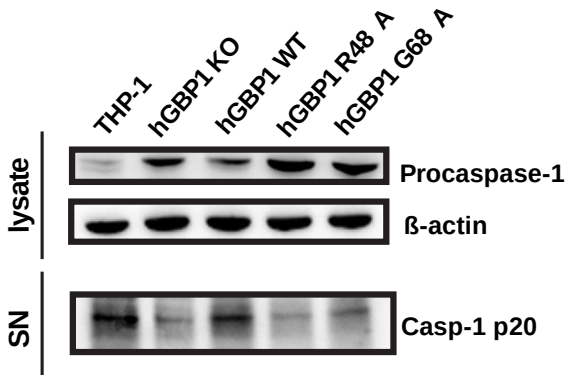

Figure 23 Western blot of caspase-1 precursor and processed p20 in infected THP-1 hGBP1 WT and mutant cell lines. Inflammasome activation was examined by immunoblotting against caspase-1. Cell lines were infected with *C. trachomatis* at MOI 30 for 24 h. The blot is a representative result of two independent experiments.

A previous study demonstrates that hGBP2 can also hydrolyze GTP to GMP but much less efficiently than hGBP1 (~10% of hGBP1) (Neun et al., 1996a). Depletion of hGBP2 in THP-1 cells led to a non-significant marginal reduction of IL-1β release and cell death (Fig. 24A), despite an efficient knock-down (Fig. 24B). Thus, activation of the inflammasome is not a general feature of all hGBPs. Instead, it may be related to the exceptionally high GMP production by hGBP1.

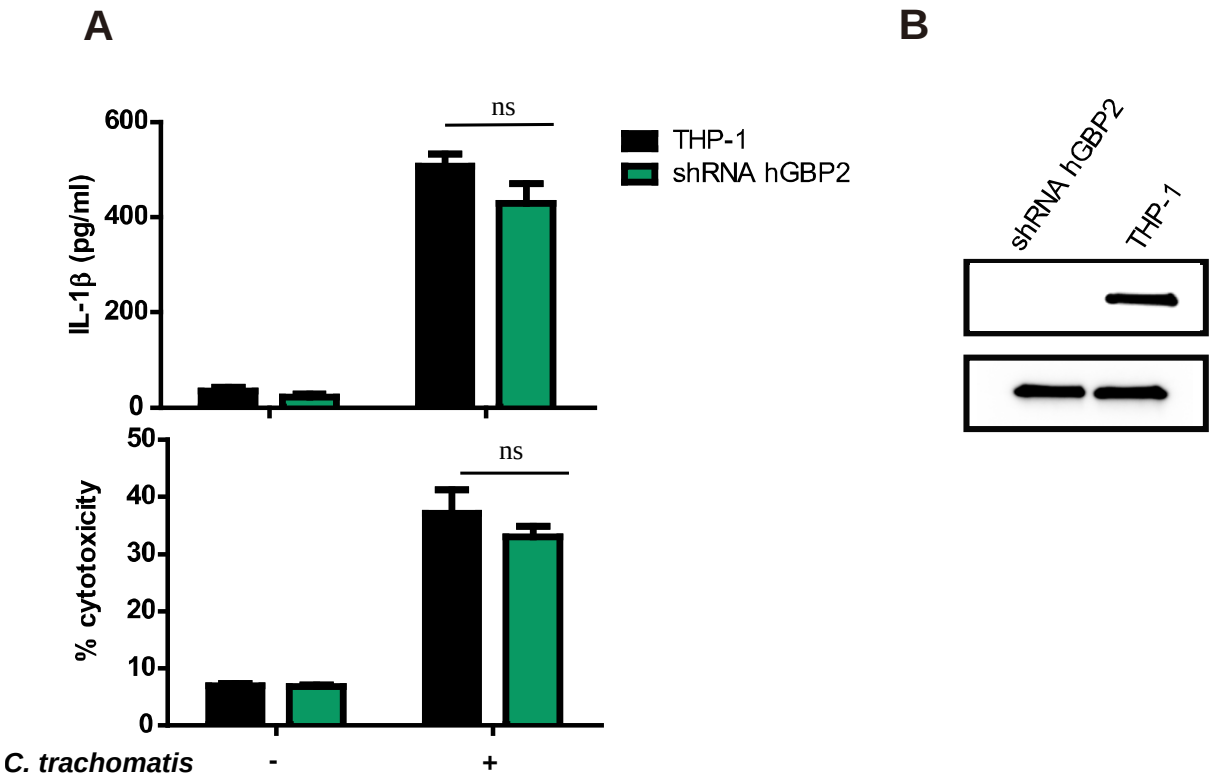

Figure 24 shRNA knockdown of hGBP2 in THP-1 cells shows hGBP2-independent inflammasome activation. (A) hGBP2 knock-down by shRNA in THP-1 cells. IL-1β ELISA and LDH release following infection with *C. trachomatis* at MOI 30 for 24 h, n=3; two-way ANOVA. (B) Stable-knock down of hGBP2 in THP-1 cells shown by immunoblotting against hGBP2. Cells were treated with IFN-γ for 16 h. All error bars indicate SEM. *P<0.05, **P<0.01, ***P<0.001.

4.4 hGBP1 activates the NLRP3 inflammasome

hGBPs have been shown to activate the canonical NOD-, LRR- and pyrin domain-containing protein 3 (NLRP3) inflammasome either directly or indirectly through the non-canonical caspase-4-mediated pathway. hGBP5 has been proposed to be part of NLRP3 to stabilize inflammasome formation (Shenoy et al., 2012) and hGBP1 has been suggested to activate NLRP3 during C. *trachomatis* infection (Finethy et al., 2015). Alternatively, hGBPs have been proposed to lyse bacterial membranes and release LPS and indirectly activate NLRP3 through the non-canonical inflammasome caspase-11/-4/5 (Meunier et al., 2014; Pilla et al., 2014). However, the exact mechanism of NLRP3 activation during *C. trachomatis* infection has been unclear.

To first confirm whether consecutive GTP hydrolysis is required for NLRP3 inflammasome activation, hGBP1 KO cells that re-express hGBP1 WT, the R48A or G68A mutant were infected with *C. trachomatis* and infection-dependent NLRP3 activation was examined by monitoring the speck formation of the inflammasome adaptor ASC (Apoptosis-associated Speck-Like protein containing a CARD). In line with the previous experiments, G68A mutants formed fewer ASC specks as compared with hGBP1 WT-expressing cells (Fig. 25A and 25B).

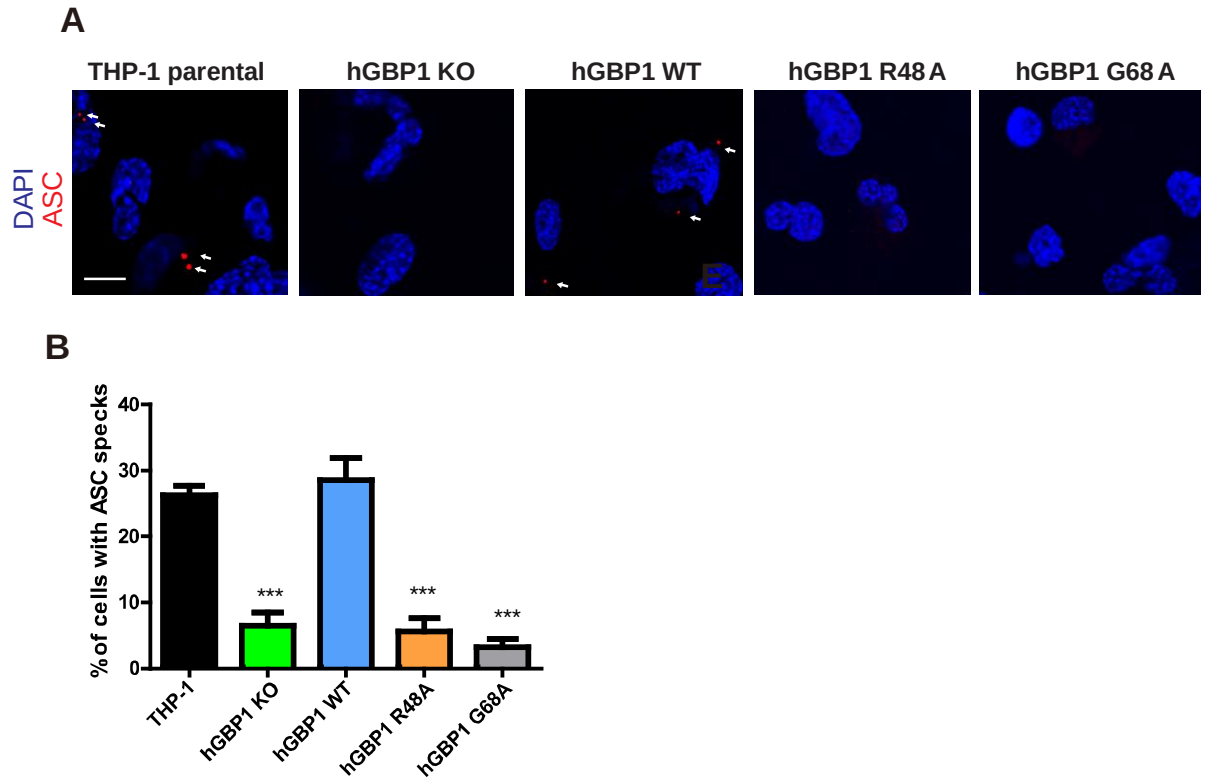

Figure 25 Differential ASC speck formation in *C. trachomatis* infected THP-1 hGBP1 cell lines. (A) Representative images of ASC specks stained in THP-1 hGBP1 cell lines infected with *C. trachomatis.* Red, ASC specks. Blue, DAPI. Scale bar, 10 µm. (B) Quantification of inflammasome ASC specks of indicated cell lines infected with *C. trachomatis* at MOI 30 for 24 h, n=3; one-way ANOVA. All error bars indicated SEM. *P<0.05, **P<0.01, ***P<0.001.

In order to verify that NLRP3 is the major inflammasome pathway induced by *C. trachomatis* infection, the cells were treated with the NLPR3 inhibitor MCC950. MCC950 treatment largely abolished infection-induced IL-1β secretion and pyroptosis (Fig. 26A). The effect of MCC950 was also confirmed in a culture of human primary macrophages (Fig. 26B).

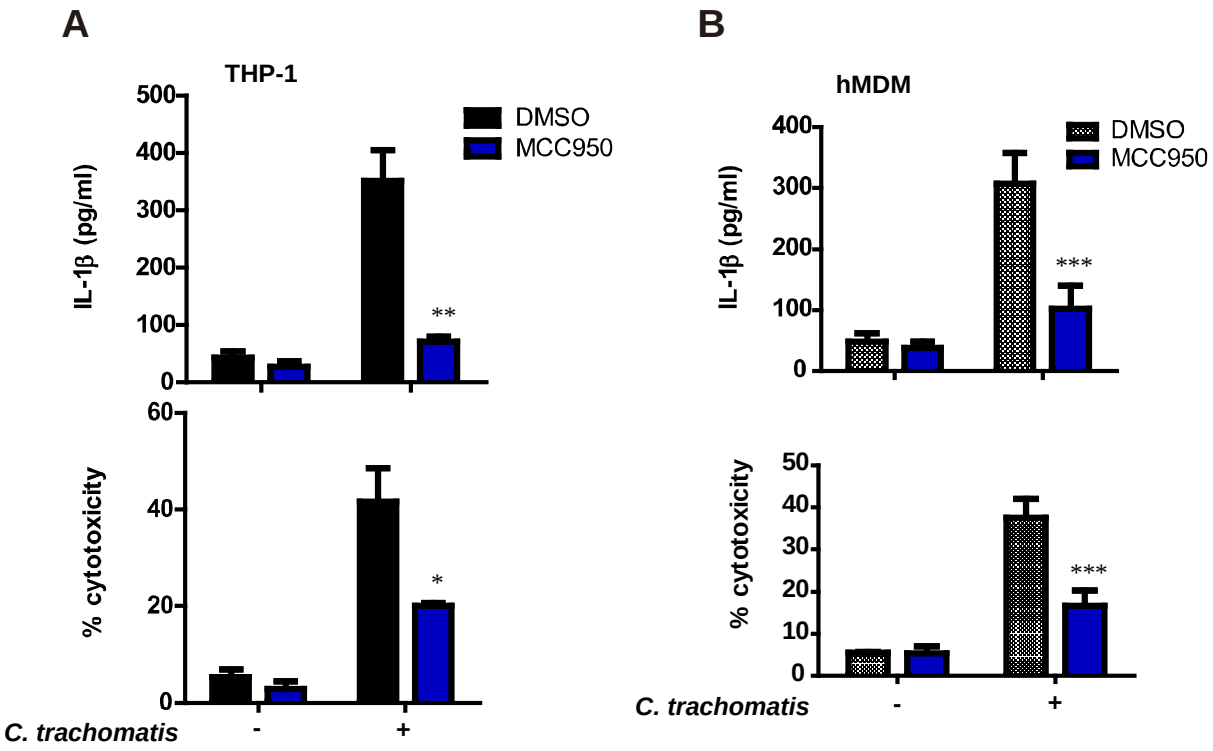

Figure 26 NLRP3 inhibitor MCC950 significantly reduces cytokine release and pyroptosis in THP-1 cells and primary human macrophages in response to *C. trachomatis* infection. (A) IL-1β ELISA and LDH release for THP-1 cells treated with MCC950 and infected with *C. trachomatis* at MOI 30 for 24 h, n=3; two-way ANOVA. (B) IL-1β ELISA and LDH release for hMDMs treated with MCC950 and infected with *C. trachomatis* at MOI 30 for 24 h, n=3; two-way ANOVA. *P<0.05, **P<0.01, ***P<0.001.

In order to test whether caspase-4 cleavage and activation cause NLRP3 inflammasome activation, caspase-4 was transiently knocked down in THP-1 cells. Transient knock down of caspase-4 inhibited IL-1β release and cell death in response to intracellular LPS, a well-established activator of caspase-4 (Fig. 27A) (Shi et al., 2014). In contrast, caspase-4 knock down had no effect on IL-1β secretion and pyroptosis following *C. trachomatis* infection (Fig. 27A). The efficiency of caspase-knockdown was confirmed by western blotting (Fig. 27B). Taken together, these results suggest that hGBP1-mediated consecutive hydrolysis of GTP to GMP is required for the canonical caspase-4-independent activation of the NLRP3 inflammasome.

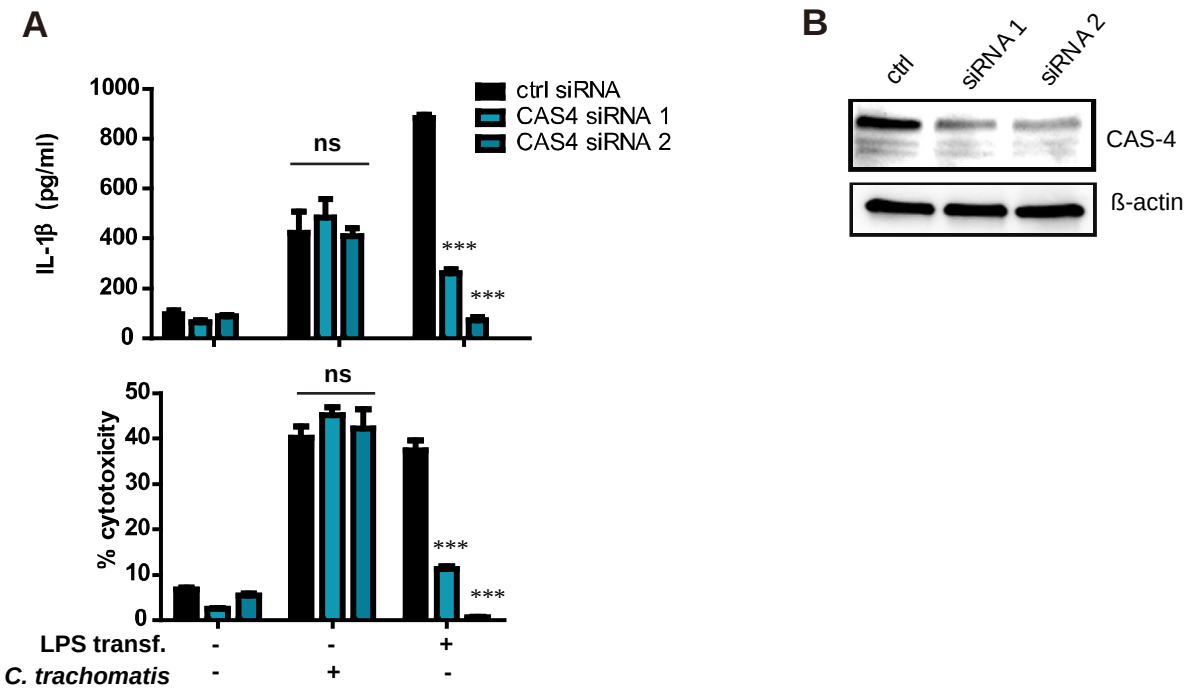

Figure 27 hGBP1 activates the caspase-4-independent NLRP3 inflammasome pathway upon *C. trachomatis* infection. (A) IL-1β ELISA and LDH release for THP-1 and THP-1 caspase-4 knock down cells, transfected with LPS or infected with *C. trachomatis* at MOI 30 for 24 h, n=3; two-way ANOVA. (B) Transient knock down of caspase-4 in THP-1 cells was validated by immunoblotting against caspase-4. Cells were primed with IFN-γ and LPS.*P<0.05, **P<0.01, ***P<0.001

4.5 Uric acid synthesis is required for inflammasome activation upon Chlamydia infection

The potential mechanism by which hGBP1 promotes NLRP3 inflammasome activation was further investigated. Several intracellular danger patterns are known to activate the NLRP3 inflammasome, among which uric acid (UA) is one (Braga et al., 2017; Kimball et al., 2019; Martinon et al., 2006a). Interestingly, GMP can be catabolized to UA through three enzymatic steps (Fig. 28). This suggests that hGBP1 oligomerization on the vacuolar membrane results in a local rise in GMP concentration. Subsequently, GMP could be catabolized to UA, which in turn would activate the NLRP3 inflammasome.

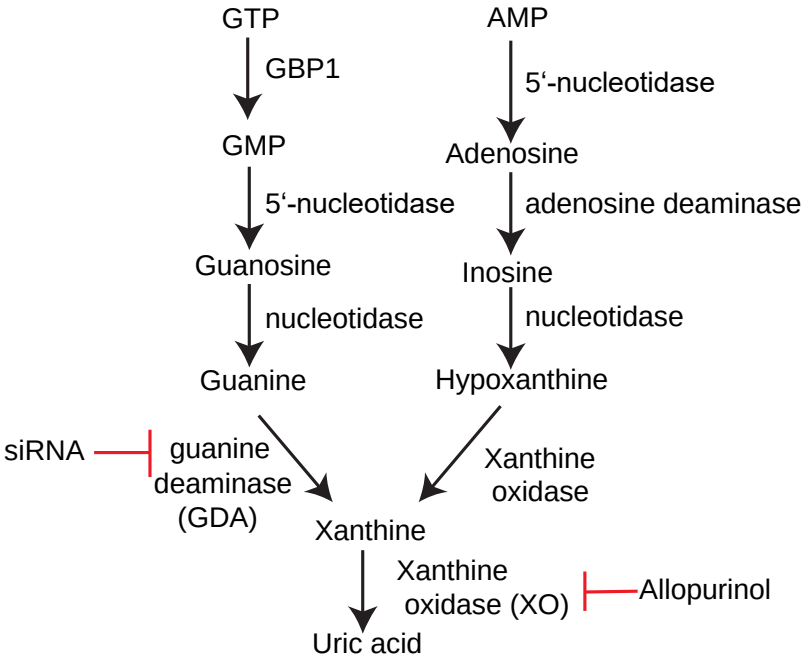

Figure 28 Metabolic pathway of GMP degradation to uric acid. The enzyme GDA was knocked down via siRNA, and the enzyme xanthine oxidase was inhibited with the chemical compound allopurinol

An essential prediction of this model is that enzymes involved in the metabolism of GMP to UA would be localized to the PCV or regulated during infection. Indeed, as Chlamydia are obligate intracellular pathogens, many metabolites and metabolic enzymes are known to be hijacked from the host system and recruited to the inclusion membrane (Saka and Valdivia, 2010). Thus, the localization of xanthine oxidase, a

key enzyme involved in the last step of xanthine oxidization to UA was examined. In uninfected cells, xanthine oxidase was evenly distributed throughout the cell. In contrast, this enzyme displayed a marked vesicular pattern in infected cells, which strongly co-localized with the inclusions (Fig. 29).

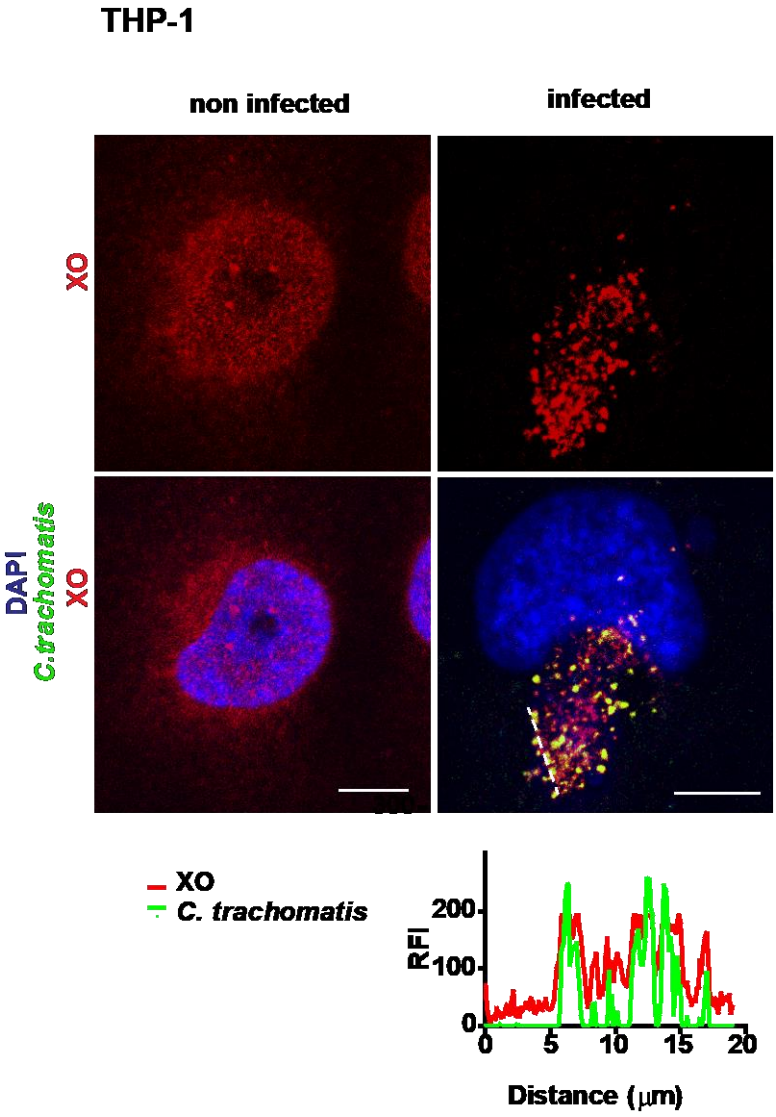

Figure 29 XO colocalizes with *C. trachomatis* in infected THP-1 Representative images of xanthine oxidase (red) immunostaining with or without *C. trachomatis* (green) infection. The line tracing quantification of the white dashed line is shown at the bottom. Scale bar = 10 µm.

Furthermore, in microarray data from a previous study, it was observed that the transcripts of guanine deaminase (GDA), which catalyzes the upstream step of

xanthine oxidase, are significantly increased upon *C. trachomatis* infection (Mehlitz et al., 2010). RT-qPCR of GDA validated these microarray results (Fig. 30).

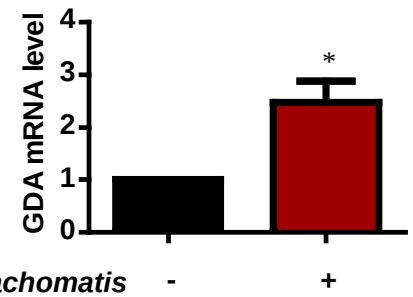

Figure 30 induction transcription of GDA upon *C. trachomatis* infection in THP-1 cells. mRNA levels of GDA in THP-1 cells upon infection with *C. trachomatis* or non-infected at MOI 30 for 24 h, n=3; two-tailed Student´s t-test

It was then investigated whether blocking UA synthesis can impair inflammasome activation in response to *C. trachomatis* infection. First, allopurinol, a clinically approved xanthine oxidase inhibitor used for gout medication, was employed. Remarkably, co-treatment of cells with allopurinol mitigated *C. trachomatis*-induced pyroptosis and ASC speck formation in a concentration-dependent manner (Fig. 31 and 32A).

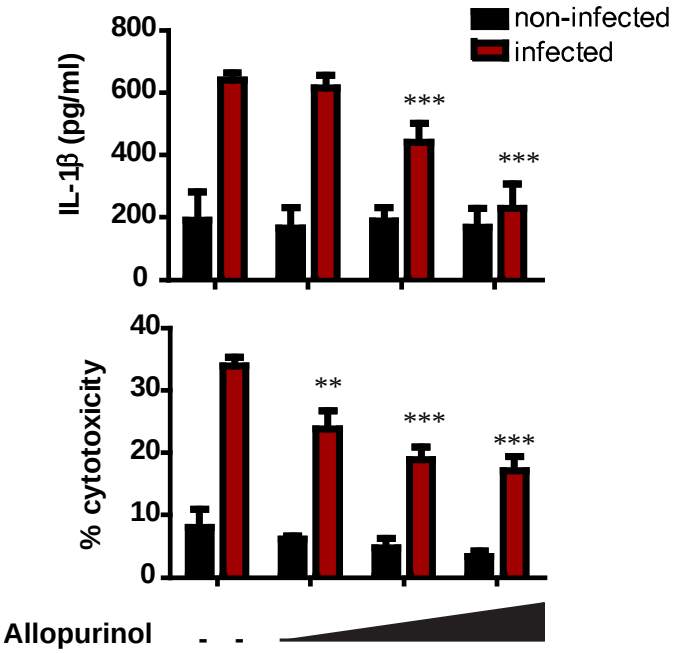

Figure 31 Allopurinol treatment of C. trachomatis infected THP-1. LDH release and IL-1β ELISA of THP-1 cells treated with increasing concentrations of allopurinol (50, 100 and 500 µM). The cells were stimulated with IFN-γ + LPS and infected with *C. trachomatis* at MOI 30 for 24 h, n=3; two-way ANOVA.

Accordingly, a sharp reduction of IL-1β secretion in the cell supernatant was detected (Fig. 31), whereas IL-1β expression was not affected at the mRNA level (Fig. 32B).

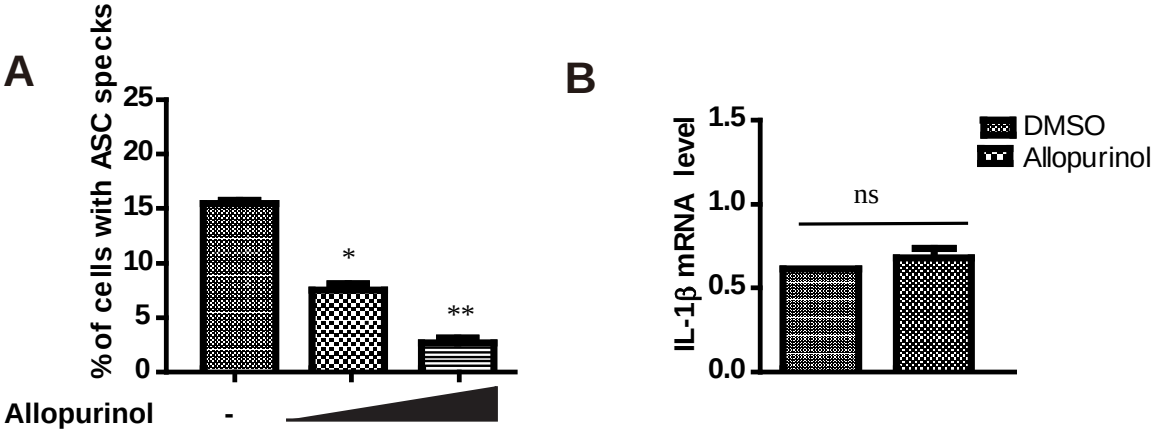

Figure 32 Dose-dependent reduction of ASC specks and IL-1β transcription level in THP-1 infected with *C. trachomatis* (A) Quantification of inflammasome ASC specks in THP-1 cells upon infection with *C. trachomatis* at MOI 30. The cells were co-treated with increasing concentrations of allopurinol (100 µM and 500 µM) for 24 h, n=3,; one-way ANOVA. (B) mRNA levels of IL-1β in THP-1 stimulated and treated or untreated with allopurinol (500 µM), n=3; two-tailed Student´s t-test.

Allopurinol blocked inflammasome activation in human primary macrophages as well (Fig. 33B). Importantly, the effect of allopurinol was specific to *C. trachomatis* infection, because it had no effect on other inflammasome activators, such as poly (dA:dT), flagellin and LPS/ATP (Fig. 33A and 33B).

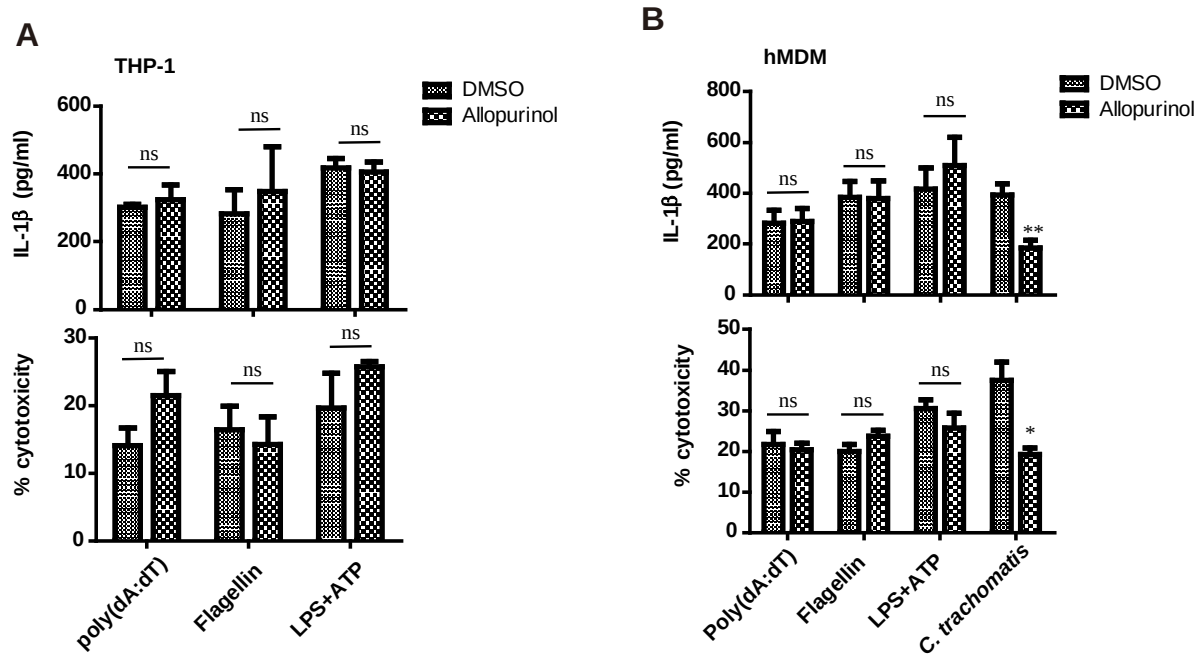

Figure 33 Inflammasome control experiments in THP-1 and hMDM. (A) IL-1β ELISA and LDH release of THP-1 cells, which were transfected with Flagellin, poly (dA:dT) or stimulated with LPS + ATP and co-treated with allopurinol (500 µM) as indicated, n=3; two-tailed Student´s t-test. (B) IL-1β ELISA and LDH release of THP-1 cells transfected with Flagellin, poly (dA:dT) or stimulated with LPS + ATP or infected with *C. trachomatis* and co-treated with allopurinol (500 µM) as indicated, n=3; two-tailed Student´s t-test.

As a second approach, the metabolic pathway of UA production was genetically inactivated. To this end, the enzyme GDA was transiently knocked down due to its specific involvement in GMP catabolism rather than that of AMP. The efficient downregulation of GDA after siRNA transfection was validated by RT-qPCR (Fig. 34).

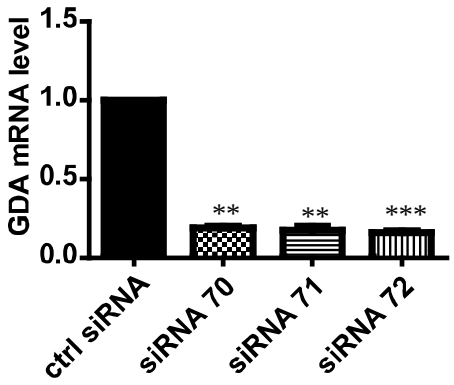

Figure 34 GDA transcription levels in THP-1 GDA knockdown cells. GDA knock down verification. GDA mRNA levels in THP-1 cells transfected with control or 3 different GDA siRNAs, n=3; one-way ANOVA.

As compared with control scrambled siRNA, all three GDA siRNAs significantly inhibited cell death and increased ASC speck formation and IL-1β secretion upon infection with *C. trachomatis* (Fig. 35A and 35B); IL-1β mRNA expression was unaffected (Fig. 35C).

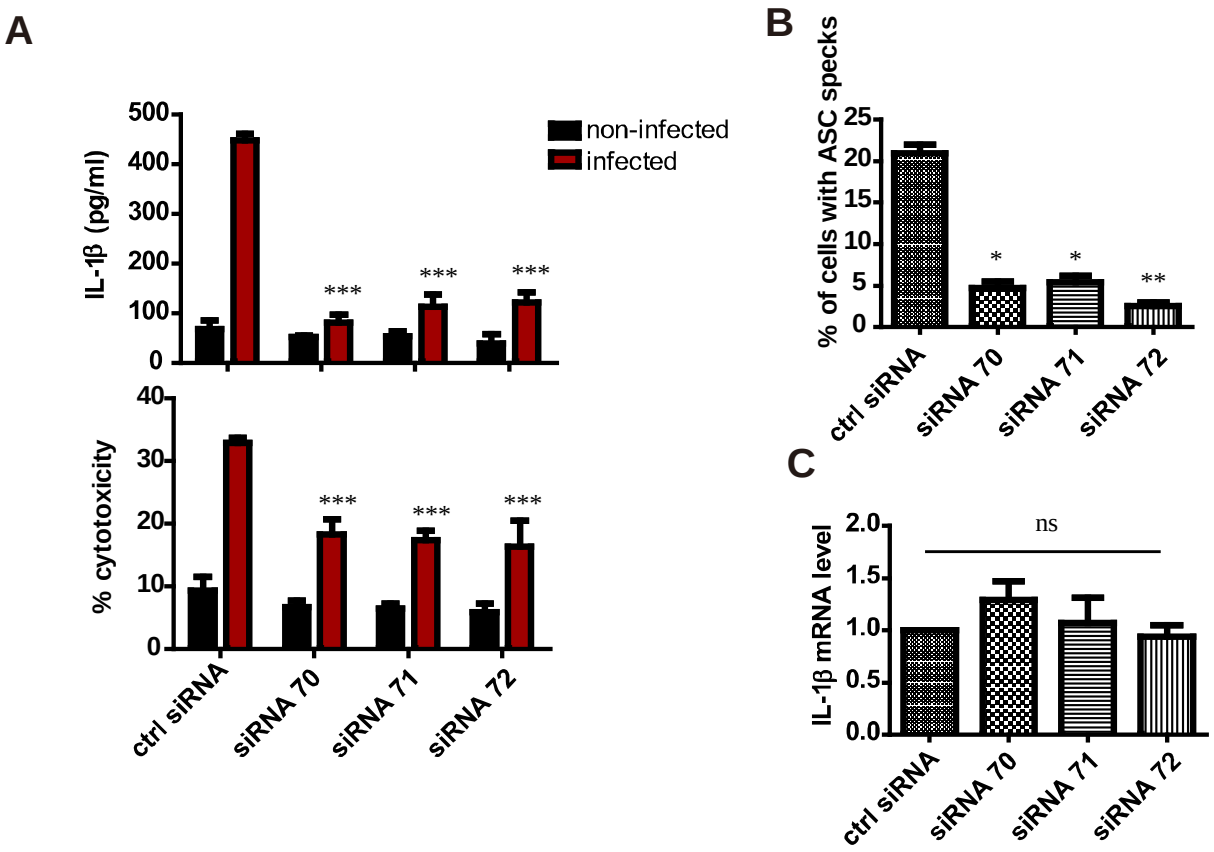

Figure 35 Knockdown of GDA in THP-1 and infection with *C. trachomatis* (A) LDH release and IL-1β ELISA of THP-1 cells transfected with control or three different siRNAs against GDA. The cells were stimulated with IFNγ + LPS and infected with *C. trachomatis* at MOI 30 for 24 h, n=3; two-way ANOVA. (B) Quantification of inflammasome ASC specks in THP-1 transfected with 3 different GDA siRNAs, and infected with *C. trachomatis* at MOI 30 for 24 h, n=3; one-way ANOVA. (C) mRNA levels of IL-1β in THP-1 cells transfected with three different GDA siRNAs (n=3; one-way ANOVA.

Notably, GDA knock down did not reduce bacterial growth, indicating that the impaired inflammasome activation is not an indirect effect of a lower bacterial load (Fig. 36).

These results indicate that catabolism of GMP to uric acid via GDA and XO is required for inflammasome activation.

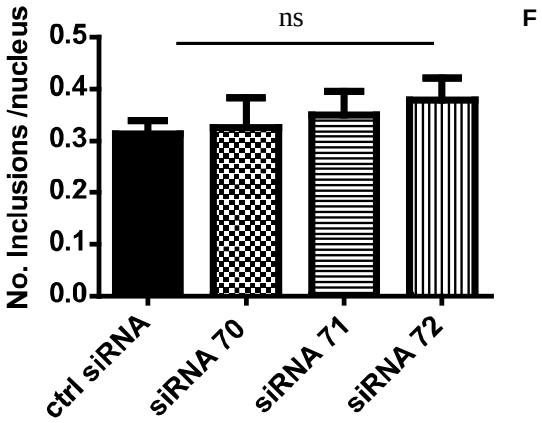

Figure 36 Number of inclusions in THP-1 GDA knockdown cells. Inclusion count of THP-1 cells transfected with three different GDA siRNAs and infected with *C. trachomatis* at MOI 5 for 24 h, n=3, one-way ANOVA.

4.6 hGBP1-produced GMP is metabolized to uric acid

To verify this hypothesis, UA concentrations upon *C. trachomatis* infection in THP-1 cells was measured. An infection-dependent increase of UA in parental cells as well as hGBP1 WT-expressing cells was observed, whereas hGBP1 KO cells, R48A mutants and G68A mutants showed no induction of UA (Fig. 37).

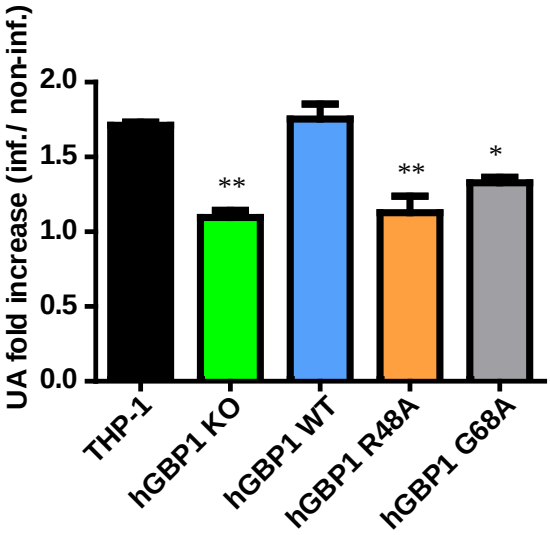

Figure 37 Relative increase of uric acid in THP-1 hGBP1 WT and mutant cell infected with *C. trachomatis*. Fold-change of UA concentrations in the cell culture supernatants of infected THP-1 cells vs. non-infected THP-1 cells. The cells were stimulated with IFN-γ + LPS and infected with *C. trachomatis* at MOI 30 for 24 h, n=3; one-way ANOVA.

Next, an antibody against UA was applied, which was originally generated for the diagnostics of rheumatic arthritis. A strong UA immunostaining around early *C. trachomatis* vacuoles as well as around mature inclusions was observed that spread throughout the cytoplasm (Fig. 38). UA staining was abolished in allopurinol-treated cells, confirming the specificity of the antibody (Fig. 38). UA has been associated with NLRP3 activation by triggering mitochondrial ROS production (Braga et al., 2017).

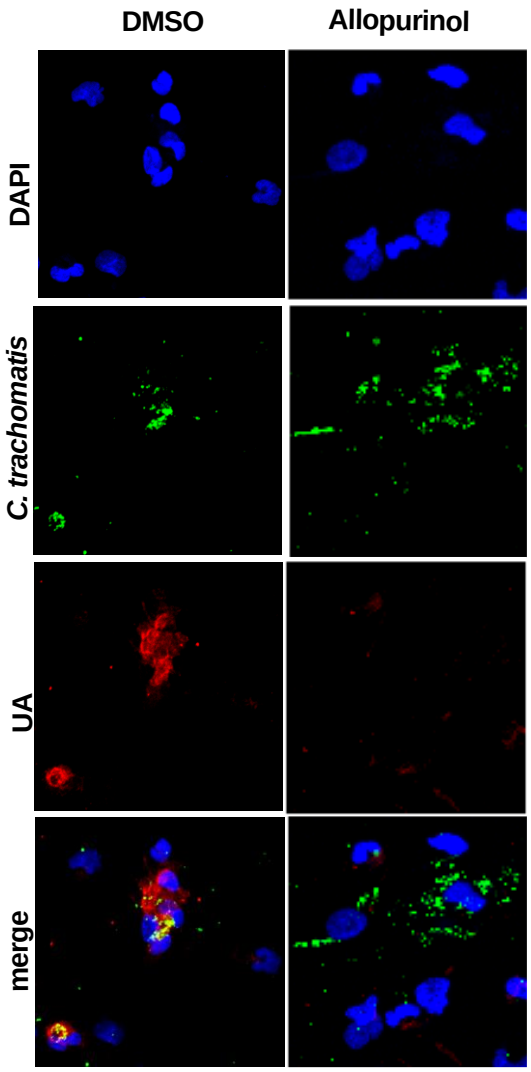

Figure 38 Uric acid staining in THP-1 cells infected with *C. trachomatis* and treated with allopurinol. THP-1 cells were stimulated with IFN-γ + LPS, infected with *C. trachomatis* at MOI 30, and treated with allopurinol or DMSO. Cells were stained for *C. trachomatis* (green), uric acid (red) and DAPI (blue).

Previous studies have suggested that mitochondrial ROS increases downstream of UA production to activate NLRP3 inflammasome (Cruz et al., 2007). Consistently, an increase of mitochondrial ROS in *C. trachomatis*-infected cell was observed, which was abolished thereof by allopurinol treatment (Fig. 39). Thus, multiple lines of evidences support the conclusion that UA is produced upon *C. trachomatis* infection in an hGBP1-dependent manner.

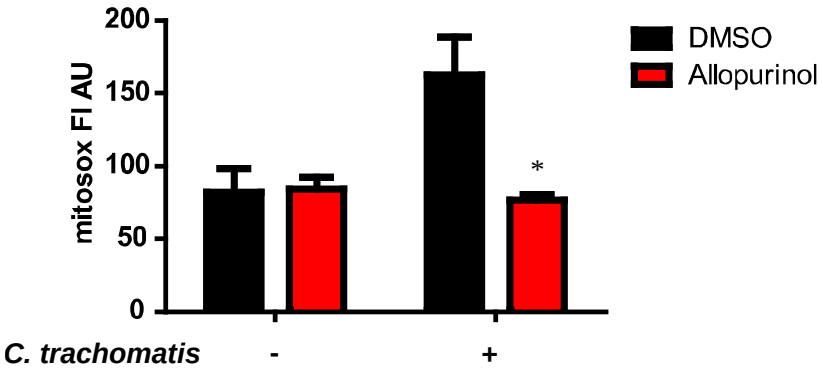

Figure 39 Production of mitochondrial ROS in THP-1 cells infected with *C. trachomatis* and treated with allopurinol. Fluorescence intensity measurements of mitochondrial ROS in THP-1 cells infected or not with *C. trachomatis* and treated or not with 500 µM allopurinol, n=3; two-way ANOVA.

Lastly, it was tested whether infection-induced inflammasome activation could be rescued in hGBP1 KO cells and G68A mutants by feeding back intermediate metabolites of UA catabolism (Fig. 40A). As GTP itself is not cell permeable nor taken up by the cells directly, cells were alternatively treated with guanine or guanosine. Remarkably, the addition of guanine and guanosine to hGBP1 KO cells and G68A mutants to a dose-dependent increase of IL-1β secretion and pyroptosis (Fig. 40A-40D).

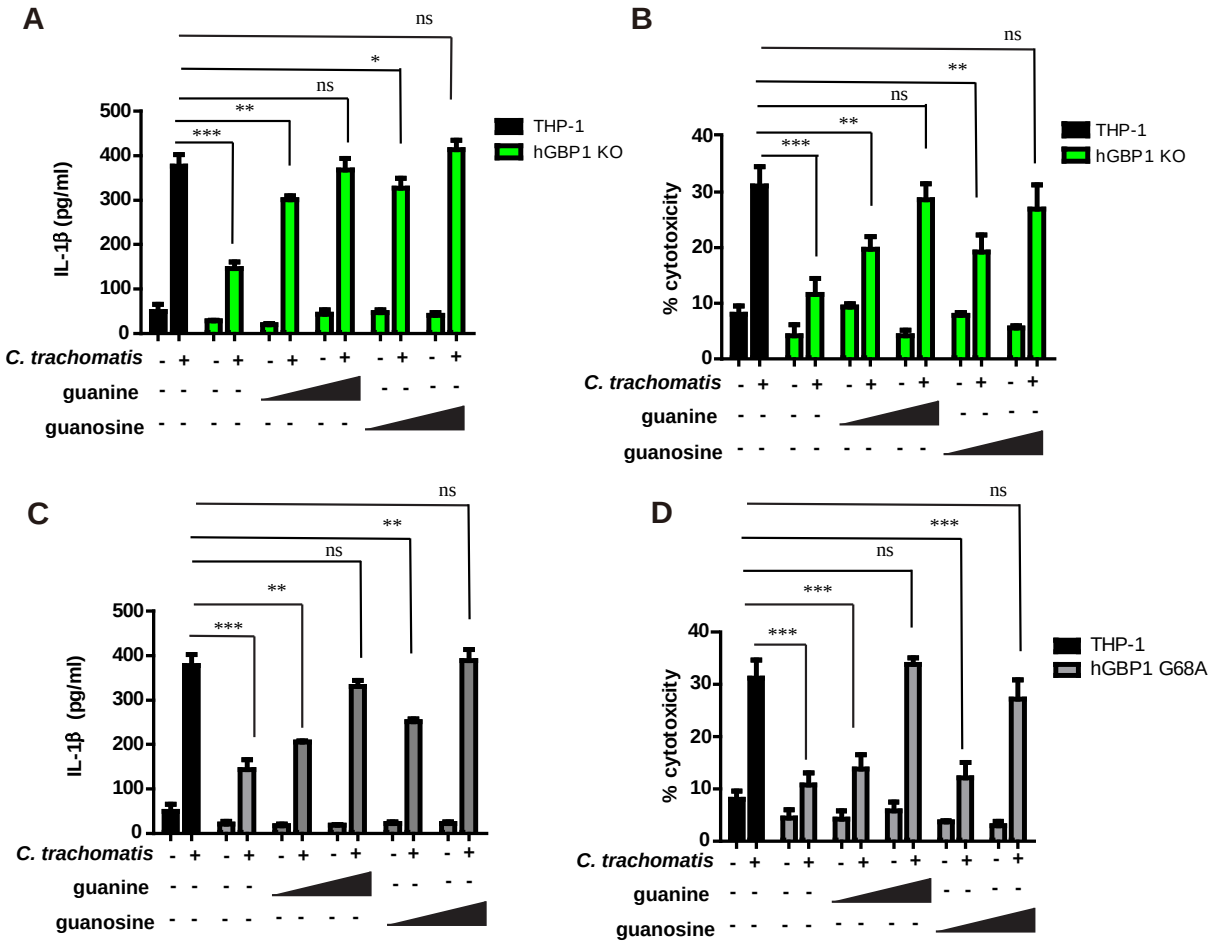

Figure 40 Rescue of inflammasome activation in hGBP1 KO and hGBP1 G68A THP-1 cells infected with *C. trachomatis*. (A) IL-1β ELISA and (B) LDH release of hGBP1 KO THP-1 cells, which were infected with *C. trachomatis* at MOI 30 for 24 h and treated with increasing concentrations of guanine or guanosine (0.5 mM and 1 mM), n=3; statistical significance was determined in comparison to the parental cell line by two-way ANOVA. IL-1β ELISA (C) and LDH release (D) of hGBP1 WT or G68A mutant cells infected with *C. trachomatis* at MOI 30 for 24 h and treated with increasing concentrations of guanine or guanosine (0.25 mM and 0.5 mM), n=3; significance was determined in comparison to the parental cells by two-way ANOVA

In summary, these results indicate that hGBP1-mediated inflammasome activation occurs through consecutive cleavage of GTP to GMP, leading to local accumulation of UA, consequently activating the NLRP3 inflammasome.

5. Discussion

In this study, a specific catalytic mutant of hGBP1 that retains cooperative GTP hydrolysis (i.e., at a comparable rate to the WT protein), while being impaired in the consecutive hydrolysis step, was generated. By employing this mutant, hGBP1's unique function in GMP production using an infection model with the obligate intracellular pathogen *C. trachomatis* was explored. hGBP1 has been implicated in restricting pathogenic growth and mediating inflammasome activation. Furthermore, it was revealed that the GTPase activity of hGBP1 tightly coordinates these two functions. Thus, similar to other dynamin-related proteins, recruitment of hGBP1 to the PCV is thought to activate GTP hydrolysis, which may be linked to membrane remodeling and the destruction of the PCV (Daumke and Praefcke, 2016; Meunier et al., 2014). Ultimately, this work demonstrates that the succeeding second nucleotide cleavage step produced GMP, which then serves as a precursor of uric acid. In this scenario, the PCV acts as a platform that mediates the recruitment of hGBP1 and xanthine oxidase to the *C. trachomatis* inclusions to convert GMP to uric acid and initiate NLRP3 inflammasome signaling, leading to inflammatory cell death and the release of pro-inflammatory cytokines. In the following, the rationale of generating a specific GMP production mutant and its implication in previous and following studies, as well as the role of the first step of GTP hydrolysis in membrane remodeling and bacterial restriction will be discussed. Furthermore, novel insights into uric acid-mediated NLRP3 inflammasome activation and future clinical implications of this work in treatment of *C. trachomatis*-induced inflammatory diseases will be elucidated.

5.1 hGBP1 G68A – a specific GMP production mutant

To date, the consecutive cleavage mechanism of hGBP1 has been studied extensively, offering novel insights into residues involved in binding and stabilizing all three nucleotides (GTP, GDP, GMP) as well as their transition states in the LG domain. However, the functional significance of this two-step cleavage mechanism in the restriction of intracellular pathogens is poorly understood and raises the demand for a specific mutation that impairs the GMP production while retaining the fast-cooperative WT-like kinetics. Mutation studies based on the consensus motifs (G1-G4) have

elucidated commonalities as well as differences between hGBP1 and other members of the dynamin superfamily and reveal that, similarly to human Atlastin-1, hGBP1 employs a catalytic arginine finger (R48) that rearranges into a catalytically active state upon nucleotide binding and LG-domain dimerization. Mutation of this arginine residue does not prevent the protein from binding nucleotide and dimerization, but the mutant remains catalytically inactive. Thus, similarly to other dynamin superfamily proteins, mutations in the conserved switch regions of hGBP1 impair GTP hydrolysis (Ponten et al., 1997; Song et al., 2004).

However, the biggest difference between hGBP1 and other members of the dynamin superfamily is the consecutive cleavage of GTP to GMP, where the two steps share the same cleavage mechanism via the same residues. This phenomenon renders the identification of residues specific to the second cleavage step a tremendous challenge. However, this special consecutive cleavage mechanism is based on the movement of the nucleotide within the binding pocket, placing the β-phosphate at the same position as the γ-phosphate. Therefore, point mutations for several glycine residues were designed that potentially sterically lock the movement of the nucleotide, suppressing the second cleavage step. Interestingly, among GBPs, GBP5 lacks the ability to cleave GTP to GMP but produces GDP instead. Most residues in the G motifs of the G domain are conserved between GBPs. Thus, whichever residues involved in enabling consecutive cleavage must differ between hGBP1 and hGBP5. G68 is located between the P-loop and switch I and is not conserved between dynamin superfamily members or GBPs. Crystal structures of hGBP1 reveal that it is in close proximity to the ribose moiety of the nucleotide and direct comparison of the amino acid sequence of GBP1 and GBP5 show that it is mutated to alanine. Therefore, G68 was a very good candidate for a point mutation to alanine that could specifically inhibit consecutive GTP hydrolysis. Indeed, mutation of G68 to alanine abolished GMP production while maintaining a fast cooperative GTP hydrolysis rate comparable to WT hGBP1.

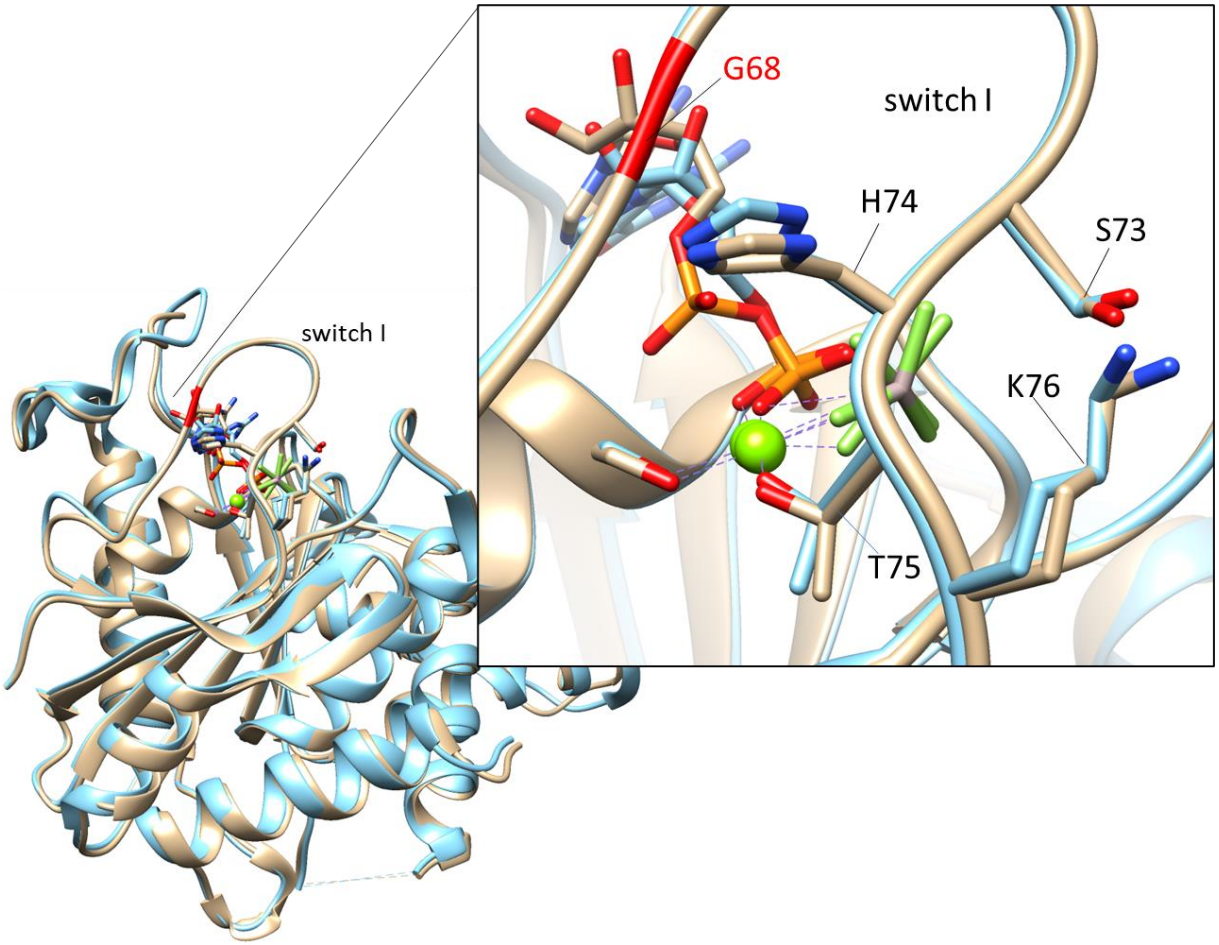

Figure 41 Residues of switch I of hGBP1 LG domain. Superimposition and magnification of hGBP1 G-domain (switch I region) structures bound to GDP·AlF_x (brown, pdb 2b92) and GMP·AlF_x (blue, pdb 2b8w). Phosphate residues are colored in orange, oxygen atoms in red, nitrogen atoms in blue, Mg^{2+} as green ball and ALF_x as green sticks.

Previous work by Praefcke and colleagues identified residues H74 and L76 of switch I as GMP production mutants. GTP hydrolysis data reveals that mutants H74A and K76A retain cooperativity but exhibit impaired GMP production and significantly reduced GTP hydrolysis activity (Praefcke et al., 2004a). This study recapitulates these findings; however, the newly identified G68A mutant not only shows impaired GMP production but also retains a similarly high GTP hydrolysis activity. Interestingly, H74 and K76 are located in switch I in between residues T75 and S73, both of which are required for positioning a catalytic water molecule (see Fig. 42) (Ghosh et al., 2006a). H74 and K76 contain large bulky side chains that can only be positioned in a restricted area within the tertiary structure of the LG-domain. When mutated to alanine,

the small CH_3 side chain allows different conformations within its allocated space, indirectly permitting higher peptide backbone flexibility and perhaps flexible positioning of residues T75 or S73, thereby mildly impairing GTP hydrolysis. Further evidence underlining the hypothesis that residue K76 (and likely H74) is a mild GTP hydrolysis mutant is shown in Fig. 13D where at a given end point of GTP hydrolysis, WT hGBP1 has hydrolyzed GTP to GMP and G68A hGBP1 has hydrolyzed GTP to GDP predominantly, whereas hGBP1 K76A has only partially hydrolyzed GTP to GDP.

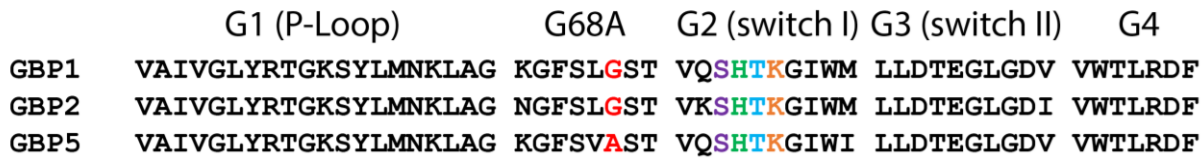

Figure 42 Sequence alignment of the G1-G4 motifs in GBP1, GBP2 and GBP5. G68 and A68 are indicated in red, S73 in purple, H74 in green, T75 in blue and K76 in orange

Lastly, the design of the G68A mutant allows a clear assignment of the function of consecutive GTP hydrolysis. In this study, G68A mutant revealed that GMP production is not required for bacterial restriction. THP-1 cells expressing hGBP1 G68A were able to restrict *C. trachomatis* growth comparable to cells expressing the WT protein, whereas cells expressing K76A show partial impairment of bacterial restriction.

According to these results, several studies that have referred to K76A or H74A as GMP production mutants need to be revisited and conclusions drawn from these experiments should be reevaluated.

Taken together, the novel GMP production mutant hGBP1 G68A reveals, for the first time, that bacterial restriction is independent of the second hydrolysis step but is required to mount the effector immune response through inflammasome activation.

5.2 Membrane remodeling function, bacterial restriction and GTP hydrolysis by GBP1

Although many studies suggest that GBPs are active on PCVs or pathogenic membranes, little is known about the nature of the membrane remodeling function. The closely related IRGs, which have been shown to target PCVs, can induce autophagy-dependent elimination and growth restriction of intracellular bacteria or direct PCV membrane destabilization (Haldar et al., 2013; Man et al., 2016; Petkova et al., 2013). A similar role has been suggested for GBPs, although several contradicting studies postulating mutually exclusive mechanisms of GBP action have been published (ref, ref, ref).

Most studies focus on murine GBPs as genetic data is more accessible *in vivo* than for the human system. However, the lack of the perhaps functionally redundant IRGs in the human system suggests that human GBPs might fulfill a greater variety of functions. Common among the 11 murine GBPs and the 7 human GBPs is that GBP1, GBP2 and GBP5 exhibit a C-terminal CAAX motif and are thus isoprenylated. This allows these GBPs to target PCVs or the membrane of cytosolic bacteria and subsequently restrict the growth of pathogens (Kravets et al., 2012; Modiano et al., 2005). How GBPs target pathogens or their vacuoles specifically remains unknown, as the PCV membrane consists of host lipids. A recent study implies that GBP1 binds LPS directly. Thus, GBP1 oligomerization was suggested to concentrate LPS, leading to disintegration of the bacterial membrane (Kutsch et al., 2020). This model potentially explains the mechanism of GBP-mediated inflammasome activation in response to cytosolic gram-negative bacteria. However, many studies show that GBPs not only target gram-negative bacteria, but also confer resistance to gram-positive bacteria and protozoa such as *Mycobacterium bovis*, *Listeria monocytogenes* and *Toxoplasma gondii* (Degrandi et al., 2013; Kim et al., 2011; Kravets et al., 2012; Shenoy et al., 2012; Yamamoto et al., 2012). Furthermore, recombinantly expressed and farnesylated human GBP1 can bind many different lipids promiscuously in a nucleotide-dependent manner (Fres et al., 2010).

In 2013, Al-Zeer and colleagues postulated that human GBP1 and GBP2 restrict *C. trachomatis* growth by mediating autophagosome fusion of inclusions and subsequent bacterial clearance from the host cell (Al-Zeer et al., 2013) . The hypothesis of a fusion

mechanism is also supported by structural similarities to Atlastin-1. Atlastin-1 is partially membrane-inserted due to its C-terminal transmembrane domain and dimerizes in a nucleotide-dependent manner, which leads to tethering of opposing ER membranes, ultimately mediating GTP hydrolysis-dependent membrane fusion (Hu et al., 2009; Orso et al., 2009). Fluorescence resonance energy transfer measurements with a soluble construct consisting of the GTPase domain and the helical bundle revealed the movements of these domains during nucleotide hydrolysis (Byrnes et al., 2013). Also, crystal structures of the Atlastin-1 dimer showed two profoundly different conformations of the helical domain relative to the GTPase domains in the GMPPNP and GDP-bound state. The GDP-bound form embodies the open conformation with the two GTPase domains facing each other and the helical domains protruding from the GTPase dimer in opposite directions. The second structure features Atlastin-1 bound to GMPPNP, in which the helical domains extend in parallel directions and interact with each other (Byrnes et al., 2013; Byrnes and Sondermann, 2011b).

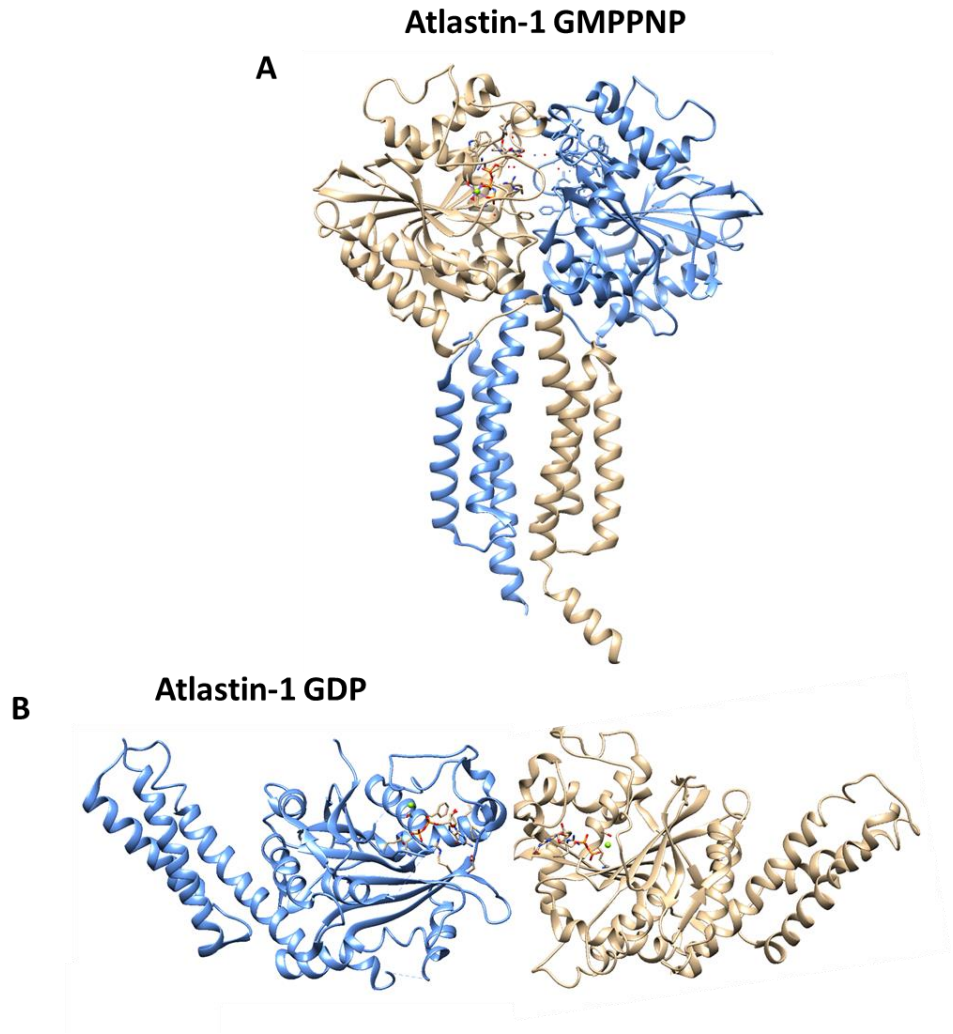

Figure 43 Conformational changes of Atlastin-1 upon GTP hydrolysis. Structure of atlastin in the (A) GMPPNP- (pdb 4IDP) and (B) GDP-bound forms (3Q5E).

Biochemical and structural studies of hGBP1 reveal a tight intramolecular interaction between the C-terminal α6/6' helices and the N-terminal LG-domain that is only released upon GTP hydrolysis, leading to major rearrangement of the helical domain (Vöpel et al., 2010). Furthermore, *in vitro* farnesylated hGBP1 can assemble into large ring-shaped oligomers in the presence of the transition state mimic GDP ALF_x that can oligomerize into rod-shaped ring polymers in the presence of GTP. These rings do not form in the presence of the slowly hydrolyzing GTP-analog GTPγS, indicating that GTP hydrolysis is required for the formation of rings. Biochemical assays show that farnesylated hGBP1 can tether giant unilamellar vesicles (GUVs) in the presence of GTP and GTPγS. Where binding to GTPγS lead to a stable attachment of two vesicles and the presence of GTP allowed for repetition of short-lived hemi-fusion events

(Shydlovskyi et al., 2017). However, the significance of the second hydrolysis step for these events have remained unknown. Results of this thesis reveal that the GMP production mutant hGBP1 G68A can bind Folch liposomes and form an oligomeric ring structure in the presence of GDP AlF_x (see Fig. 16), but the functionality of this mutant in tethering GUVs has not been tested. The ability of THP-1 cells expressing hGBP1 G68A to restrict the growth of C. *trachomatis* with similar efficiency as the WT protein would suggest, that GMP production is not required for hemi-fusion of GUVs or any membrane remodeling event of hGBP1 that is significant *in vivo*. In contrast, other studies indicate that GBPs might lyse PCVs or bacterial membranes. Arguably, Salmonella PCVs that stain positive for GBPs, also are stained positive for galectin-8, a protein known to bind β-galactins of the inner leaflet of the PCV membrane, indicating that a PCV membrane rupture must have occurred. Also, more cytosolic Salmonella were found in WT BMDMs compared to GBP^{chr3} KO, suggesting that more salmonella escape the PCV in the presence of GBPs (Pilla et al., 2014). Additional studies demonstrate PCV lysis of the parasite Toxoplasma *gondii* in BMDM and MEF cells (Kravets et al., 2016). However, later studies with *Francisella novidica* and *Legionella pneumophila* indicate that GBP- dependent bacteriolysis occurs after PCV rupture (Liu et al., 2018; Man et al., 2015; Meunier et al., 2014; Meunier et al., 2015). Most studies share the consensus that GBPs liberate PAMPs of pathogens that can be subsequently sensed by either canonical or non-conical inflammasomes, supporting a lysis mechanism. However, studies of the murine pathogen C. *muridarum* suggest that inflammasome activation occurs independently of membrane targeting by GBPs, as GBPs do not localize to C. *muridarum* inclusions but can still activate the NLRP3 inflammasome (Finethy et al., 2015). In summary, the results of this thesis suggest that GBP-mediated bacterial restriction based on membrane remodeling occurs independent of the second hydrolysis step of GTP. Clearly, further investigation is required to characterize the nature of the membrane remodeling activity performed by GBPs.

5.3 GBPs in the activation of inflammasome and cell death pathways

Murine and human GBPs have been demonstrated to activate a plethora of inflammasome and cell death pathways. Except for *C. muridarum*, mouse GBPs can localize to PCVs or bacterial membranes, which is followed by PCV or bacteriolysis by a so far unknown mechanism. Subsequently, bacterial PAMPs such as LPS are released that can be sensed by caspase 11 (caspase-4/5 in human) and leads to the cleavage and activation of gasdermin-D, a pore forming protein that translocates to the plasma membrane and causes pyroptosis (Kayagaki et al., 2015; Lagrange et al., 2018; Meunier et al., 2014; Pilla et al., 2014). Another PAMP that is released into the cytosol is bacterial DNA, which can lead to the activation of the canonical AIM2 inflammsome in response to *Francisella novidica* infection (Meunier et al., 2015). In the case of *C. muridarum* where inclusion localization is not detected or *C. trachomatis*, Gbp^{Chr3} mediate activation of the canonical NLRP3 or AIM2 inflammasome (Finethy et al., 2015). Also, mouse GBP5 is proposed to be involved in the activation of the canonical inflammasome pathway during infection with the gram-positive bacterium *L. monocytogenes* (Shenoy et al., 2012). Human GBPs have been shown to localize to the *C. trachomatis* inclusion, *S. typhimurium* vacuole and to the outer membrane of *Shigella flexneri* (Al-Zeer et al., 2013; Meunier et al., 2014). hGBP1 has been demonstrated to promote caspase-4 dependent pyroptosis in response to *S. typhimurium* infection (Santos et al., 2020) and hGBP2 in response to *F. novidica* infection (Lagrange et al., 2018). Human GBP1 can not only promote inflammatory cell death but also apoptosis during *Toxoplasma gondii* infection over AIM2 and caspase-8 activation (Fisch et al., 2019). Recent studies suggest that direct binding of LPS by GBP1 leads to the activation of the non-canonical inflammasome either through LPS dependent bacteriolysis or subsequent recruitment of other GBPs to form an activation platform for caspase-4 in response to Shigella and Salmonella infection (Kutsch et al., 2020; Santos et al., 2020). However, there is no consensus between the studies, which specific LPS antigen is involved or whether nucleotide is necessary for LPS binding. In this work, human GBP1 was shown to mediate canonical NLRP3 activation during *C. trachomatis* infection through consecutive GTP hydrolysis in a mechanism independent of bacterial restriction. The consensus among all studies is that GBPs restrict pathogenic growth within the host cell and mediate inflammasome activation. Yet, the existence of one common mechanism to explain these key

functions is rather unlikely. Moreover, it seems that the inflammasome pathway activated is specific to the pathogen invading the host cell, rendering GBPs flexible and versatile factors in antimicrobial defense. Since several independent effector mechanism of GBPs appear to exist, it would be intriguing to test the newly generated GMP production mutant in the context of different infection models and further dissect the specificity of this unique function in host defense.

5.4 Uric acid as a NLRP3 activator

Uric acid is the main product of purine catabolism and is regularly secreted in urine (Maesaka and Fishbane, 1998). Compared to other organisms, higher apes and humans lack an enzyme called uricase that oxidizes uric acid to 5-hydroxyisourate that can spontaneously dissociate into allantoin and water. Therefore, uric acid levels in humans are several times higher than in other organisms (Oda et al., 2002). Accumulation of uric acid can lead to crystal formation, a DAMP released from deoxygenated tissues and dying cells (Shi et al., 2003). This DAMP can activate the immune system as it leads to an increase in ROS, decrease in nitric oxide, activates chemotaxes, induces pro-inflammatory signaling pathways and triggers the expression of pro-inflammatory cytokines (Di Giovine et al., 1987; Martinon et al., 2006b; So and Thorens, 2010). Besides uric acid, silica and cholesterol crystals are known to induce inflammasome activation (Dostert et al., 2008; Duewell et al., 2010; Hornung et al., 2008), by causing lysosomal damage and the release of lysosomal content into the cytosol (Lima et al., 2013). Lysosomal proteases can damage vital proteins in the cytosol and affect other organelles such as mitochondria, which leads to an increase in mitochondrial ROS (mtROS) production (Schaefer, 2014), release of oxidized mitochondrial DNA and NLRP3 inflammasome activation (Shimada et al., 2012b). Uric acid crystals can also directly interact with membranes and activate potassium-ion (K^+) efflux, suggesting the convergence of many NLRP3 activating pathways (Mariathasan et al., 2006). Recent studies reveal that serum uric acid levels are associated with inflammatory diseases such as gout-related disease and preeclampsia (Acauan Filho et al., 2016; Crișan et al., 2016) and soluble uric acid can activate the NLRP3 inflammasome in a mtROS dependent manner (Braga et al., 2017). Elevated uric acid levels are often associated with purine-rich diets of modern humans (Zhang et al., 2012), but other causes remain unexplored.

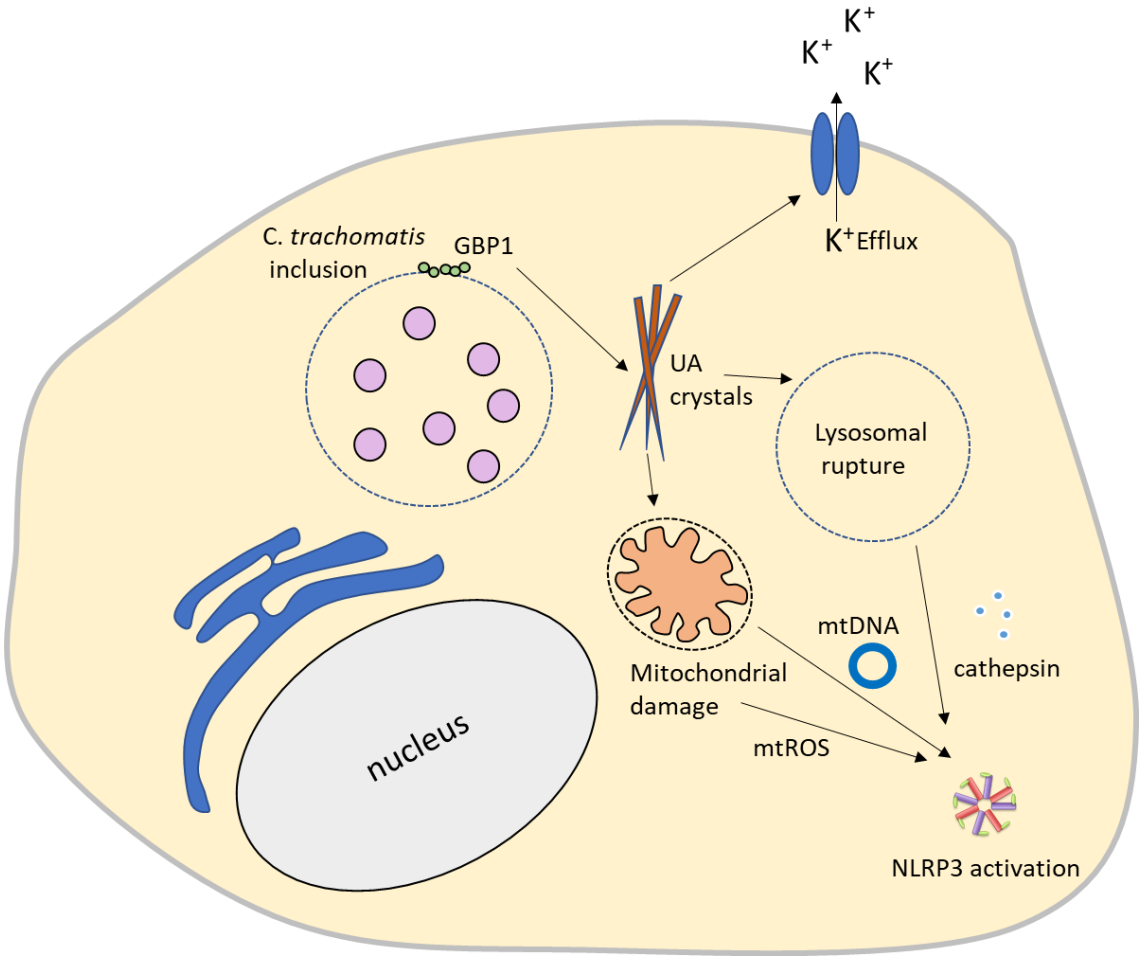

Figure 44 NLRP3 activation by uric acid. Uric acid accumulates as a degradation product of GMP produced by hGBP1. Uric acid crystals can stimulate NLRP3 activation by inducing mitochondrial or lysosomal damage, leading to the release of mitochondrial DNA (mtDNA), mitochondrial ROS (mtROS) or cathepsin. Uric acid also induces K^+ Efflux that is a NLRP3 activating DAMP.

Results in this thesis indicate that uric acid accumulates in cells infected with *C. trachomatis* and that this accumulation is a direct cause of GBP1-mediated GMP production. THP-1 cells that do not express GBP1 or GTP hydrolysis mutants lead to lower levels of uric acid and impaired NLRP3 inflammasome activation. The results further demonstrate that the succeeding second nucleotide cleavage step by GBP1 produces GMP, which then serves as a precursor of uric acid. In this scenario, the PCV acts as a platform that mediates the recruitment of hGBP1 and xanthine oxidase to the *C. trachomatis* inclusions to initiate inflammasome signaling. At the same time, *C. trachomatis* infection leads to an increase in GDA expression (Fig. 30). Thus far, it has been unclear whether this regulation of nucleotide metabolizing enzymes is merely part of a host defense mechanism or a way of *C. trachomatis* to redirect the

host metabolism as part of a survival strategy. Downregulation of GDA did not affect pathogenic growth, suggesting that GDA activity and UA formation are not required for survival of *C. trachomatis* under regular conditions. However, loss of hGBP1-mediated GMP production reduced *C. trachomatis*-induced cell death, implying a direct link between guanine catabolism and inflammasome activation. Although a contribution of hGBP2 to *C. trachomatis*-dependent UA formation was ruled out, it cannot be excluded for other hGBPs that execute the second hydrolysis step. Another recent study indicates that uric acid crystals form during infection of enteropathogenic *Escherichia coli* (EPEC) and Shiga-toxic *E.coli* (STEC) in the gastrointestinal tract (Crane et al., 2016). Although the physical state of uric acid that triggers NLPR3 inflammasome activation has not been addressed in this thesis, staining data with an antibody that detects uric acid crystals as an epitope indicate that uric acid crystals accumulate in THP-1 macrophages upon C. *trachomatis* infection. Furthermore, mtROS is produced during C. *trachomatis* infection that can be reduced with an inhibitor of the nucleotide-uric acid catabolism pathway, suggesting that NLRP3 activation occurs in a mtROS-dependent manner caused by uric acid crystal formation. Interestingly, intracellular levels of uric acid in THP-1 cells did not differ between non-infected and infected cells. In fact, differences in uric acid levels were only detected in the low-serum medium supernatant upon infection, suggesting that uric acid is secreted rapidly, when accumulated. While treatment with NLRP3 inhibitor MCC950 did significantly reduce pyroptosis, it did not lead to better detection of intracellular uric acid levels. Therefore, extracellular accumulation of uric acid may occur through direct damage of the plasma membrane by uric acid crystals.

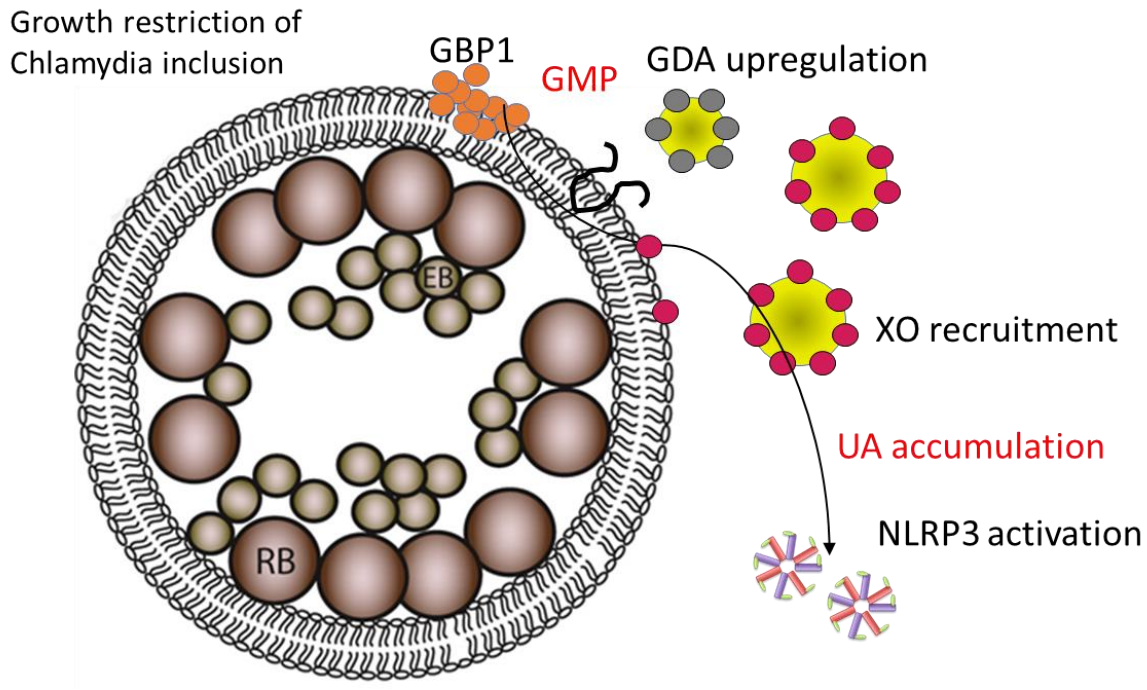

Figure 45 Model for hGBP1-mediated NLRP3 inflammasome activation during C. *trachomatis* infection. Upon *C. trachomatis* infection, hGBP1 is recruited to the Chlamydia inclusion and oligomerizes on the inclusion membrane. C. *trachomatis* infection leads to the upregulation of GDA expression and recruitment of XO to the inclusion membrane. GMP produced by hGBP1 is catabolized to uric acid in a specialized pipeline. Uric acid leads to NLRP3 activation.

In summary, this study describes a novel model of canonical inflammasome activation through GBP1 in response to *C. trachomatis* infection. In this scenario, GBP1 produces GMP that is rapidly converted into the danger signal uric acid, which in turn activates the NLRP3 inflammasome leading to cytokine release and pyroptosis. In the future, it might be useful to test whether inflammasome activation is triggered via the same pathway in response to other obligate intracellular pathogens.

5.5 Future implications of allopurinol in the treatment of *C. trachomatis* infection induced acute inflammation

While GBPs have been associated with inflammasome activation in response to infection with C. *trachomatis* and other intracellular pathogen, the mechanism of GBP-mediated inflammasome activation was unclear. Results of this thesis demonstrate that NLRP3 inflammasome activation occurs through GBP1-mediated GMP production that is further catabolized to uric acid. Inhibition of the catabolism of GMP to uric acid by gene silencing of GDA leads to impaired NLRP3 inflammasome activation, cytokine release and pyroptosis. Treatment with the clinically approved XO inhibitor allopurinol showed the same effects in a dose-dependent manner in THP-1 cells. Additionally, allopurinol leads to reduction of C. *trachomatis* infection induced mtROS generation in THP-1 cells, suggesting that increase in mtROS is directly dependent on uric acid production. As an obligate intracellular pathogen, *C. trachomatis* cannot synthesize purines or pyrimidines and depends on the host cell for these metabolites (Tipples and McClarty, 1993). However, neither reduction of the GDA protein level nor treatment with allopurinol significantly reduced the number of *C. trachomatis* inclusions in THP-1 24 h post infection. A possible explanation for this phenomenon is, that other purine and pyrimidines could be acquired by interconversion of intermediate metabolites in the pathway. Although the immediate growth of *C. trachomatis* was not affected, the influence of the inhibition of nucleotide catabolism pathways during further development of the infectious progeny has not been tested. Mouse macrophages utilize multiple inflammasome pathways in response to *C. trachomatis* infection (Finethy et al., 2015). Conversely, results of this thesis indicate that the uric acid-NLRP3 axis is mainly responsible for the host response to *C. trachomatis* infections in humans. Furthermore, the data suggest that inflammasome activation in human macrophages in response to C. *trachomatis* infection is rather independent of PAMP liberation by hGBPs, substantiating the finding that inflammation occurs over a unified pathway. Therefore, allopurinol could be a potential therapeutic application in reducing acute inflammation in patients suffering from *C. trachomatis* infection. Thus far, allopurinol has been applied in the treatment of acute gout to reduce the accumulation of uric acid crystals in joints and reduce acute inflammation (Hitchings and Elion, 1963; Pacher et al., 2006). However, it would be intriguing to test whether inflammasome activation is triggered via the same pathway

in response to other intracellular pathogen and could be acutely treated with allopurinol.

6. Summary

Human guanylate binding protein 1 (hGBP1) belongs to the dynamin superfamily of GTPases and conveys host defense against intracellular bacteria and parasites. During infection, hGBP1 is recruited to pathogen-containing vacuoles, such as *Chlamydia trachomatis* inclusions, restricts pathogenic growth, and induces the activation of the inflammasome pathway. hGBP1 has a unique catalytic activity to hydrolyze GTP to GMP in two consecutive cleavage steps. However, the functional significance of this activity in host defense remains elusive. In this thesis, a structure-guided mutant that specifically abrogates GMP production, while maintaining fast cooperative GTP hydrolysis, was generated. Complementation experiments in human monocytes/macrophages show that hGBP1-mediated GMP production is dispensable for restricting *Chlamydia trachomatis* growth but is required for inflammasome activation. Mechanistically, GMP is catabolized to uric acid, which in turn activates the NLRP3 inflammasome via induction of mitochondrial ROS. Our study demonstrates that the unique enzymology of hGBP1 coordinates bacterial growth restriction and inflammasome signaling.

7. Zusammenfassung

Das zur Dynamin-Superfamilie gehörende humane Guanylate Binding Protein 1 (hGBP1) ist für die zelluläre Immunabwehr gegen Bakterien und Parasiten verantwortlich. Bei einer Infektion wird hGBP1 zu bakteriellen Vakuolen, z.B. *Chlamydia trachomatis* Inklusionen, rekrutiert, wodurch es zur Restriktion des bakteriellen Wachstums kommt. Zudem trägt hGBP1 zur Aktivierung des Inflammasoms bei. hGBP1 hat einen einzigartigen katalytischen Mechanismus, durch den es GTP zu GMP in zwei aufeinander folgenden Stufen hydrolysieren kann. Die funktionelle Relevanz dieses Mechanismus in der bakteriellen Abwehr ist allerdings noch nicht erforscht.

In dieser Doktorarbeit wurde diese Frage mit Hilfe einer Kristallstruktur-basierten Mutante erforscht. Diese Mutante hydrolysierte GTP nur noch zu GDP, dies aber mit derselben kooperativen Aktivität wie der Wildtyp. Die Funktionalität dieser Mutante wurde mit Hilfe von Komplementationsexperimenten in humanen Monozyten und Makrophagen ermittelt. Die Ergebnisse zeigen, dass GMP Produktion durch hGBP1 nicht notwendig für die Restriktion bakteriellen Wachstums ist. Stattdessen ist der zweite Hydrolyse-Schritt für die Aktivierung des NLRP3 Inflammasoms wichtig. Hierbei wird das von hGBP1 produzierte GMP zur Harnsäure umgesetzt, welches das NLRP3 Inflammasom durch mitochondrialen reaktiven Sauerstoff aktiviert. Diese Doktorarbeit zeigt daher auf, wie hGBP1 die Restriktion bakteriellen Wachstums und die Inflammasom Aktivierung durch seinen einzigartigen enzymatischen Mechanismus koordiniert.

8. Appendix

Appendix A-Dynamin superfamily structures displayed

Protein	PDB code	Nucleotide loading state	Species	Method	Resolution (Å)	Reference
GBP1	1DG3	Nucleotide-free	Homo sapiens	X-ray diffraction	1.8	(Prakash et al., 2000)
	2B8W	GMP·AlF_x	Homo sapiens	X-ray diffraction	2.22	(Ghosh et al., 2006a)
	2B92	GDP·AlF_x	Homo sapiens	X-ray diffraction	3.2	(Ghosh et al., 2006a)
Atlastin-1	4IDP	GMPPNP	Homo sapiens	X-Ray diffraction	2.59	(Byrnes et al., 2013)
	3Q5E	GDP	Homo sapiens	X-Ray diffraction	3.01	(Byrnes and Sondermann, 2011a)

Appendix B-List of instruments

Instruments	Manufacturer
Agarose Gel Electrophoresis System	*Biometra Göttingen D*
Äkta FPLC	OLS,Bremen D
Äkta Prime Plus	Invitrogen, Darmstadt D
Äkta Purifier	Biorad, Hercules, USA
Amicon centrifugal filter devices	Millipore, Billersica, USA
Benchtop Centrifuge 5415 D	Eppendorf, Hamburg, D
Benchtop Centrifuge 5415 R	Thermofisher Scientific, Dreiech, D
Benchtop Centrifuge 5804 R	Eppendorf, Hamburg, D
Butyl Sepharose 4B Fast Flow	GE Healthcare, Piscataway, USA
Cell culture flasks	Eppendorf, Hamburg, D
Cell culture plates	Eppendorf, Hamburg, D
Centrifuge Avanti J-26 XP	Pneumatic Microfluidics, Newton, USA
Chromotography column GST HP 1 mL	Beckman Coulter, Krefeld, D
Chromotography column HisTrap 1 mL	Beckman Coulter, Krefeld, D
Chromotography column material GSH Sepharose 4B	Beckman Coulter, Krefeld, D
Chromotography column Ni Sepharose HP	GE Healthcare, Piscataway, USA
Chromotography column Superdex 200 16/60,10/300	GE Healthcare, Piscataway, USA
Epoch2 microplate reater	GE Healthcare, Piscataway, USA
Fluidizer M-110L	GE Healthcare, Piscataway, USA
Heracell 150 cell culture incubator	GE Healthcare, Piscataway, USA
HPLC Infinity	Ismatec, Glattbrug, CH
Hypersil ODS guard column	GE Healthcare, Piscataway, USA
Peristaltic Pump Reglo Analog ISM827B	GE Healthcare, Piscataway, USA
pH-Meter	GE Healthcare, Piscataway, USA
Photometer BioPhotometer	Agilent Technologies, Santa Clara, USA
Photometer NanoDrop 2000	Agilent Technologies, Santa Clara, USA

Reversed-phase ODS-2 Hypersil HLPC column	Thermofisher Scientific, Dreiech, D
Scales	Mettler-Toledo, Giessen, D
SDS OAGE System Xcell sure Lock	Satorius, Göttingen, D
Shaker incubator Innova44	New Brunswick Scientific, Edison, USA
Synergy H1 plate fluorescence microplate reader	TPP, Trasadingen, CH
Thermocycler TGradient	TPP, Trasadingen, CH
Ultracentrifuge Optima L-100K	Biotek, Winooski, USA
Ultracentrifuge Optima TLX	Biotek, Winooski, USA
Western blot system	Corning®, corning,USA
White, polystyrene medium binding 96-well ELISA plates	Carl Zeiss, Oberkochen, D
Zeiss EM910	Carl Zeiss, Oberkochen, D
ZEISS LSM 700 Confocal Laser Scanning Microscope	Carl Zeiss, Oberkochen, D
Zeiss standard 20	Thermofisher Scientific, Dreiech, D

Appendix C-List of Chemicals

Chemical	Catalog number	Manufacturer
2-Log DNA ladder	N3200S	NEB, Frankfurt a.M., D
Acetic acid	3783.5	Roth, Karlsruhe, D
Acetone	9372.2	Roth, Karlsruhe, D
Acetonitrile	CN20.2	Roth, Karlsruhe, D
Agarose	2267.3	Roth, Karlsruhe, D
Allopurinol	10012597	Cayman Chemical Company, Ann Arbor, USA
Aluminum chloride	563919	Sigma-Aldrich, Steinheim. D
Bafilomycin A1	ab120497	Abcam,UK
carbenicillin disodium salt	6344.2	Roth, Karlsruhe, D
Coomassie brilliant blue R 250	3862.2	Roth, Karlsruhe, D
DTT	6908.2	Roth, Karlsruhe, D
EDTA	8040.2	Roth, Karlsruhe, D
Ethanol	5054.2	Roth, Karlsruhe, D
Ethidium bromide	2218.1	Roth, Karlsruhe, D
Ferrostatin-1	A13247	Adooq Bioscience, Irvine, USA
Fetal bovine serum	A11,211	PAA laboratories
Flagellin	AG-40B-0025-C010	AdipoGen, Liestal, CH
GDP	A11-211	PAA laboratories,Pasching, D
Glutathione Sepharose 4B	27-4574-01	Amersham,Piscatawy,USA
Glycerol	3783.1	Roth, Karlsruhe, D
GSH reduced	3541	Calbiochem, Darmstadt, D
GTP	NU-1012-1G	Jena Bioscience, D
Guanidinehydrochloride	37.1	Roth, Karlsruhe,D
HEPES	9105.4	Roth, Karlstuhe, D
Horse serum	26050088	Gibco/Thermofisher Scientific, Dreiech, D
Human recombinant IFN-γ	IF002	Merck Millipore
Human recombinant M-CSF	M6518	Sigma-Aldrich,Steinheim,D
IM54	13323	Cayman Chemical Company, Ann Arbor, USA

Imidazole	3899.3	Roth, Karlsruhe, D
Isopropanol	9866.5	Roth, Karlsruhe, D
Isopropyl-β-D-thiogalactopyranosid	2316.5	Roth, Karlsruhe, D
Kanamycinsulfate	T823.4	Roth, Karlsruhe, D
LPS, E. Coli O111:B4	LPS25	Merck Millipore, Burlington, USA
Magnesium chloride Hexahydrate	63065	Sigma-Aldrich, Steinheim, D
Mark12 unstained standard	LC5677	Life technologies, Karlsruhe, D
MCC950	M6164	AbMole Bioscience, Houston, USA
Methonol	4627.5	Roth, Karlsruhe
Necrostatin-1	M2315	AbMole Bioscience, Houston, USA
Ni Sepharose HP	71-5027-67 AD	Ge Healthcare, München
NuPAGE LDS Sample Buffer	NP0007	Life Technologies, Karlsruhe, D
NuPAGE MES SDS Buffer	NP0060	Life Technologies, Karlsruhe, D
NuPAGE MOPS SDS Buffer	NP0050	Life Technologies, Karlsruhe, D
Paraformaldehyde	158127	Sigma-Aldrich,Steinheim,D
Penicillin-Streptomycin	15140-122	Life Technologies, Karlsruhe, D
Phorbol 12-Myristate 13-Acetate	524400	Sigma-Aldrich, Steinheim, D
PMSF	6367.4	Roth, Karlsruhe, D
Poly (dA:dT)	P0883-10UN	Sigma-Aldrich, Steinheim, D
Sodium chloride	9265.2	Roth, Karlsruhe, D
Western blot detection reagent ECL	RPN2232	Amersham, GE healthcare, München
Z-DEVD-FMK	S7312	Selleckchem, Houston, USA

Appendix D - List of Enzymes

Enzyme	**Manufacturer**
DNase I	NEB, Frankfurt a.M., D
T4 DNA Ligase	NEB, Frankfurt a.M., D
T4 Pol*ynucleotide kinase*	NEB, Frankfurt a.M., D
Restriction Endonucleases	NEB, Frankfurt a.M., D

Appendix E-List of Kits

Kits	Manufacturer
Plasmid Mini Prep Kit	Jena Bioscience, Jena,D
Plasmid Midi Prep Kit	QIAGEN, Hilden, D
CytoTox-ONE™ Homogeneous Membrane Integrity Assay	Promega, Walldorf, D
Uric Acid/Uricase Assay kit	Cell Biolabs, inc., San Diego, USA
MitoSOX™ Red Mitochondrial Superoxide Indicator	Thermo Fisher Scientific, Dreeich, D
Human IL-1 beta/IL-1F2 DuoSet ELISA kit	R&D Biosystems, Wiesbaden, D
FuGENE® HD Transfection Reagent	Promega, Walldorf, D
Profect-P1-lipid based protein delivery reagent	Targeting Systems, El Cajon, USA
Lipofectamine™ RNAiMAX Transfection Reagent	Thermo Fisher Scientific, Dreiech, D
SYBR green qPCR mastermix	Thermofisher Scientific, Dreiech, D
KOD Hot Start polymerase Kit	Merck Millipore, Darmstadt, D
Phusion high fidelity polymerase	NEB, Frankfurt a.M., D

Appendix F-List of Media

Medium	Manufacturer
Terrific Borth (TB)	Roth, Karlsruhe, D
DMEM	Gibco/Thermofisher Scientific, Dreiech, D
RPMI 1640	Gibco/Thermofisher Scientific, Dreiech, D
Opti-MEM	Gibco/Thermofisher Scientific, Dreiech, D
PBS	Gibco/Thermofisher Scientific, Dreiech, D

Appendix G-List of Buffers

Buffer	Components
Resuspension buffer	50 mM Tris–HCl (pH 8.0), 5 mM $MgCl_2$, 300 mM NaCl, 5 mM β-mercaptoethanol, 10% (v/v) glycerol, 20 mM imidazole, 100 µM phenylmethylsulfonyl fluoride (PMSF), 1 µg/mL DNase I
Equilibration buffer	50 mM Tris–HCl (pH 8.0), 5 mM $MgCl_2$, 300 mM NaCl, 5 mM β-mercaptoethanol, 10% (v/v) glycerol, 20 mM imidazole,
Washing buffer	50 mM Tris–HCl (pH 8.0), 5 mM $MgCl_2$, 500 mM NaCl, 5 mM β-mercaptoethanol, 10% (v/v) glycerol, 20 mM imidazole,
Dialysis buffer	50 mM HEPES pH 7.5, 150 mM NaCl, 5 mM $MgCl_2$ and 2 mM dithiothreitol
Elution buffer	50 mM Tris–HCl (pH 8.0), 5 mM $MgCl_2$, 500 mM NaCl, 5 mM β-mercaptoethanol, 10% (v/v) glycerol, 20 mM imidazole,
SEC buffer	50 mM HEPES pH 7.5, 150 mM NaCl, 5 mM $MgCl_2$ and 2 mM dithiothreitol
Hydrophobic gradien buffer A	50 mM Tris-HCl, pH 8.0, 2 mM $MgCl_2$, 2 mM DTT, 1.5 mM $(NH_4)_2SO_4$
Hydrophobic gradien buffer B	50 mM Tris-HCl, pH 8.0, 2 mM $MgCl_2$, 2 mM DTT,
Liposome buffer	25 mM HEPES, pH 7.5, 150 mM NaCl and 1 mM $MgCl_2$
GTPase buffer	20 mM HEPES pH 7.5, 150 mM NaCl, 2 mM $MgCl_2$
GDP·AlFx complex formation buffer	20 mM HEPES pH 7.5, 150 mM NaCl, 2 mM $MgCl_2$, 200 µM GDP, 300 µM AlF_3 and 10 mM NaF

HPLC buffer	100 mM potassium phosphate buffer pH 6.5, 10 mM tetrabutylammonium bromide, 7.5% acetonitrile

Appendix H - List of Constructs

Protein	Mutation	Species	Plasmid
hGBP1	N/A	Homo sapiens	pSKB-LNB2
hGBP1	G68A	Homo sapiens	pSKB-LNB2
hGBP1	R48A	Homo sapiens	pSKB-LNB2
hGBP1	K76A	Homo sapiens	pSKB-LNB2
hGBP1	N/A	Homo sapiens	pCMV-GFP Hygro
hGBP1	G68A	Homo sapiens	pCMV-GFP Hygro
hGBP1	R48A	Homo sapiens	pCMV-GFP Hygro
hGBP1	K76A	Homo sapiens	pCMV-GFP Hygro
hGBP1	CRISPR KO sgRNA1	Homo sapiens	plenti-CRISPR-V2
hGBP1	CRISPR KO sgRNA2	Homo sapiens	plenti-CRISPR-V2

Appendix I - List of Abbreviations

Abbreviation	meaning
APC	antigen presenting cell
ASC	adaptor molecule apoptosis-associate speck-like protein containing a caspase recruitment domain
CARD	caspase activation and recruitment domain
CRISPR	Clustered Regularly Interspaced Short Palindromic Repeat
DAMP	danger-associated molecular pattern
EB	elementary bodies
ELISA	enzyme-linked immunosorbant assay
EPEC	enteropathogenic *E. coli*
ERK	extracellular signal-regulated kinases
GBP	guanylate binding protein
Gbp^{Chr3}	gbp genes on mouse chromosome 3
GDA	guanine deaminase
IAP	baculoviral inhibitor of apoptosis
IFIT1	interferon- induced protein with tetratricopeptide repeats 1
IFNGR	IFN-γ receptor
IFN-γ	Interferon-γ
IKKβ	inhibitor of nuclear factor kappa-B kinase subunit beta
IL	Interleukin
IL1R1	IL-1β type 1 receptor
IL-1RAP	IL-1 receptor accessory protein
Inc	inclusion membrane protein
IRAK4	IL-1 receptor-associated kinase
IRF3	interferon regulatory factor 3
IRG	immune related GTPase
ISG	interferon stimulated gene
IκB	nuclear factor kappa-B inhibitor
JAK	Janus kinase
JNK	c-Jun N-terminal kinases
LDH	lactate dehydrogenase
LG	large GTPase
LPS	lipopolysaccharides
LRR	leucine rich repeat
MAP2K	mitogen-activated protein kinase kinase
MAP3K	mitogen-activated protein kinase kinase kinase
MAPK	mitogen-activated protein kinase
MOMP	major outer membrane protein
MTOC	microtubule organizing center
MYD88	myeloid differentiation primary response gene 88
NACHT	NAIP (neuronal apoptosis inhibitory protein), CIITA (MHC class II transcription activator), HET-E (incompatibility locus protein from Podospora anserina) and TP1 (telomerase-associated protein)

Nek7	NIMA-related kinase 7
NF-κB	nuclear factor 'kappa-light-chain-enhancer' of activated B-cells
NLR	NOD-like receptor
NOS	nitric oxide synthase
PAMP	pathogen-associated molecular pattern
PCV	pathogen containing vacuole
PRR	pattern recognition receptor
PYD	Pyrin domain
RB	reticulate bodies
ROS	reactive oxygen species
STAT	signal transducer and activator of transcription
STEC	Shiga-toxic *E. coli*
STING	synthase stimulator of interferon genes
TAB	TAK1-binding proteins
TAK	TGF-β-activated kinase
TIR	Toll- and IL-1R–like
TLR	toll-like receptor
TNF	tumor necrosis factor
TNF-α	tumor necrosis factor α
TOLLIP	Toll-interacting protein
TRAF	tumor necrosis factor-associated factor
TRAM	TRIF-related adapter molecule
TRIF	TIR-domain-containing adapter-inducing interferon-β
UA	uric acid
VLIG	very large inducible GTPases
XO	xanthine oxidase

9.References

Abdul-Sater, A.A., Saïd-Sadier, N., Lam, V.M., Singh, B., Pettengill, M.A., Soares, F., Tattoli, I., Lipinski, S., Girardin, S.E., Rosenstiel, P.*, et al.* (2010). Enhancement of reactive oxygen species production and chlamydial infection by the mitochondrial Nod-like family member NLRX1. The Journal of biological chemistry *285*, 41637-41645.

Abu-Lubad, M., Meyer, T.F., and Al-Zeer, M.A. (2014). Chlamydia trachomatis inhibits inducible NO synthase in human mesenchymal stem cells by stimulating polyamine synthesis. J Immunol *193*, 2941-2951.

Acauan Filho, B.J., Pinheiro da Costa, B.E., Ogando, P.B., Vieira, M.C., Antonello, I.C., and Poli-de-Figueiredo, C.E. (2016). Serum nitrate and NOx levels in preeclampsia are higher than in normal pregnancy. Hypertension in pregnancy *35*, 226-233.

Acuner Ozbabacan, S.E., Gursoy, A., Nussinov, R., and Keskin, O. (2014). The structural pathway of interleukin 1 (IL-1) initiated signaling reveals mechanisms of oncogenic mutations and SNPs in inflammation and cancer. PLoS Comput Biol *10*, e1003470-e1003470.

Agostini, L., Martinon, F., Burns, K., McDermott, M.F., Hawkins, P.N., and Tschopp, J. (2004). NALP3 forms an IL-1beta-processing inflammasome with increased activity in Muckle-Wells autoinflammatory disorder. Immunity *20*, 319-325.

Akira, S., and Takeda, K. (2004). Toll-like receptor signalling. Nature Reviews Immunology *4*, 499-511.

Akira, S., Uematsu, S., and Takeuchi, O. (2006). Pathogen recognition and innate immunity. Cell *124*, 783-801.

Al-Zeer, M.A., Al-Younes, H.M., Braun, P.R., Zerrahn, J., and Meyer, T.F. (2009). IFN-γ-Inducible Irga6 Mediates Host Resistance against Chlamydia trachomatis via Autophagy. PLOS ONE *4*, e4588.

Al-Zeer, M.A., Al-Younes, H.M., Lauster, D., Abu Lubad, M., and Meyer, T.F. (2013). Autophagy restricts Chlamydia trachomatis growth in human macrophages via IFNG-inducible guanylate binding proteins. Autophagy *9*, 50-62.

Amer, A., Franchi, L., Kanneganti, T.D., Body-Malapel, M., Ozören, N., Brady, G., Meshinchi, S., Jagirdar, R., Gewirtz, A., Akira, S.*, et al.* (2006). Regulation of Legionella phagosome maturation and infection through flagellin and host Ipaf. The Journal of biological chemistry *281*, 35217-35223.

Anand, P.K., Malireddi, R.K.S., Lukens, J.R., Vogel, P., Bertin, J., Lamkanfi, M., and Kanneganti, T.-D. (2012). NLRP6 negatively regulates innate immunity and host defence against bacterial pathogens. Nature *488*, 389-393.

Anttila, T., Saikku, P., Koskela, P., Bloigu, A., Dillner, J., Ikäheimo, I., Jellum, E., Lehtinen, M., Lenner, P., Hakulinen, T.*, et al.* (2001). Serotypes of Chlamydia trachomatis and risk for development of cervical squamous cell carcinoma. Jama *285*, 47-51.

Bachmann, N.L., Polkinghorne, A., and Timms, P. (2014). Chlamydia genomics: providing novel insights into chlamydial biology. Trends in microbiology *22*, 464-472.

Bastidas, R.J., Elwell, C.A., Engel, J.N., and Valdivia, R.H. (2013). Chlamydial intracellular survival strategies. Cold Spring Harbor perspectives in medicine *3*, a010256.

Bian, X., Klemm, R.W., Liu, T.Y., Zhang, M., Sun, S., Sui, X., Liu, X., Rapoport, T.A., and Hu, J. (2011). Structures of the atlastin GTPase provide insight into homotypic fusion of endoplasmic reticulum membranes. Proc Natl Acad Sci U S A *108*, 3976-3981.

Bohlson, S., O'Conner, S., Hulsebus, H., Ho, M.-M., and Fraser, D. (2014). Complement, C1q, and C1q-Related Molecules Regulate Macrophage Polarization. Frontiers in immunology *5*, 402.

Braga, T.T., Forni, M.F., Correa-Costa, M., Ramos, R.N., Barbuto, J.A., Branco, P., Castoldi, A., Hiyane, M.I., Davanso, M.R., Latz, E.*, et al.* (2017). Soluble Uric Acid Activates the NLRP3 Inflammasome. Sci Rep *7*, 39884-39884.

Braun, E., Hotter, D., Koepke, L., Zech, F., Groß, R., Sparrer, K.M.J., Müller, J.A., Pfaller, C.K., Heusinger, E., Wombacher, R.*, et al.* (2019). Guanylate-Binding Proteins 2 and 5 Exert Broad Antiviral Activity by Inhibiting Furin-Mediated Processing of Viral Envelope Proteins. Cell Reports *27*, 2092-2104.e2010.

Brikos, C., Wait, R., Begum, S., O'Neill, L.A., and Saklatvala, J. (2007). Mass spectrometric analysis of the endogenous type I interleukin-1 (IL-1) receptor signaling complex formed after IL-1 binding identifies IL-1RAcP, MyD88, and IRAK-4 as the stable components. Molecular & cellular proteomics : MCP *6*, 1551-1559.

Britzen-Laurent, N., Bauer, M., Berton, V., Fischer, N., Syguda, A., Reipschläger, S., Naschberger, E., Herrmann, C., and Stürzl, M. (2010). Intracellular Trafficking of Guanylate-Binding Proteins Is Regulated by Heterodimerization in a Hierarchical Manner. PLoS ONE *5*, e14246.

Brunham, R.C., and Rey-Ladino, J. (2005). Immunology of Chlamydia infection: implications for a Chlamydia trachomatis vaccine. Nature Reviews Immunology *5*, 149-161.

Byrnes, L.J., Singh, A., Szeto, K., Benvin, N.M., O'Donnell, J.P., Zipfel, W.R., and Sondermann, H. (2013). Structural basis for conformational switching and GTP loading of the large G protein atlastin. Embo j *32*, 369-384.

Byrnes, L.J., and Sondermann, H. (2011a). Structural basis for the nucleotide-dependent dimerization of the large G protein atlastin-1/SPG3A. Proc Natl Acad Sci U S A *108*, 2216-2221.

Byrnes, L.J., and Sondermann, H. (2011b). Structural basis for the nucleotide-dependent dimerization of the large G protein atlastin-1/SPG3A. Proceedings of the National Academy of Sciences *108*, 2216-2221.

Cao, Z., Henzel, W.J., and Gao, X. (1996a). IRAK: a kinase associated with the interleukin-1 receptor. Science *271*, 1128-1131.

Cao, Z., Xiong, J., Takeuchi, M., Kurama, T., and Goeddel, D.V. (1996b). TRAF6 is a signal transducer for interleukin-1. Nature *383*, 443-446.

Case, E.D., Chong, A., Wehrly, T.D., Hansen, B., Child, R., Hwang, S., Virgin, H.W., and Celli, J. (2014). The Francisella O-antigen mediates survival in the macrophage cytosol via autophagy avoidance. Cell Microbiol *16*, 862-877.

Cates, W., Jr., and Wasserheit, J.N. (1991). Genital chlamydial infections: epidemiology and reproductive sequelae. American journal of obstetrics and gynecology *164*, 1771-1781.

Chang, L., and Karin, M. (2001). Mammalian MAP kinase signalling cascades. Nature *410*, 37-40.

Chappie, J.S., Acharya, S., Leonard, M., Schmid, S.L., and Dyda, F. (2010). G domain dimerization controls dynamin's assembly-stimulated GTPase activity. Nature *465*, 435-440.
Chen, G.Y., Liu, M., Wang, F., Bertin, J., and Núñez, G. (2011). A functional role for Nlrp6 in intestinal inflammation and tumorigenesis. J Immunol *186*, 7187-7194.

Chen, J., and Chen, Z.J. (2018). PtdIns4P on dispersed trans-Golgi network mediates NLRP3 inflammasome activation. Nature *564*, 71-76.

Chen, Y.S., Bastidas, R.J., Saka, H.A., Carpenter, V.K., Richards, K.L., Plano, G.V., and Valdivia, R.H. (2014). The Chlamydia trachomatis type III secretion chaperone Slc1 engages multiple early effectors, including TepP, a tyrosine-phosphorylated protein required for the recruitment of CrkI-II to nascent inclusions and innate immune signaling. PLoS Pathog *10*, e1003954.

Chiu, R., Boyle, W.J., Meek, J., Smeal, T., Hunter, T., and Karin, M. (1988). The c-fos protein interacts with c-JunAP-1 to stimulate transcription of AP-1 responsive genes. Cell *54*, 541-552.

Chung, C.T., Niemela, S.L., and Miller, R.H. (1989). One-step preparation of competent Escherichia coli: transformation and storage of bacterial cells in the same solution. Proc Natl Acad Sci U S A *86*, 2172-2175.

Clausen, J.D., Christiansen, G., Holst, H.U., and Birkelund, S. (1997). Chlamydia trachomatis utilizes the host cell microtubule network during early events of infection. Molecular microbiology *25*, 441-449.

Crane, J.K., Broome, J.E., and Lis, A. (2016). Biological Activities of Uric Acid in Infection Due to Enteropathogenic and Shiga-Toxigenic Escherichia coli. Infection and immunity *84*, 976-988.

Crișan, T.O., Cleophas, M.C., Oosting, M., Lemmers, H., Toenhake-Dijkstra, H., Netea, M.G., Jansen, T.L., and Joosten, L.A. (2016). Soluble uric acid primes TLR-induced proinflammatory cytokine production by human primary cells via inhibition of IL-1Ra. Annals of the rheumatic diseases *75*, 755-762.

Cruz, C.M., Rinna, A., Forman, H.J., Ventura, A.L.M., Persechini, P.M., and Ojcius, D.M. (2007). ATP activates a reactive oxygen species-dependent oxidative stress response and secretion of proinflammatory cytokines in macrophages. The Journal of biological chemistry *282*, 2871-2879.

Danis, V.A., Kulesz, A.J., Nelson, D.S., and Brooks, P.M. (1990). Cytokine regulation of human monocyte interleukin-1 (IL-1) production in vitro. Enhancement of IL-1 production by interferon (IFN) gamma, tumour necrosis factor-alpha, IL-2 and IL-1, and inhibition by IFN-alpha. Clinical and experimental immunology *80*, 435-443.

Daumke, O., Lundmark, R., Vallis, Y., Martens, S., Butler, P.J., and McMahon, H.T. (2007). Architectural and mechanistic insights into an EHD ATPase involved in membrane remodelling. Nature *449*, 923-927.

Daumke, O., and Praefcke, G.J. (2016). Invited review: Mechanisms of GTP hydrolysis and conformational transitions in the dynamin superfamily. Biopolymers *105*, 580-593.

Davis, B.K., Wen, H., and Ting, J.P. (2011). The inflammasome NLRs in immunity, inflammation, and associated diseases. Annual review of immunology *29*, 707-735.

Dawkins, R., Krebs, J.R., Maynard Smith, J., and Holliday, R. (1979). Arms races between and within species. Proceedings of the Royal Society of London Series B Biological Sciences *205*, 489-511.

Degrandi, D., Konermann, C., Beuter-Gunia, C., Kresse, A., Würthner, J., Kurig, S., Beer, S., and Pfeffer, K. (2007). Extensive Characterization of IFN-Induced GTPases mGBP1 to mGBP10 Involved in Host Defense. The Journal of Immunology *179*, 7729-7740.

Degrandi, D., Kravets, E., Konermann, C., Beuter-Gunia, C., Klümpers, V., Lahme, S., Wischmann, E., Mausberg, A.K., Beer-Hammer, S., and Pfeffer, K. (2013). Murine Guanylate Binding Protein 2 (mGBP2) controls Toxoplasma gondii replication. Proceedings of the National Academy of Sciences *110*, 294-299.

Di Giovine, F.S., Malawista, S.E., Nuki, G., and Duff, G.W. (1987). Interleukin 1 (IL 1) as a mediator of crystal arthritis. Stimulation of T cell and synovial fibroblast mitogenesis by urate crystal-induced IL 1. J Immunol *138*, 3213-3218.

Dinarello, C.A. (2009). Immunological and inflammatory functions of the interleukin-1 family. Annual review of immunology *27*, 519-550.

Dostert, C., Pétrilli, V., Van Bruggen, R., Steele, C., Mossman, B.T., and Tschopp, J. (2008). Innate immune activation through Nalp3 inflammasome sensing of asbestos and silica. Science *320*, 674-677.

Duewell, P., Kono, H., Rayner, K.J., Sirois, C.M., Vladimer, G., Bauernfeind, F.G., Abela, G.S., Franchi, L., Nuñez, G., Schnurr, M.*, et al.* (2010). NLRP3 inflammasomes are required for atherogenesis and activated by cholesterol crystals. Nature *464*, 1357-1361.

Elwell, C., Mirrashidi, K., and Engel, J. (2016). Chlamydia cell biology and pathogenesis. Nature Reviews Microbiology *14*, 385-400.

Faelber, K., Dietrich, L., Noel, J.K., Wollweber, F., Pfitzner, A.-K., Mühleip, A., Sánchez, R., Kudryashev, M., Chiaruttini, N., Lilie, H.*, et al.* (2019). Structure and assembly of the mitochondrial membrane remodelling GTPase Mgm1. Nature *571*, 429-433.

Faelber, K., Gao, S., Held, M., Posor, Y., Haucke, V., Noé, F., and Daumke, O. (2013). Oligomerization of dynamin superfamily proteins in health and disease. Progress in molecular biology and translational science *117*, 411-443.

Faelber, K., Posor, Y., Gao, S., Held, M., Roske, Y., Schulze, D., Haucke, V., Noe, F., and Daumke, O. (2011). Crystal structure of nucleotide-free dynamin. Nature *477*, 556-560.

Ferrante, C.J., and Leibovich, S.J. (2012). Regulation of Macrophage Polarization and Wound Healing. Advances in Wound Care *1*, 10-16.

Finethy, R., Jorgensen, I., Haldar, A.K., de Zoete, M.R., Strowig, T., Flavell, R.A., Yamamoto, M., Nagarajan, U.M., Miao, E.A., and Coers, J. (2015). Guanylate Binding Proteins Enable Rapid Activation of Canonical and Noncanonical Inflammasomes in Chlamydia-Infected Macrophages. Infection and Immunity *83*, 4740-4749.

Fisch, D., Bando, H., Clough, B., Hornung, V., Yamamoto, M., Shenoy, A.R., and Frickel, E.-M. (2019). Human GBP1 is a microbe-specific gatekeeper of macrophage apoptosis and pyroptosis. The EMBO journal *38*, e100926-e100926.

Franchi, L., Amer, A., Body-Malapel, M., Kanneganti, T.D., Ozören, N., Jagirdar, R., Inohara, N., Vandenabeele, P., Bertin, J., Coyle, A.*, et al.* (2006). Cytosolic flagellin requires Ipaf for activation of caspase-1 and interleukin 1beta in salmonella-infected macrophages. Nat Immunol *7*, 576-582.

Fres, J.M., Müller, S., and Praefcke, G.J.K. (2010). Purification of the CaaX-modified, dynamin-related large GTPase hGBP1 by coexpression with farnesyltransferase. Journal of Lipid Research *51*, 2454-2459.

Gao, S., von der Malsburg, A., Paeschke, S., Behlke, J., Haller, O., Kochs, G., and Daumke, O. (2010). Structural basis of oligomerization in the stalk region of dynamin-like MxA. Nature *465*, 502-506.

Ghosh, A., Praefcke, G.J., Renault, L., Wittinghofer, A., and Herrmann, C. (2006a). How guanylate-binding proteins achieve assembly-stimulated processive cleavage of GTP to GMP. Nature *440*, 101-104.

Ghosh, A., Praefcke, G.J.K., Renault, L., Wittinghofer, A., and Herrmann, C. (2006b). How guanylate-binding proteins achieve assembly-stimulated processive cleavage of GTP to GMP. Nature *440*, 101-104.

Greenfeder, S.A., Nunes, P., Kwee, L., Labow, M., Chizzonite, R.A., and Ju, G. (1995). Molecular cloning and characterization of a second subunit of the interleukin 1 receptor complex. The Journal of biological chemistry *270*, 13757-13765.

Groß, C.J., Mishra, R., Schneider, K.S., Médard, G., Wettmarshausen, J., Dittlein, D.C., Shi, H., Gorka, O., Koenig, P.A., Fromm, S.*, et al.* (2016). K(+) Efflux-Independent NLRP3 Inflammasome Activation by Small Molecules Targeting Mitochondria. Immunity *45*, 761-773.
Gunjan, K., Mohsin, R., and Brijendra, K.T. (2018). Interferon-gamma (IFN-γ): Exploring its implications in infectious diseases. Biomolecular Concepts *9*, 64-79.

Hackstadt, T., Fischer, E.R., Scidmore, M.A., Rockey, D.D., and Heinzen, R.A. (1997). Origins and functions of the chlamydial inclusion. Trends in microbiology *5*, 288-293.

Hackstadt, T., Scidmore-Carlson, M.A., Shaw, E.I., and Fischer, E.R. (1999). The Chlamydia trachomatis IncA protein is required for homotypic vesicle fusion. Cell Microbiol *1*, 119-130.

Hafner, L.M. (2015). Pathogenesis of fallopian tube damage caused by Chlamydia trachomatis infections. Contraception *92*, 108-115.

Haldar, A.K., Saka, H.A., Piro, A.S., Dunn, J.D., Henry, S.C., Taylor, G.A., Frickel, E.M., Valdivia, R.H., and Coers, J. (2013). IRG and GBP Host Resistance Factors Target Aberrant, "Non-self" Vacuoles Characterized by the Missing of "Self" IRGM Proteins. PLoS Pathog *9*, e1003414.

Hazuda, D.J., Lee, J.C., and Young, P.R. (1988). The kinetics of interleukin 1 secretion from activated monocytes. Differences between interleukin 1 alpha and interleukin 1 beta. The Journal of biological chemistry *263*, 8473-8479.

He, Y., Zeng, M.Y., Yang, D., Motro, B., and Núñez, G. (2016). NEK7 is an essential mediator of NLRP3 activation downstream of potassium efflux. Nature *530*, 354-357.

Heuer, D., Rejman Lipinski, A., Machuy, N., Karlas, A., Wehrens, A., Siedler, F., Brinkmann, V., and Meyer, T.F. (2009). Chlamydia causes fragmentation of the Golgi compartment to ensure reproduction. Nature *457*, 731-735.

Hitchings, G.H., and Elion, G.B. (1963). Chemical suppression of the immune response. Pharmacological reviews *15*, 365-405.

Hornung, V., Bauernfeind, F., Halle, A., Samstad, E.O., Kono, H., Rock, K.L., Fitzgerald, K.A., and Latz, E. (2008). Silica crystals and aluminum salts activate the NALP3 inflammasome through phagosomal destabilization. Nat Immunol *9*, 847-856.

Hu, J., Shibata, Y., Zhu, P.P., Voss, C., Rismanchi, N., Prinz, W.A., Rapoport, T.A., and Blackstone, C. (2009). A class of dynamin-like GTPases involved in the generation of the tubular ER network. Cell *138*, 549-561.

Hybiske, K., and Stephens, R.S. (2007). Mechanisms of host cell exit by the intracellular bacterium Chlamydia. Proc Natl Acad Sci U S A *104*, 11430-11435.

Janeway, C.A., Jr. (1989). Approaching the asymptote? Evolution and revolution in immunology. Cold Spring Harbor symposia on quantitative biology *54 Pt 1*, 1-13.

Kang, T.J., Basu, S., Zhang, L., Thomas, K.E., Vogel, S.N., Baillie, L., and Cross, A.S. (2008). Bacillus anthracis spores and lethal toxin induce IL-1beta via functionally distinct signaling pathways. European journal of immunology *38*, 1574-1584.

Kanneganti, T.D., Lamkanfi, M., and Núñez, G. (2007). Intracellular NOD-like receptors in host defense and disease. Immunity *27*, 549-559.

Kayagaki, N., Stowe, I.B., Lee, B.L., O'Rourke, K., Anderson, K., Warming, S., Cuellar, T., Haley, B., Roose-Girma, M., Phung, Q.T.*, et al.* (2015). Caspase-11 cleaves gasdermin D for non-canonical inflammasome signalling. Nature *526*, 666-671.

Khare, S., Dorfleutner, A., Bryan, N.B., Yun, C., Radian, A.D., de Almeida, L., Rojanasakul, Y., and Stehlik, C. (2012). An NLRP7-containing inflammasome mediates recognition of microbial lipopeptides in human macrophages. Immunity *36*, 464-476.

Kim, B.-H., Shenoy, A.R., Kumar, P., Das, R., Tiwari, S., and MacMicking, J.D. (2011). A Family of IFN-γ–Inducible 65-kD GTPases Protects Against Bacterial Infection. Science *332*, 717-721.

Kim, B.H., Chee, J.D., Bradfield, C.J., Park, E.S., Kumar, P., and MacMicking, J.D. (2016). Interferon-induced guanylate-binding proteins in inflammasome activation and host defense. Nat Immunol *17*, 481-489.

Kimball, A.S., Davis, F.M., denDekker, A., Joshi, A.D., Schaller, M.A., Bermick, J., Xing, X., Burant, C.F., Obi, A.T., Nysz, D.*, et al.* (2019). The Histone Methyltransferase Setdb2 Modulates Macrophage Phenotype and Uric Acid Production in Diabetic Wound Repair. Immunity *51*, 258-271.e255.

Kofoed, E.M., and Vance, R.E. (2011). Innate immune recognition of bacterial ligands by NAIPs determines inflammasome specificity. Nature *477*, 592-595.

Kojima, H., Aizawa, Y., Yanai, Y., Nagaoka, K., Takeuchi, M., Ohta, T., Ikegami, H., Ikeda, M., and Kurimoto, M. (1999). An Essential Role for NF-κB in IL-18-Induced IFN-γ Expression in KG-1 Cells. The Journal of Immunology *162*, 5063.

Krapp, C., Hotter, D., Gawanbacht, A., McLaren, Paul J., Kluge, Silvia F., Stürzel, Christina M., Mack, K., Reith, E., Engelhart, S., Ciuffi, A.*, et al.* (2016). Guanylate Binding Protein (GBP) 5 Is an Interferon-Inducible Inhibitor of HIV-1 Infectivity. Cell Host & Microbe *19*, 504-514.

Kravets, E., Degrandi, D., Ma, Q., Peulen, T.-O., Klümpers, V., Felekyan, S., Kühnemuth, R., Weidtkamp-Peters, S., Seidel, C.A., and Pfeffer, K. (2016). Guanylate binding proteins directly attack Toxoplasma gondii via supramolecular complexes. Elife *5*, e11479.

Kravets, E., Degrandi, D., Weidtkamp-Peters, S., Ries, B., Konermann, C., Felekyan, S., Dargazanli, J.M., Praefcke, G.J.K., Seidel, C.A.M., Schmitt, L.*, et al.* (2012). The GTPase activity of murine guanylate-binding protein 2 (mGBP2) controls the intracellular localization and recruitment to the parasitophorous vacuole of Toxoplasma gondii. Journal of Biological Chemistry.

Krzyszczyk, P., Schloss, R., Palmer, A., and Berthiaume, F. (2018). The Role of Macrophages in Acute and Chronic Wound Healing and Interventions to Promote Pro-wound Healing Phenotypes. Front Physiol *9*, 419-419.

Kumar, Y., and Valdivia, R.H. (2009). Leading a sheltered life: intracellular pathogens and maintenance of vacuolar compartments. Cell Host Microbe *5*, 593-601.

Kutsch, M., Sistemich, L., Lesser, C.F., Goldberg, M.B., Herrmann, C., and Coers, J. (2020). Direct binding of polymeric GBP1 to LPS disrupts bacterial cell envelope functions. Embo j *39*, e104926.

Lagrange, B., Benaoudia, S., Wallet, P., Magnotti, F., Provost, A., Michal, F., Martin, A., Di Lorenzo, F., Py, B.F., Molinaro, A.*, et al.* (2018). Human caspase-4 detects tetra-acylated LPS and cytosolic Francisella and functions differently from murine caspase-11. Nature Communications *9*, 242.

Levinsohn, J.L., Newman, Z.L., Hellmich, K.A., Fattah, R., Getz, M.A., Liu, S., Sastalla, I., Leppla, S.H., and Moayeri, M. (2012). Anthrax lethal factor cleavage of Nlrp1 is required for activation of the inflammasome. PLoS Pathog *8*, e1002638.

Lima, H., Jr., Jacobson, L.S., Goldberg, M.F., Chandran, K., Diaz-Griffero, F., Lisanti, M.P., and Brojatsch, J. (2013). Role of lysosome rupture in controlling Nlrp3 signaling and necrotic cell death. Cell cycle (Georgetown, Tex) *12*, 1868-1878.

Liu, B.C., Sarhan, J., Panda, A., Muendlein, H.I., Ilyukha, V., Coers, J., Yamamoto, M., Isberg, R.R., and Poltorak, A. (2018). Constitutive Interferon Maintains GBP Expression Required for Release of Bacterial Components Upstream of Pyroptosis and Anti-DNA Responses. Cell Reports *24*, 155-168.e155.

Liu, T., Zhang, L., Joo, D., and Sun, S.-C. (2017). NF-κB signaling in inflammation. Signal Transduct Target Ther *2*, 17023.

Lu, A., and Wu, H. (2015). Structural mechanisms of inflammasome assembly. FEBS J *282*, 435-444.

Macaluso, F., Nothnagel, M., Parwez, Q., Petrasch-Parwez, E., Bechara, F.G., Epplen, J.T., and Hoffjan, S. (2007). Polymorphisms in NACHT-LRR (NLR) genes in atopic dermatitis. Experimental dermatology *16*, 692-698.

Madeira, F., Park, Y.m., Lee, J., Buso, N., Gur, T., Madhusoodanan, N., Basutkar, P., Tivey, A.R.N., Potter, S.C., Finn, R.D.*, et al.* (2019). The EMBL-EBI search and sequence analysis tools APIs in 2019. Nucleic Acids Res *47*, W636-W641.

Maesaka, J.K., and Fishbane, S. (1998). Regulation of renal urate excretion: a critical review. American journal of kidney diseases : the official journal of the National Kidney Foundation *32*, 917-933.

Malhotra, M., Sood, S., Mukherjee, A., Muralidhar, S., and Bala, M. (2013). Genital Chlamydia trachomatis: an update. The Indian journal of medical research *138*, 303-316.

Man, S.M., Karki, R., Malireddi, R.K.S., Neale, G., Vogel, P., Yamamoto, M., Lamkanfi, M., and Kanneganti, T.-D. (2015). The transcription factor IRF1 and guanylate-binding proteins target activation of the AIM2 inflammasome by Francisella infection. Nat Immunol *16*, 467-475.

Man, S.M., Karki, R., Sasai, M., Place, D.E., Kesavardhana, S., Temirov, J., Frase, S., Zhu, Q., Malireddi, R.K.S., Kuriakose, T.*, et al.* (2016). IRGB10 Liberates Bacterial Ligands for Sensing by the AIM2 and Caspase-11-NLRP3 Inflammasomes. Cell *167*, 382-396.e317.

Mariathasan, S., Weiss, D.S., Newton, K., McBride, J., O'Rourke, K., Roose-Girma, M., Lee, W.P., Weinrauch, Y., Monack, D.M., and Dixit, V.M. (2006). Cryopyrin activates the inflammasome in response to toxins and ATP. Nature *440*, 228-232.

Martinez, F.O., and Gordon, S. (2014). The M1 and M2 paradigm of macrophage activation: time for reassessment. F1000Prime Rep *6*, 13-13.

Martinon, F., Burns, K., and Tschopp, J. (2002). The inflammasome: a molecular platform triggering activation of inflammatory caspases and processing of proIL-beta. Molecular cell *10*, 417-426.

Martinon, F., Pétrilli, V., Mayor, A., Tardivel, A., and Tschopp, J. (2006a). Gout-associated uric acid crystals activate the NALP3 inflammasome. Nature *440*, 237-241.

Meade, K.G., and O'Farrelly, C. (2019). β-Defensins: Farming the Microbiome for Homeostasis and Health. Frontiers in immunology *9*, 3072-3072.

Mehlitz, A., Banhart, S., Mäurer, A.P., Kaushansky, A., Gordus, A.G., Zielecki, J., Macbeath, G., and Meyer, T.F. (2010). Tarp regulates early Chlamydia-induced host cell survival through interactions with the human adaptor protein SHC1. J Cell Biol *190*, 143-157.

Meunier, E., Dick, M.S., Dreier, R.F., Schurmann, N., Broz, D.K., Warming, S., Roose-Girma, M., Bumann, D., Kayagaki, N., Takeda, K.*, et al.* (2014). Caspase-11 activation requires lysis of pathogen-containing vacuoles by IFN-induced GTPases. Nature *509*, 366-370.

Meunier, E., Wallet, P., Dreier, R.F., Costanzo, S., Anton, L., Ruhl, S., Dussurgey, S., Dick, M.S., Kistner, A., Rigard, M.*, et al.* (2015). Guanylate-binding proteins promote activation of the AIM2 inflammasome during infection with Francisella novicida. Nat Immunol *16*, 476-484.

Miao, E.A., Leaf, I.A., Treuting, P.M., Mao, D.P., Dors, M., Sarkar, A., Warren, S.E., Wewers, M.D., and Aderem, A. (2010). Caspase-1-induced pyroptosis is an innate immune effector mechanism against intracellular bacteria. Nat Immunol *11*, 1136-1142.

Mills, C.D., Kincaid, K., Alt, J.M., Heilman, M.J., and Hill, A.M. (2000). M-1/M-2 macrophages and the Th1/Th2 paradigm. J Immunol *164*, 6166-6173.

Mital, J., and Hackstadt, T. (2011). Diverse requirements for SRC-family tyrosine kinases distinguish chlamydial species. mBio *2*.

Modiano, N., Lu, Y.E., and Cresswell, P. (2005). Golgi targeting of human guanylate-binding protein-1 requires nucleotide binding, isoprenylation, and an IFN-γ-inducible cofactor. Proceedings of the National Academy of Sciences of the United States of America *102*, 8680-8685.

Motta, V., Soares, F., Sun, T., and Philpott, D.J. (2015). NOD-like receptors: versatile cytosolic sentinels. Physiological reviews *95*, 149-178.

Muñoz-Planillo, R., Kuffa, P., Martínez-Colón, G., Smith, B.L., Rajendiran, T.M., and Núñez, G. (2013). K^+ efflux is the common trigger of NLRP3 inflammasome activation by bacterial toxins and particulate matter. Immunity *38*, 1142-1153.

Nathan, C.F., Murray, H.W., Wiebe, M.E., and Rubin, B.Y. (1983). Identification of interferon-gamma as the lymphokine that activates human macrophage oxidative metabolism and antimicrobial activity. J Exp Med *158*, 670-689.

Neun, R., Richter, M.F., Staeheli, P., and Schwemmle, M. (1996a). GTPase properties of the interferon-induced human guanylate-binding protein 2. *390*, 69-72.

Neun, R., Richter, M.F., Staeheli, P., and Schwemmle, M. (1996b). GTPase properties of the interferon-induced human guanylate-binding protein 2. FEBS Letters *390*, 69-72.

Ngo, C.C., and Man, S.M. (2017). Mechanisms and functions of guanylate-binding proteins and related interferon-inducible GTPases: Roles in intracellular lysis of pathogens. Cellular Microbiology *19*, e12791.

Nickel, W., and Rabouille, C. (2009). Mechanisms of regulated unconventional protein secretion. Nature Reviews Molecular Cell Biology *10*, 148-155.

Nordmann, A., Wixler, L., Boergeling, Y., Wixler, V., and Ludwig, S. (2012). A new splice variant of the human guanylate-binding protein 3 mediates anti-influenza activity through inhibition of viral transcription and replication. The FASEB Journal *26*, 1290-1300.

Oda, M., Satta, Y., Takenaka, O., and Takahata, N. (2002). Loss of urate oxidase activity in hominoids and its evolutionary implications. Molecular biology and evolution *19*, 640-653.

Oeckinghaus, A., and Ghosh, S. (2009). The NF-kappaB family of transcription factors and its regulation. Cold Spring Harbor perspectives in biology *1*, a000034.

Ohno, S., Kinoshita, T., Ohno, Y., Minamoto, T., Suzuki, N., Inoue, M., and Suda, T. (2008). Expression of NLRP7 (PYPAF3, NALP7) protein in endometrial cancer tissues. Anticancer research *28*, 2493-2497.

Okada, K., Hirota, E., Mizutani, Y., Fujioka, T., Shuin, T., Miki, T., Nakamura, Y., and Katagiri, T. (2004). Oncogenic role of NALP7 in testicular seminomas. Cancer science *95*, 949-954.

Omsland, A., Sixt, B.S., Horn, M., and Hackstadt, T. (2014). Chlamydial metabolism revisited: interspecies metabolic variability and developmental stage-specific physiologic activities. FEMS microbiology reviews *38*, 779-801.

Orso, G., Pendin, D., Liu, S., Tosetto, J., Moss, T.J., Faust, J.E., Micaroni, M., Egorova, A., Martinuzzi, A., McNew, J.A*., et al.* (2009). Homotypic fusion of ER membranes requires the dynamin-like GTPase atlastin. Nature *460*, 978-983.

Pacher, P., Nivorozhkin, A., and Szabó, C. (2006). Therapeutic effects of xanthine oxidase inhibitors: renaissance half a century after the discovery of allopurinol. Pharmacological reviews *58*, 87-114.

Paciello, I., Silipo, A., Lembo-Fazio, L., Curcuru, L., Zumsteg, A., Noel, G., Ciancarella, V., Sturiale, L., Molinaro, A., and Bernardini, M.L. (2013). Intracellular Shigella remodels its LPS to dampen the innate immune recognition and evade inflammasome activation. Proc Natl Acad Sci U S A *110*, E4345-4354.

Pavletic, A.J., Wölner-Hanssen, P., Paavonen, J., Hawes, S.E., and Eschenbach, D.A. (1999). Infertility following pelvic inflammatory disease. Infect Dis Obstet Gynecol *7*, 145-152.
Petkova, D.S., Viret, C., and Faure, M. (2013). IRGM in autophagy and viral infections. Frontiers in immunology *3*, 426-426.

Pettersen, E.F., Goddard, T.D., Huang, C.C., Couch, G.S., Greenblatt, D.M., Meng, E.C., and Ferrin, T.E. (2004). UCSF Chimera—A visualization system for exploratory research and analysis. *25*, 1605-1612.

Pilla-Moffett, D., Barber, M.F., Taylor, G.A., and Coers, J. (2016). Interferon-Inducible GTPases in Host Resistance, Inflammation and Disease. Journal of Molecular Biology *428*, 3495-3513.

Pilla, D.M., Hagar, J.A., Haldar, A.K., Mason, A.K., Degrandi, D., Pfeffer, K., Ernst, R.K., Yamamoto, M., Miao, E.A., and Coers, J. (2014). Guanylate binding proteins promote caspase-11–dependent pyroptosis in response to cytoplasmic LPS. Proceedings of the National Academy of Sciences *111*, 6046-6051.

Ponten, A., Sick, C., Weeber, M., Haller, O., and Kochs, G. (1997). Dominant-negative mutants of human MxA protein: domains in the carboxy-terminal moiety are important for oligomerization and antiviral activity. Journal of Virology *71*, 2591.

Pospischil, A., Thoma, R., Hilbe, M., Grest, P., and Gebbers, J.O. (2002). Abortion in woman caused by caprine Chlamydophila abortus (Chlamydia psittaci serovar 1). Swiss medical weekly *132*, 64-66.

Praefcke, G.J., Geyer, M., Schwemmle, M., Robert Kalbitzer, H., and Herrmann, C. (1999a). Nucleotide-binding characteristics of human guanylate-binding protein 1 (hGBP1) and identification of the third GTP-binding motif. J Mol Biol *292*, 321-332.

Praefcke, G.J., Kloep, S., Benscheid, U., Lilie, H., Prakash, B., and Herrmann, C. (2004a). Identification of residues in the human guanylate-binding protein 1 critical for nucleotide binding and cooperative GTP hydrolysis. J Mol Biol *344*, 257-269.

Praefcke, G.J., and McMahon, H.T. (2004a). The dynamin superfamily: universal membrane tubulation and fission molecules? Nature reviews Molecular cell biology *5*, 133-147.

Praefcke, G.J.K., Geyer, M., Schwemmle, M., Kalbitzer, H.R., and Herrmann, C. (1999b). Nucleotide-binding characteristics of human guanylate-binding protein 1 (hGBP1) and identification of the third GTP-binding motif11Edited by P. E. Wright. Journal of Molecular Biology *292*, 321-332.

Praefcke, G.J.K., Kloep, S., Benscheid, U., Lilie, H., Prakash, B., and Herrmann, C. (2004b). Identification of Residues in the Human Guanylate-binding Protein 1 Critical for Nucleotide Binding and Cooperative GTP Hydrolysis. Journal of Molecular Biology *344*, 257-269.

Praefcke, G.J.K., and McMahon, H.T. (2004b). The dynamin superfamily: universal membrane tubulation and fission molecules? Nature Reviews Molecular Cell Biology *5*, 133-147.

Prakash, B., Praefcke, G.J.K., Renault, L., Wittinghofer, A., and Herrmann, C. (2000). Structure of human guanylate-binding protein 1 representing a unique class of GTP-binding proteins. Nature *403*, 567-571.

Rathinam, V.A.K., and Fitzgerald, K.A. (2016). Inflammasome Complexes: Emerging Mechanisms and Effector Functions. Cell *165*, 792-800.

Redgrove, K.A., and McLaughlin, E.A. (2014). The Role of the Immune Response in Chlamydia trachomatis Infection of the Male Genital Tract: A Double-Edged Sword. Front Immunol *5*, 534.

Rosmarin, D.M., Carette, J.E., Olive, A.J., Starnbach, M.N., Brummelkamp, T.R., and Ploegh, H.L. (2012). Attachment of Chlamydia trachomatis L2 to host cells requires sulfation. Proceedings of the National Academy of Sciences *109*, 10059.

Saka, H.A., and Valdivia, R.H. (2010). Acquisition of nutrients by Chlamydiae: unique challenges of living in an intracellular compartment. Current Opinion in Microbiology *13*, 4-10.

Santos, J.C., Boucher, D., Schneider, L.K., Demarco, B., Dilucca, M., Shkarina, K., Heilig, R., Chen, K.W., Lim, R.Y.H., and Broz, P. (2020). Human GBP1 binds LPS to initiate assembly of a caspase-4 activating platform on cytosolic bacteria. Nat Commun *11*, 3276.

Saraste, M., Sibbald, P.R., and Wittinghofer, A. (1990). The P-loop--a common motif in ATP- and GTP-binding proteins. Trends in biochemical sciences *15*, 430-434.
Sato, S., Sanjo, H., Takeda, K., Ninomiya-Tsuji, J., Yamamoto, M., Kawai, T., Matsumoto, K., Takeuchi, O., and Akira, S. (2005). Essential function for the kinase TAK1 in innate and adaptive immune responses. Nat Immunol *6*, 1087-1095.

Schaefer, L. (2014). Complexity of danger: the diverse nature of damage-associated molecular patterns. The Journal of biological chemistry *289*, 35237-35245.

Schneider, W.M., Chevillotte, M.D., and Rice, C.M. (2014). Interferon-stimulated genes: a complex web of host defenses. Annual review of immunology *32*, 513-545.

Schroder, K., Hertzog, P.J., Ravasi, T., and Hume, D.A. (2004). Interferon-gamma: an overview of signals, mechanisms and functions. Journal of leukocyte biology *75*, 163-189.

Schwemmle, M., and Staeheli, P. (1994). The interferon-induced 67-kDa guanylate-binding protein (hGBP1) is a GTPase that converts GTP to GMP. *269*, 11299-11305.

Sharif, H., Wang, L., Wang, W.L., Magupalli, V.G., Andreeva, L., Qiao, Q., Hauenstein, A.V., Wu, Z., Núñez, G., Mao, Y.*, et al.* (2019). Structural mechanism for NEK7-licensed activation of NLRP3 inflammasome. Nature *570*, 338-343.

Shenoy, A.R., Wellington, D.A., Kumar, P., Kassa, H., Booth, C.J., Cresswell, P., and MacMicking, J.D. (2012). GBP5 Promotes NLRP3 Inflammasome Assembly and Immunity in Mammals. Science *336*, 481-485.

Shi, H., Wang, Y., Li, X., Zhan, X., Tang, M., Fina, M., Su, L., Pratt, D., Bu, C.H., Hildebrand, S.*, et al.* (2016). NLRP3 activation and mitosis are mutually exclusive events coordinated by NEK7, a new inflammasome component. Nat Immunol *17*, 250-258.

Shi, J., Zhao, Y., Wang, Y., Gao, W., Ding, J., Li, P., Hu, L., and Shao, F. (2014). Inflammatory caspases are innate immune receptors for intracellular LPS. Nature *514*, 187-192.

Shi, Y., Evans, J.E., and Rock, K.L. (2003). Molecular identification of a danger signal that alerts the immune system to dying cells. Nature *425*, 516-521.

Shimada, K., Crother, T.R., and Arditi, M. (2012a). Innate immune responses to Chlamydia pneumoniae infection: role of TLRs, NLRs, and the inflammasome. Microbes and infection *14*, 1301-1307.

Shimada, K., Crother, T.R., Karlin, J., Dagvadorj, J., Chiba, N., Chen, S., Ramanujan, V.K., Wolf, A.J., Vergnes, L., Ojcius, D.M.*, et al.* (2012b). Oxidized mitochondrial DNA activates the NLRP3 inflammasome during apoptosis. Immunity *36*, 401-414.

Shydlovskyi, S., Zienert, A.Y., Ince, S., Dovengerds, C., Hohendahl, A., Dargazanli, J.M., Blum, A., Günther, S.D., Kladt, N., Stürzl, M.*, et al.* (2017). Nucleotide-dependent farnesyl switch orchestrates polymerization and membrane binding of human guanylate-binding protein 1. *114*, E5559-E5568.

Sica, A., and Mantovani, A. (2012). Macrophage plasticity and polarization: in vivo veritas. The Journal of Clinical Investigation *122*, 787-795.

So, A., and Thorens, B. (2010). Uric acid transport and disease. J Clin Invest *120*, 1791-1799.
Song, B., Leonard, M., and Schmid, S. (2004). Dynamin GTPase Domain Mutants That Differentially Affect GTP Binding, GTP Hydrolysis, and Clathrin-mediated Endocytosis. The Journal of biological chemistry *279*, 40431-40436.

Stoeber, M., Stoeck, I.K., Hänni, C., Bleck, C.K., Balistreri, G., and Helenius, A. (2012). Oligomers of the ATPase EHD2 confine caveolae to the plasma membrane through association with actin. Embo j *31*, 2350-2364.

Sun, H.S., Sin, A.T., Poirier, M.B., and Harrison, R.E. (2016). Chlamydia trachomatis Inclusion Disrupts Host Cell Cytokinesis to Enhance Its Growth in Multinuclear Cells. Journal of cellular biochemistry *117*, 132-143.

Tietzel, I., El-Haibi, C., and Carabeo, R.A. (2009). Human Guanylate Binding Proteins Potentiate the Anti-Chlamydia Effects of Interferon-γ. PLoS ONE *4*, e6499.

Ting, J.P., Lovering, R.C., Alnemri, E.S., Bertin, J., Boss, J.M., Davis, B.K., Flavell, R.A., Girardin, S.E., Godzik, A., Harton, J.A.*, et al.* (2008). The NLR gene family: a standard nomenclature. Immunity *28*, 285-287.

Tipples, G., and McClarty, G. (1993). The obligate intracellular bacterium Chlamydia trachomatis is auxotrophic for three of the four ribonucleoside triphosphates. Molecular microbiology *8*, 1105-1114.

Tretina, K., Park, E.-S., Maminska, A., and MacMicking, J.D. (2019). Interferon-induced guanylate-binding proteins: Guardians of host defense in health and disease. J Exp Med *216*, 482-500.

Tuma, P.L., and Collins, C.A. (1994). Activation of dynamin GTPase is a result of positive cooperativity. The Journal of biological chemistry *269*, 30842-30847.

Vöpel, T., Hengstenberg, C.S., Peulen, T.-O., Ajaj, Y., Seidel, C.A.M., Herrmann, C., and Klare, J.P. (2014). Triphosphate Induced Dimerization of Human Guanylate Binding Protein 1 Involves Association of the C-Terminal Helices: A Joint Double Electron–Electron Resonance and FRET Study. Biochemistry *53*, 4590-4600.

Vöpel, T., Syguda, A., Britzen-Laurent, N., Kunzelmann, S., Lüdemann, M.-B., Dovengerds, C., Stürzl, M., and Herrmann, C. (2010). Mechanism of GTPase-Activity-Induced Self-Assembly of Human Guanylate Binding Protein 1. Journal of Molecular Biology *400*, 63-70.

Wang, N., Liang, H., and Zen, K. (2014). Molecular mechanisms that influence the macrophage m1-m2 polarization balance. Front Immunol *5*, 614.

Wang, S.-p., Kuo, C.-c., Barnes, R.C., Stephens, R.S., and Grayston, J.T. (1985). Immunotyping of Chlamydia trachomatis with Monoclonal Antibodies. The Journal of Infectious Diseases *152*, 791-800.

Warnock, D.E., Hinshaw, J.E., and Schmid, S.L. (1996). Dynamin self-assembly stimulates its GTPase activity. The Journal of biological chemistry *271*, 22310-22314.

Weber, A., Wasiliew, P., and Kracht, M. (2010). Interleukin-1 (IL-1) pathway. Science signaling *3*, cm1.

Wehner, M., and Herrmann, C. (2010). Biochemical properties of the human guanylate binding protein 5 and a tumor-specific truncated splice variant. *277*, 1597-1605.

WHO (2018). Report on global sexually transmitted infection surveillance, 2018.

Wolf, A.J., Reyes, C.N., Liang, W., Becker, C., Shimada, K., Wheeler, M.L., Cho, H.C., Popescu, N.I., Coggeshall, K.M., Arditi, M.*, et al.* (2016). Hexokinase Is an Innate Immune Receptor for the Detection of Bacterial Peptidoglycan. Cell *166*, 624-636.

Wolf, K., and Fields, K.A. (2013). Chlamydia pneumoniae impairs the innate immune response in infected epithelial cells by targeting TRAF3. J Immunol *190*, 1695-1701.

Wolf, K., Plano, G.V., and Fields, K.A. (2009). A protein secreted by the respiratory pathogen Chlamydia pneumoniae impairs IL-17 signalling via interaction with human Act1. Cell Microbiol *11*, 769-779.

Yamamoto, M., Okuyama, M., Ma, Ji S., Kimura, T., Kamiyama, N., Saiga, H., Ohshima, J., Sasai, M., Kayama, H., Okamoto, T.*, et al.* (2012). A Cluster of Interferon-γ-Inducible p65 GTPases Plays a Critical Role in Host Defense against Toxoplasma gondii. Immunity *37*, 302-313.

Zhang, Y., Chen, C., Choi, H., Chaisson, C., Hunter, D., Niu, J., and Neogi, T. (2012). Purine-rich foods intake and recurrent gout attacks. Annals of the rheumatic diseases *71*, 1448-1453.

Zhang, Y., Yeruva, L., Marinov, A., Prantner, D., Wyrick, P.B., Lupashin, V., and Nagarajan, U.M. (2014). The DNA sensor, cyclic GMP-AMP synthase, is essential for induction of IFN-β during Chlamydia trachomatis infection. J Immunol *193*, 2394-2404.

Zhou, R., Yazdi, A.S., Menu, P., and Tschopp, J. (2011). A role for mitochondria in NLRP3 inflammasome activation. Nature *469*, 221-225.